Università degli Studi di Bergamo, Italy
Department of Management, Information and Production Engineering

Health Monitoring of Electro-Mechanical Actuators for primary flight surfaces

Yamuna Maccarana

in fulfillment of the requirements
for the degree of

Doctor of Philosophy in
Engineering and Applied Sciences

XXXI Cycle

Advisor: Prof. Fabio Previdi
Co-advisor: Ing. Mirko Mazzoleni

September 2018

Acknowledgements

I would like to thank my advisor Fabio as well as all of my colleagues, Alberto, Michele, Claudio, Fabio, Paolo, Mirko, Stefano, Dario, Gabriele, Matteo, Valerio and I who accompanied me from the beginning to the accomplishing of my P.h.D..

Especially, I would also like to thank *"mamma e papà"*, and all those people who supported me with smiles and good vibes during all these three years.

Abstract

This thesis has been developed under the funded project named REPRISE (Reliable Electromechanical actuator for PRImary SurfacE with health monitoring), which aims to design a novel Electro-Mechanical Actuator (EMA) to be used on primary flight surfaces of small aircrafts. The main feature of the enhanced system is a novel embedded Health Monitoring (HM) component, which aims at assessing the grade of deterioration of the specimen without resorting to additional sensing within the EMA, but by monitoring the indirect effects that the operating degradation of the mechanical transmission elements has on measurements not directly related to their status.

The entire work has been validated experimentally by the employment of a dedicated test bench to perform endurance tests, gradually leading the mechanical components to final failure. The deterioration has been evaluated also by visual inspection and screw thread profile measurements. The effectiveness of the CD algorithm has been proven despite there was no evidence of loss of ability in pursuing the EMA main function of position tracking.

This work delivers an important contribution to the More Electric Aircraft mission and lies the foundation for the development of an HM module able to estimate the Remaining Useful Life (RUL) of the specimen and thus allowing maintenance actions when the an upcoming failure is advised, in a Predictive Maintenance strategy.

Contents

Preface

The first chapter of this thesis is to provide the background and motivation of this work together with the main purposes. The work has been published in internationals conferences papers.

Background and motivation

In the past several years, several industrial programmes have initiated the concept of a More Electric Aircraft. The aero-equipment industry has in particular launched several studies and developments for more extensive electrical actuation with Electro Hydrostatic Actuators (EHA) and started to introduce EMAs (electromechanical actuators) for auxiliary equipment. This has provided incremental approaches to address hydraulic circuit issues with Power-by-Wire technologies (A320, B777 and Falcon 7X), introduction of the 2-hydraulic/2-electric (2H/2E) power distribution architecture, where flight controls are powered in backup mode by EHAs using a local hydraulic reservoir (A380, A350XWB) and use of EMAs for specific systems (spoilers, brakes and engine starters). The adoption of electrical equipment for flight-critical applications in future aircrafts is motivated by a number of economic and environmental considerations. However, the actual implementation of such equipment requires that several breakthroughs are achieved to meet envelope, cost and safety barriers that currently prevent the introduction of a fully electric actuation architecture. For this reason, new aircraft are still relying on hydraulic actuation for primary flight-control surfaces and landing gear. It must then be emphasized that new aircraft developed by newcomers (Avic, Irkut, etc.) tend to be cost competitive by using equipment of proven technology produced in low-cost countries. A need is thus perceived by the European aviation community

for moving towards new technologies able to offer a more efficient, environmentally friendly and reliable product that will be competitive versus the corresponding products based on old technology offered by competitors.

The entire presented work lies under a funded project named REPRISE (Reliable Electromechanical actuator for PRImary SurfacE with health monitoring) beneath the Clean Sky 2 Joint Undertaking research program concealed by the European Union's Horizon 2020.

Figure 1: Funder logos

The partners of the REPRISE project are:

- Piaggio Aerospace (topic manager), one of the most important multinational aerospace manufacturing company, headquartered in Genoa, Italy.
- Umbra Cuscinetti S.p.A, a company that works in aerospace field since 1972, specialized in bearings, based in Foligno, Italy.
- Zettlex, an English company that projects and builds sensors for precise measurement of position and velocity for harsh conditions.

Figure 2: Umbra Cuscinetti S.p.A, Piaggio Aerospace and Zettelex logos

The REPRISE project aims at supporting the improvement of the Technological Readiness Level (TRL) for electromechanical Flight-Control Systems of small aircrafts. The final aim of the project is to design and realize an Electro-Mechanical

Actuator endowed with a Health Monitoring system in order to perform Condition Assessment (CA) on the mechanical parts of the system, especially of the ballscrew.

Aims and results

Aims - This thesis is dedicated to the development of an advanced *Health Monitoring* (HM) algorithm, developed through *Fault Detection and Isolation* (FDI) and *Condition Assessment* (CA) techniques, of a novel *Electro-Mechanical Actuator* for primary flight surfaces handling. More in details, the final aim of this work is to identify any degradation in the mechanical transmission elements (ballscrew and other components such as bearings) without resorting to additional sensing on internal components.
Results - The aims have been achieved as the HM system is able to detect anomalies in the prototype, even if there is no evident loss of ability of the EMA in pursuing its main function (position tracking). As result for future development, the HM system, embedded on the EMA, will serve as a *Predictive Maintenance* scheduler, significantly reducing costs and improving the overall component reliability.

Alongside the algorithm implementation, a large experimental activity has been carried out on a 1:1 scale EMA by means of a dedicated test rig, with the purpose of bringing the actuator close to failure, by progressive deterioration of the parts in overload operating conditions. The effectiveness of the HM algorithm in detecting the mechanical transmission degradation has been experimentally proven. The deterioration has been confirmed by visual inspection in spite of the fact that the actuator was still able to perform position tracking in an effective way, even when ballscrew was severe damaged. Performance evaluation studies have been performed to verify the capability of the EMA, that comprises a fault tolerant control system, in achieving the imposed reference position profile, even in degraded conditions.

Thesis outline

The work has been organized into three main parts:

- *Part I: State of the art*, provides a survey on state of the art of Fault Detection and Isolation, with attention to Health Monitoring techniques and in-depth analysis of the aerospace environment, in particular of aeronautical

Electro-Mechanical Actuators. The state of the art investigation lays the foundations to understand the Author's proposal.

- *Part II: Experimental setup*, necessary to describe the vast experimental procedure that has been carried out during this project to test and validate the effectiveness of the proposed Health Monitoring module based on Change Detection algorithms, that is presented in the last part.
- *Part III: Health Monitoring based on Change Detection algorithms*, that contains the core of the work and presents a new Health Monitoring system based on Change Detection algorithms, discussing the results. The comprehension of this part is strictly related to the awareness of the first part and of the second part.

More in details, this thesis is structured as follows:

Part I: State of the Art

- *Chapter 1* introduces the general matter of this thesis, providing basic concepts and key definitions
- *Chapter 2* is to explore the state of the art of Health Monitoring techniques and FDI methods and a general approach to the matter
- *Chapter 3* investigates specific studies on FDI in aerospace environment
- *Chapter 4* achieves a deep research on FDI techniques applied to Electro-Mechanical Actuators (EMAs) in aerospace environment, with references to case studies

Part II: Experimental setup

- *Chapter 5* is devoted to the illustration of the test rig
- *Chapter 6* is dedicated to the description of the test procedures
- *Chapter 7* evaluates the performance of the actuator in healthy and faulty conditions

Part III:Health Monitoring based on Change Detection algorithms

- *Chapter 8* presents the concepts and the theory behind the developed Health Monitoring module based on Change Detection algorithms

- *Chapter 9* implements the HM system in MATLAB environment
- *Chapter 10* discuss the testing and the results of the HM system on the measurements of the experimental tests

Part I

State of the art

The state of the art of Health Monitoring (HM) techniques via Fault Detection and Isolation (FDI) methodologies, with in-depth analysis in the aerospace environment, is investigated in this part.

CHAPTER 1

Topic description and definitions

Nowadays, the world is facing a situation of great and fast technical and technological development. The term *development* indicates a change in methods or equipment that is achieved to accomplish new tasks. Often, new tasks are not intended in terms of new capabilities, but instead they concern higher performance level requirements or lower efforts and consumptions while accomplishing the same goal. This causes a consequent increasing of the complexity of several systems in many different high technology industries, leading to numerous benefits with regard to economical saving, resources optimization, power enhancing, environmental preservation and so on. Although, all this also brings to major risks in the matters of safety, pollution, product quality level observance etcetera. Here is where malfunctions and faults have a greater probability to happen.

Next, a series of definitions is given following the trace of [1] [2] [3].

- **Malfunction***: an intermittent unpermitted alteration of one or more elements of the system during the fulfillment of a task.*
- **Fault***: an unpermitted alteration of one or more elements of the system.*
- **Incipient fault***: a fault that is originating but still has limited or no effects on the overall system.*

Faults can result in performance reduction, parts degradation or damages occurring, with consequent deleterious impacts on the system and on the whole process of technical and technological development.

- **Symptom***: a visible effect of the alteration of one or more elements of the*

system.
Furthermore, severe faults can culminate in a failure of the entire system.
- Failure*: a permanent halt of the system operating condition.*
In fact, there is no point in enhancing more and more technological and better-performing systems if reliability is not developed at the same pace. Reliability defines how well a system works, even in case of unexpected events, such as faults. The reliability of a system can be improved in different ways, however, often a redundancy is introduced. The latter can be of two types:

- Hardware (HW) redundancy
- Software (SW) redundancy

A HW redundancy can be obtained by providing multiple physical copies of a hardware components. Although this increases the overall reliability of the system, it implies more costs and additional weight and space consumption. Sometimes, HW redundancy cannot even be achieved because of limited space or extreme performance requirements (as is often the case of aerospace environment, which will be considered in section 3). For this reason, usually SW redundancy is introduced in the form of the so called *Fault Detection and Isolation* methods.
- Fault detection*: the ability to predict or promptly notice undesired states in a system or a process.*
The ultimate aim of fault detection is to inform a supervisor so that it can take appropriate actions to avoid or limit accidents and breakages [4]. The supervisor can be a human, a fully automated entity or a cross between the two.
- Supervisor*: the entity which manages the output of a fault detection analysis.*
However, when the fault is detected, more information such as the position of the alteration can significantly improve the supervisor actions. This is obtained by a fault isolation process.
- Fault isolation*: the ability to locate the detected faults in a system or a process.*
Moreover, besides the fault detection and isolation process, more accurate actions can be taken by the supervisor if the type and entity of the occurred fault can be defined.
- Fault identification*: the ability to classify the type and entity of detected faults in a system or a process.*
Thus, through FDI techniques, the supervisor is able to assess the condition of a system. The continued action of supervising the status of health of a system is called Health Monitoring (HM).

- Health monitoring*: the continued oversight of the progression of the degradation of a system, a process or a component.*
The HM process, through FDI techniques, could also be able to achieve a continuous evaluation of the progression of deterioration of the system, accomplishing the so called Condition Assessment (CA).
- Condition Assessment*: the evaluation of the state of health of a system, a process or a component.*

In Figure 1.1 the overall general scheme of the FDI procedure is reported. During this thesis, the attention is focused on the *Detection*, *Isolation* and *Classification* phases, while the task of informing and resolving is not part of this project aim.

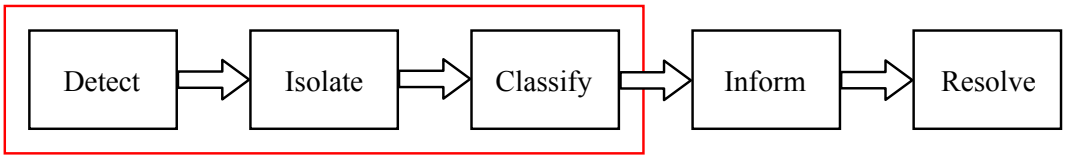

Figure 1.1: Methodological chain for FDI and fault management

The two-step idea for the Fault Detection and Isolation (FDI) procedure was introduced in the 1980's [5], and is composed of two tasks:

- Residual generation
- Residual evaluation

- Residual*: an indicator of the faults happening, based on a deviation between the estimations from the models and the real measurements.*
However, other methodologies for the extraction of indicators containing information on the ongoing faults were employed. Also, other strategies have been developed for the classification phase. For this reason, different strategies can be employed for the Fault Detection, Isolation and Classification, giving birth to the following so called methodologies [6]:

- Model-based method
- Signal-based method
- Knowledge-based method
- Hybrid method

With the definitions given in this chapter the general matter of this thesis has been introduced. In the next chapter, together with a general overview of the Health Monitoring task on fault tolerant systems, the state of the art of all the cited FDI methodologies is presented.

CHAPTER 2

General Methodological Overview on FDI

With increasing demands for efficiency and product quality and progressing integration of automatic control systems in high-cost and safety-critical processes, the field of monitoring (or supervision) plays an important role [7]. Also, fault detection and diagnosis belong to the general area of *supervision* [8]. The term supervision is often associated with the term *Health Monitoring (HM)*. In fact, the supervisor is the entity that is responsible of the monitoring of the health of a system. The HM process relies on FDI techniques. In fact, as stated in chapter 1, HM is able to achieve the *Condition Assessment (CA)* of the system through FDI techniques. This logic is illustrated in Figure 2.1.

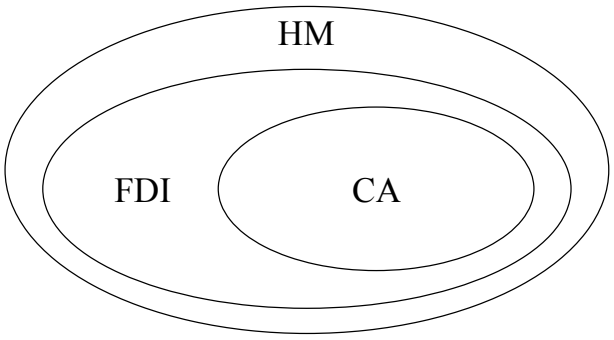

Figure 2.1: Health Monitoring, via Fault Detection and Isolation techniques to achieve Condition Assessment

The matter has been largely investigated for decades in several environments and applications [9] and is presented in the next sections.

2.1 HM task in fault tolerant systems

The process of HM is achieved differently depending on the type of the system and control loop (open loop and closed loop control systems). The next sections are to present an analytical description of HM in open and closed loop systems.

2.1.1 HM in open loop systems

A general system **P** that operates in open loop is considered. Refer to Figure 2.2.

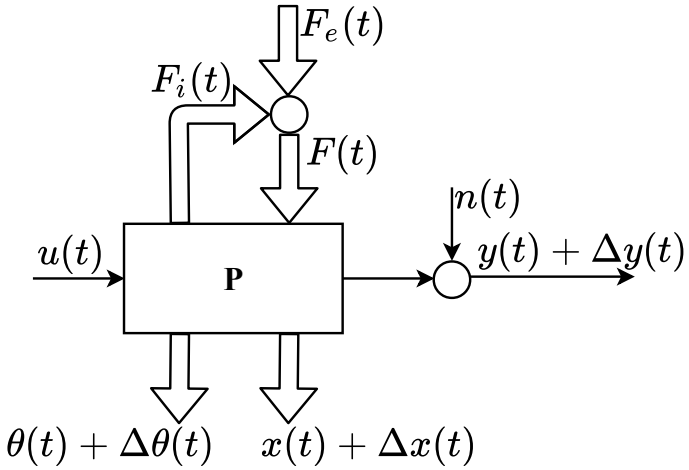

Figure 2.2: Scheme of an open loop operating system

The signals $\mathbf{u}(t)$ and $\mathbf{y}(t)$ are, respectively, measurable input and output signals. $\mathbf{x}(t)$ is the state vector and $\boldsymbol{\theta}(t)$ the internal system parameter vector. When internal or external faults $\mathbf{F_i}(t)$ and $\mathbf{F_e}(t)$ occur, the overall fault $\mathbf{F}(t)$ makes the state vector, the output and the parameter vector subjected to deviations, indicated as, respectively, $\Delta\mathbf{x}(t)$, $\Delta\mathbf{y}(t)$ and $\Delta\boldsymbol{\theta}(t)$.

Certainly, a large amount of information is included in such Δ quantities. In ideal cases, an effective FDI method should have the ability to extract knowledge over this deviations. However, it has to be considered that also natural process disturbances and noise $\mathbf{n}(t)$ affects the system. In general, for a process that is operating in open loop, a remaining fault $\mathbf{f}(t)$ (part of $\mathbf{F}(t)$) results in a permanent offset $\Delta\mathbf{y}(t)$ in the output [8] [10]. Thus, in this case, a relation can be studied between the fault and its direct effect on the output. Moreover, if the system is observable, the states can be renconstructed. However, also the states may have been affected by the fault. This could lead to a misalignment between the actual states and the reconstructed states that derives from the fault effect. Thus,

it is possible to affirm that the possibility of observing the effect of the fault on the output is related to the observability property of the system. Normally, the supervision of a system is made by limit or threshold checking of measured variables. An advice is given only if the Δ exceeds tolerance zone. This process is also called *monitoring*.

Nevertheless, most of the control applications (especially in critical environments such as the aerospace one and the case study of this work), presents a closed loop control system. This avoids, in the operational limits of the components, the permanent offsets caused by faults or incipient faults. This makes the system intrinsically fault-tolerant and complicates the task of the FDI, as the symptoms may be hidden, especially if monitoring only input and output signals. The next section describes this more in details.

2.1.2 HM in closed loop systems

In Figure 2.3 the signal $\mathbf{w}(t)$ is the reference signal, while $\mathbf{e}(t)$ is the error given by the difference $\mathbf{e}(t) = \mathbf{w}(t) - \mathbf{y}(t)$.

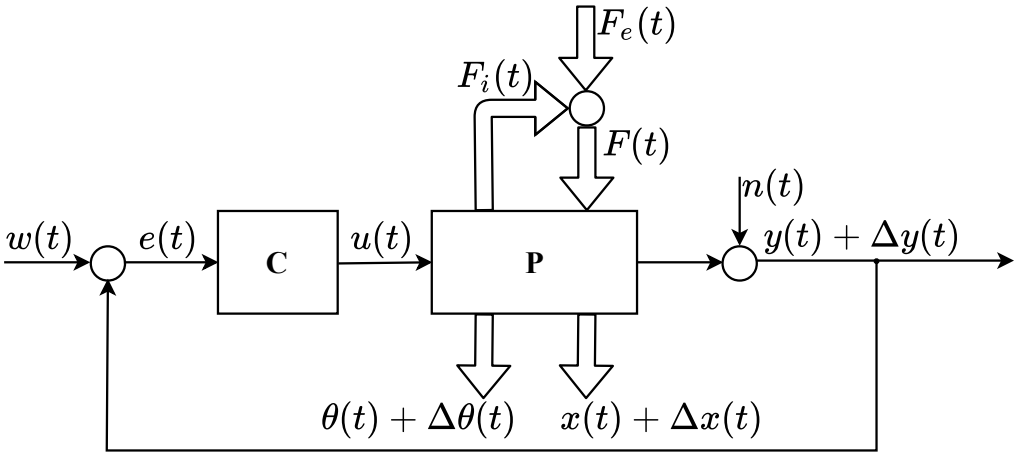

Figure 2.3: Scheme of a closed loop operating system

Depending on the time history of parameter changes $\Delta\boldsymbol{\theta}(t)$ or state-variable changes $\Delta\mathbf{x}(t)$, if a suitable controller is employed in the system (e.g. controller with integral action), the output presents a deviation $\Delta\mathbf{y}(t)$ which will be different from the one in the open loop system. In particular, the effects of the fault and of the noise will be vanishing on the output $\mathbf{y}(t)$ while the control variable $\mathbf{u}(t)$ will present a permanent offset $\Delta\mathbf{u}(t)$ for proportionally acting processes. For this reason, it is clear that, if monitoring only the output variable with respect to the

reference, the fault may not be detected because it could have no effects on $\mathbf{y}(t)$, furthermore considering also the corruption generated by the noise. This happens because the controller in a closed loop configuration is able to compensate not only for disturbances but also for parameter changes $\Delta\boldsymbol{\theta}(t)$ and state changes $\Delta\mathbf{x}(t)$ with respect to the control variable. Thus, the faults $\mathbf{F}(t)$ may be completely compensated, unless the fault is severe enough to induce the control variables to reach saturation. In the latter case the deviation $\Delta\mathbf{y}(t)$ may increase. Hence, for processes in closed loop, the input $\mathbf{u}(t)$ shall be supervised as well. For a better understanding, a visual comparison of the time behaviors of measurable signals $\Delta\mathbf{y}(t)$ and $\Delta\mathbf{u}(t)$ in relation to a parameter change $\Delta\boldsymbol{\theta}(t)$ following a fault $\mathbf{F}(t)$ in open loop and closed loop systems is depicted in Figure 2.4.

It is clear how the closed loop system, on the contrary of the open loop system, is able counteract the fault, allowing the system to operate in pseudo-normal condition and concealing the fault. This makes the task of fault detection somehow more complex and introduces the concept of *intrinsically fault tolerant control systems*.

- **Intrinsically fault tolerant system***: a system able to counteract faults, compensating their effects with a control action in closed loop configuration.*

Moreover, most of the modern systems are in a closed loop configuration. This justifies the importance and complexity of FDI methodologies and techniques. The intrinsic feature of fault tolerant control systems is the ability to follow a reference signal accurately, despite disturbances and system degradations. Depending on the performances of the control strategy, this action can be achieved fast and precisely, hiding eventual symptoms of incipient faults (some more serious faults may lead to system failures or jamming).

Normally, the supervised variables are the error $\mathbf{e}(t)$ and the output $\mathbf{y}(t)$. As previously stated, these two variables, if an integral action is present in the control loop, will not show the presence of small faults. Only a small number of events (faults) produce unusual behaviors of the system (and often too late) in closed loop systems [11]. However, unusual behaviors may be avoided or limited by an overwork of the controller. This results in a strained operational condition of the system that could lead to a failure. For this reason, a FDI algorithm should be able to determine, as accurately as possible, which part of the system is failing, and which kind of fault it is facing, even in case of incipient faults. Thus, additional sensors may be needed to the aim of FDI in closed loop systems, in a HW redundancy solution. However, in some cases it is not possible to add supplementary measurement hardware on the specimen (e.g. in aerospace

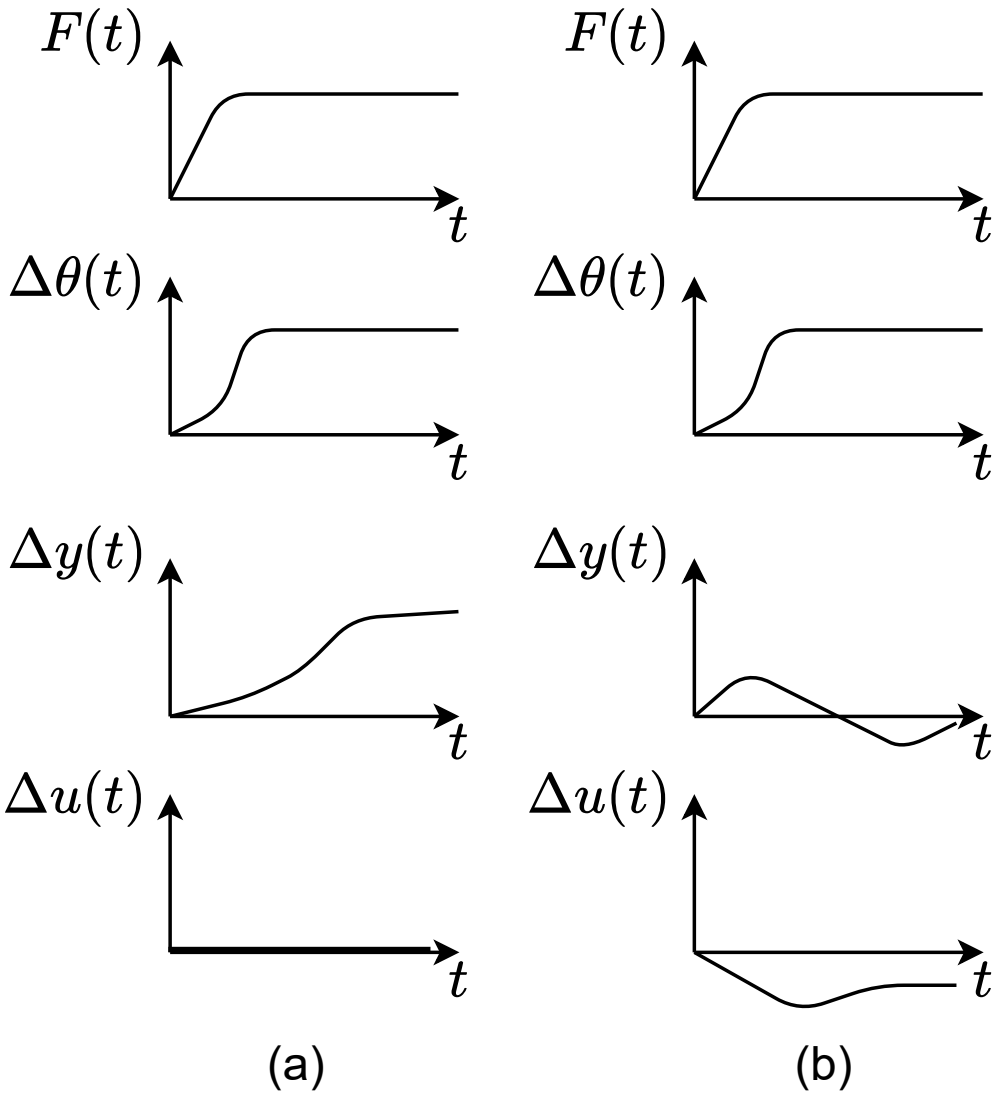

Figure 2.4: Comparison of time behavior of a parameter change and measurable signals of a fault in (a) open loop and (b) closed loop

application where space and weight is a strict requirement). Thus, there exist some techniques toward the FDI without resorting to additional hardware. For example, it is possible to monitor performances of the system by considering also the control variable $\mathbf{u}(t)$ and the reference variable $\mathbf{w}(t)$ and in particular their variance, steady-state deviation, eventual overshoots, frequency spectra and so on. The next sections are dedicated to a vast overview, in which the general approach to the FDI is presented in a methodological way.

2.2 Model-based approach method

This section is meant to present a rigorous methodological approach to fault detection and isolation via model-based methods. The model-based algorithms state of the art relies its foundations in the '70s [12], [13] and has been largely investigated in the last decades [14] [15] [16] [17] [18] until the last years [6] [19] [20] [21] [22] and nowadays [8].

The idea of the model-based approach is to supervise the dependencies between different measured signals of a process or system. For example, some measured variables have physical relations to other measured variables. This relation can be expressed by mathematical process models. Over the process model, a fault detection is achieved by generating the following features:

- $\mathbf{r}(t)$: residuals
- $\hat{\theta}(t)$: parameter estimates
- $\hat{\mathbf{x}}(t)$: state estimates

The features are obtained through several methods, such as parameter and state estimation and observers, parity equations and others [23], as further investigated in the next sections. At first, when the system is in healthy conditions, features are extracted and stored as benchmark for future comparisons. Here is where the real FD process takes place: the new features extracted over time are compared with the initial features. If changes are detected, analytical symptoms $\mathbf{s}(t)$ are highlighted. Once symptoms have been highlighted, a FI phase is needed to lead to the fault identification. The whole model-based general procedure is depicted in Figure 2.5.

However, in the model-based FDI method, often a model of the fault is employed. There exist different fault models depending on the type of the faults. This is explained in the next section.

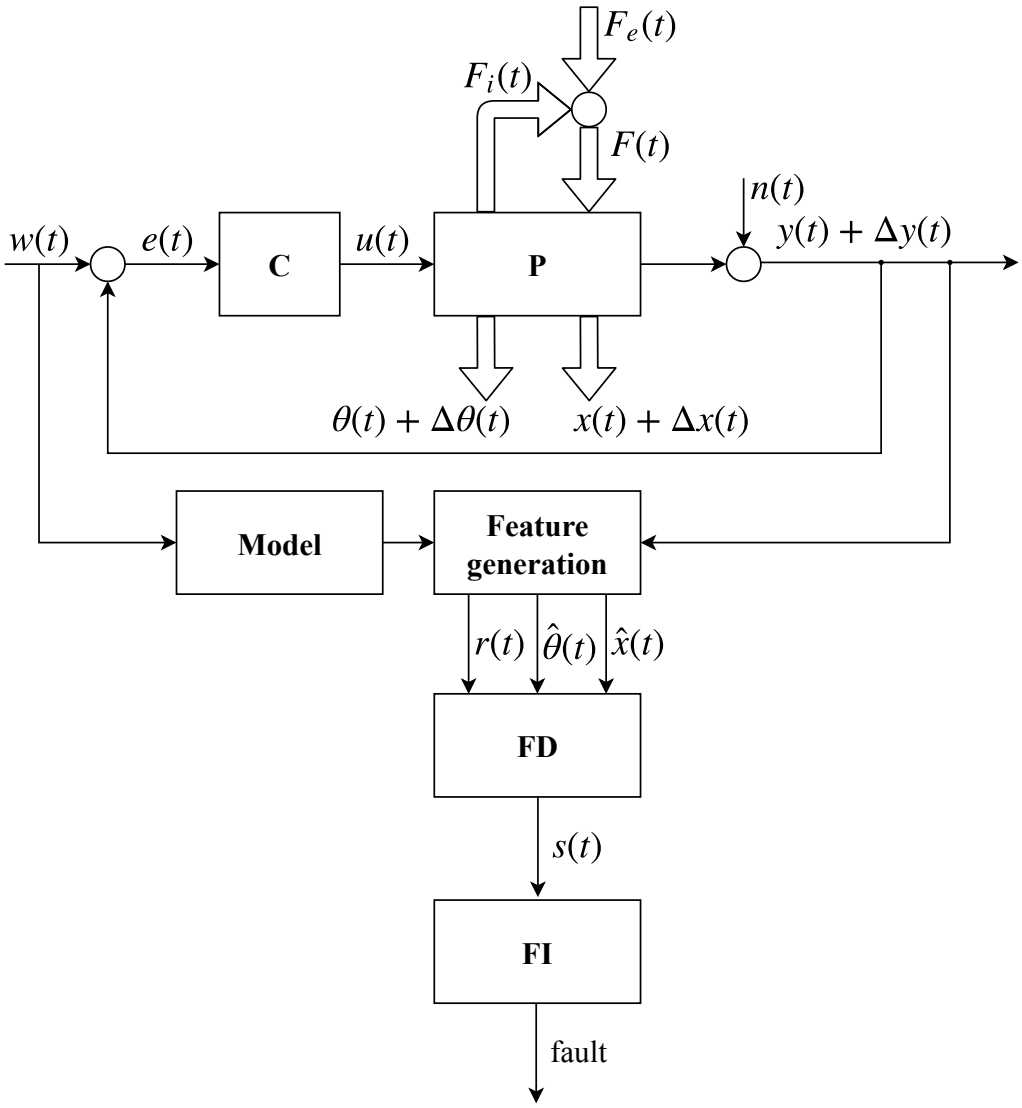

Figure 2.5: General scheme of model-based FDI methods

2.2.1 Fault Modeling

There exists different types of faults. The faults that are time dependent can be divided in:

- abrupt: a fault that brings to a stepwise change in the features
- incipient: a fault that leads to a drift-like change in the features
- intermittent: a fault that evidences its effects in sporadic manner in the features

The three are depicted in Figure 2.6, where the vertical dashed line indicates the fault happening in a certain instant and the plots show the behavior of the features changing $feat(t)$ in time t.

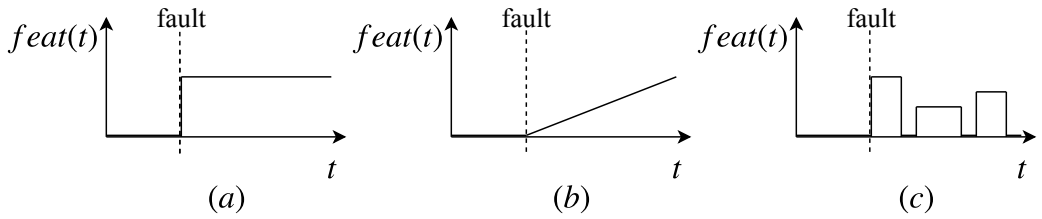

Figure 2.6: Types of time dependent faults: (a) abrupt, (b) incipient and (c) intermittent

Faults can influence the system output variable $\mathbf{y}(t)$ in several ways, however, the basic models of faults are:

- additive: by an addition of a variable $\mathbf{f}(t)$ to the output
- multiplicative: by the product of the control variable $\mathbf{u}(t)$ by $\mathbf{f}(t)$

Examples of additive faults can be an offset of measures given by sensors, while examples of multiplicative faults are usually related to parameter changes in a process. The effect of additive and multiplicative faults are described in Figure 2.7, where the output $Y(t)$, in the additive fault case, is equal to the output given by the control variable through the system $Y_u(t)$ with the constant contribute f of a fault, while the output $Y(t)$, in the multiplicative fault case, in equal to a sum of the control variable $U(t)$ multiplied by a (the effect of the system) plus the contribute of the fault f multiplied by the control variable.

However, there exists numerous different models of faults depending on the application and on the FDI specific purpose. Usually, fault trees (see section 3.2)

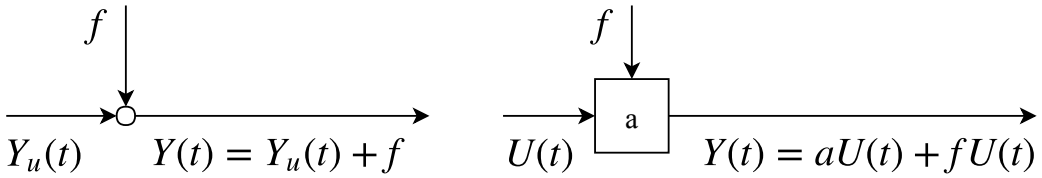

Figure 2.7: Basic models of faults: (a) additive and (b) multiplicative

are developed in order to classify the anomaly that the system faces. In the next sections, instead, modeling techniques are presented along with model-based FDI methods.

2.2.2 Residuals

Considering Figure 2.5, $\mathbf{r}(t)$ is the residual vector, that is calculated as a combination of the output $\mathbf{y}(t)$ and it eventual deviation $\Delta\mathbf{y}(t)$ and the reference $\mathbf{w}(t)$ (or control variable $\mathbf{u}(t)$). There exists several methodologies for the residuals generation, however, each of such methodology refers to a general representation, briefly explained next.

The base idea, giving also the definition of residuals in chapter 1, is that no information should be included in the residuals if no faults are occurring:

$$\mathbf{r}(t) = 0 \Leftrightarrow \mathbf{f}(t) = 0 \tag{2.1}$$

Thus, it is possible to say that the residuals and the faults are somehow related by a *fault transfer matrix* G_{rf} [21] and, with simplification of the system in Figure 2.5, it is possible to obtain the dynamic of the residual signal as:

$$\mathbf{r}(s) = \sum_{i=1}^{q} G_{rf_i}(s)\mathbf{f}_i(s) \tag{2.2}$$

where $\mathbf{f}_i(s)$ is the i-th component of the fault vector, that is q-long. Thus, as long as the $G_{rf_i}(s)$, that is the i-th column of G_{rf}, is non-zero (this condition is named *fault detectability condition*), then the fault $\mathbf{f}_i(s)$ has a visible effect on the residual and is, therefore, detectable.

Once the effect of the fault has been included in the residuals, then the residual evaluation phase starts. Such phase can be fulfilled on a single residual or, better, on a set of residuals. In order to accomplish the FI task, in [24] two different concepts have been presented in a geometric framework in which a residual vector

spans the residual space:

- in the Structured Residual Set each residual is supposed to be affected only by a specific subset of faults
- in the Fixed Direction Residual Set each residual is supposed to be affected only by one specific faults

However, each fault leaves some information in the form of a specific *signature* in the residuals and, assuming to be able to lead each signature to each fault, then, in the geometric framework, it is possible to identify each fault by comparing its signature in the residuals [25].

Also, there exists other approaches for the residual evaluation [4]:

- threshold (constant or time varying) [26] [27]
- neural networks and pattern recognition [28]
- fuzzy logic [29]

The residuals generation and evaluation method can be flanked or replaced in the FDI by other techniques, presented in the next sections.

2.2.3 Parameter estimation

Model based FDI methods require an accurate knowledge of the system and of its mathematical and physical processes, usually by means of differential equations or frequency response. This implies that all system parameters have to be known. However, this does not always happen, for example if some physical coefficient are partially or not known at all. In this case, a process of parameter estimation is needed.

The process of going from observed data to a mathematical model is fundamental in science and engineering [30]. In the control area this process has been termed *System Identification* and the objective is to define dynamical models (difference or differential equations) from observed input and output signals. Thus, the aim of the identification procedure is to estimate systems models starting from experimental data. This process is useful especially in those cases where it is necessary to obtain a robust model over a hard-measurable physical system or over a system in which the knowledge of some dynamics may be partial or even totally void. The procedure is characterized by four basic ingredients:

- the observed data
- a model (or a set of candidate models)
- a criterion of fit (objective function)
- a validation method

Generally, it is possible to define three types of identification:

- white box identification, in which the model is obtained by the description of the system components through physical law
- grey box identification, in which the structure of the model is known but one or more parameters are not and they have to be estimated due to experimental observations
- black box identification, in which nothing is known about the system. In this case a group of general models is considered and their parameters do not have a direct physical meaning, but instead, they are just simple vehicles to define the input/output transfer function of the system

For example, white box identification can be employed only when the physics of the system (together with its parameters) are known. In this case, the use of differential equation is suggested. Instead, if nothing is known about the structure of the systems, the model identification will be based on the input/output measurable signals together with some model structure assumptions: many trials may be needed. In this case, neural networks and impulse response are the techniques to be used. In between, the grey box identification can be additionally divided in light-grey and dark-grey box identification, depending on the known information. In this case, it is possible to employ differential equations and fuzzy models with parameter estimation.

However, more in details, the process of identification consists in the research of those parameters which minimize an objective function that represents the distance between the simulated output signals (from the model) and the experimental ones (the observed data). The objective function can also be named *loss function* or *cost function*. The minimization of the output error is achieved as depicted in Figure 2.8, in which the recursive approach is based on the recursion of the comparison between experimental output from the real system and the simulated output from the model. Similarly, there exists another approaches by minimization of the objective function for the parameter estimation that employs a non-recursive manner [7] [17].

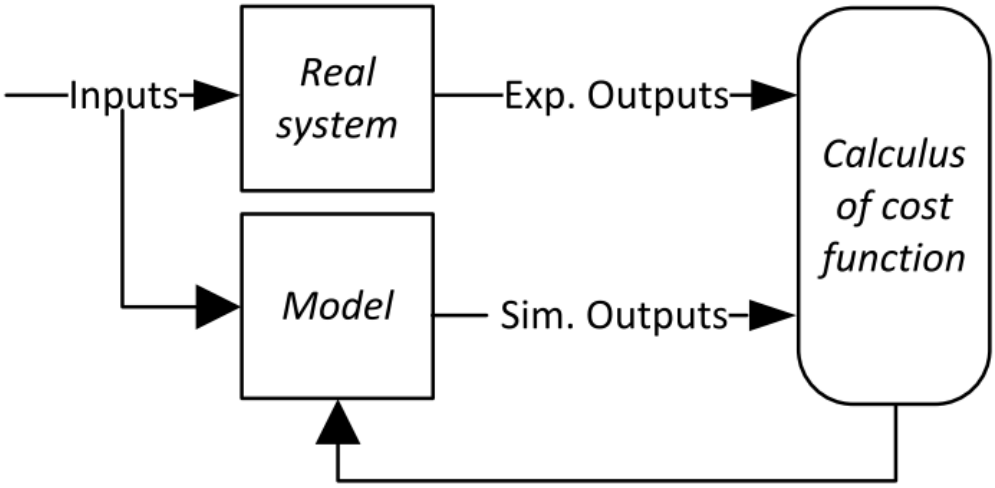

Figure 2.8: Recursive identification process

The criterion of fit (from which the cost function is defined) depends on each specific application and has to be set in order to reach the best possible result in simulation with respect to the reality. There exists many different methodologies for the parameter estimation to find the optimal solution, depending mostly on the linearity or non-linearity of the model (when known) [31]. In the end, parameters can be compared over time and eventual faults happening in the FDI process. Of course, each fault has a different effect on one or more system parameters.

Instead, the next section is to describe the case in which the system parameters are known (or well estimated) and states and/or outputs are, for some reasons, not measurable.

2.2.4 State and output observers and estimation

In the case where the system parameters are known, observers can be employed to estimate states which may not be measurable. Next, a LTI dynamic system with additive faults f_L to the input and f_M to the output is considered. The process model becomes:

$$\begin{aligned} \dot{\mathbf{x}}(t) &= A\mathbf{x}(t) + B\mathbf{u}(t) + F\mathbf{v}(t) + L\mathbf{f}_L(t) \\ \mathbf{y}(t) &= C\mathbf{x}(t) + N\mathbf{n}(t) + M\mathbf{f}_M(t) \end{aligned} \tag{2.3}$$

where $\mathbf{v}(t)$ and $\mathbf{n}(t)$ are the disturbance signals, F, L, N and M the weight matrices of the respective signals.

At this point both states and outputs may be observed. The observer equations

filter (in discrete form) are:

$$\begin{aligned} \hat{\mathbf{x}}(k+1) &= A\hat{\mathbf{x}}(k) + B\mathbf{u}(k) + H\mathbf{e}(k) \\ \mathbf{e}(k) &= \mathbf{y}(k) - C\hat{\mathbf{x}}(k) \\ \hat{\mathbf{y}}(k) &= C\hat{\mathbf{x}}(k) \end{aligned} \tag{2.4}$$

where H is the matrix multiplied by the error. In other words, the output estimation error is defined as the measured output minus the estimated output:

$$\mathbf{e}(t) = \mathbf{y}(t) - \hat{\mathbf{y}}(t) \tag{2.5}$$

A similar reasoning is made for the state estimation error. The residuals are then generated by the design of a matrix W, so that the residual generation results as:

$$\mathbf{r}(t) = W\mathbf{e}(t) \tag{2.6}$$

Considering the equations 2.4, in the form of equation 2.6, the residual signal contains information of both fault and disturbance signals. A similar reasoning is made for the residuals generated by the state estimation error [14]. The symptoms that can be found as results of the observations are the same as for both the state and the output estimations. As before, observations can be compared over time for the fault detection and identification.

Similarly to the state observers approach, the Kalman filter can be used if considerable stochastic disturbances act on the system. Also, other filters such as the Extended Kalman Filter or the Particle Filter for nonlinear state filtering can be employed [32] [33] [34] [35] [36].

2.2.5 Parity equations

Following the idea of that depicted in Figure 2.8, a fixed model G_M can be considered and run in parallel to the process G_P. There exist different forms of parity equations:

- output error (refer to Figure 2.9), in which the outputs are compared to create the output residuals:

$$r_{OUT}(t) = y(t) - y_M(t) \tag{2.7}$$

  where G_P indicates the considered process, and y_M the model output.

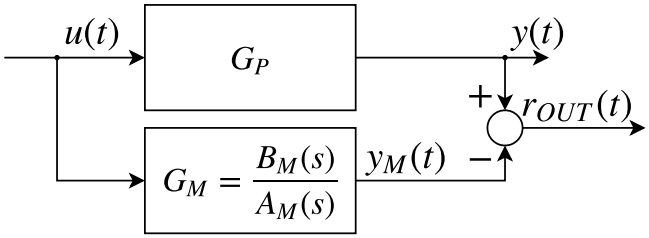

Figure 2.9: Output error parity equation scheme

- equation error (refer to Figure 2.10), with the following equations:

$$r_{EQ}(t) = A_M(s)y(t) - B_M(s)u(t) \tag{2.8}$$

where A_M and B_M are, respectively, the denominator and numerator of G_M.

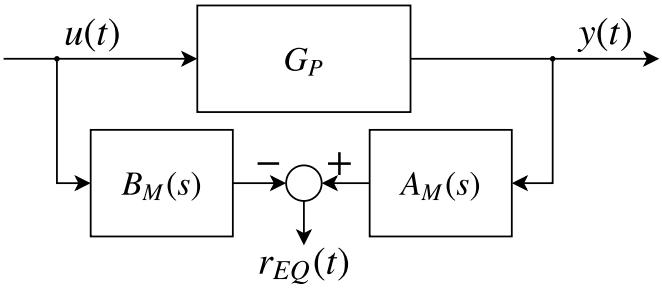

Figure 2.10: Equation error parity equation scheme

- input error (refer to Figure 2.11), with the following equations:

$$r_{IN}(t) = u(t) - \frac{A_M(s)}{B_M(s)}y(t) \tag{2.9}$$

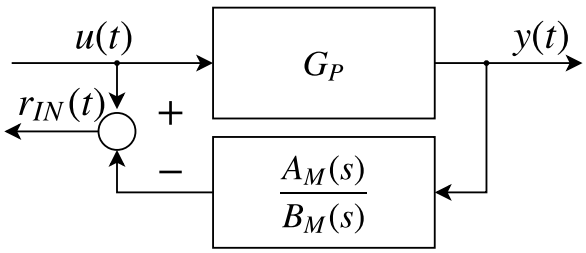

Figure 2.11: Input error parity equation scheme

In all cases, the residuals only depend on the input and output faults $f_u(t)$ and $f_y(t)$. Similarly, in MIMO systems, it is possible to generate structured residuals for a better isolation of faults [18].

Next, a conclusive comparison is made.

2.2.6 Model-based approaches comparison

To conclude the model-based approach method to FDI, a comparative section is presented. This entire section lays the foundations for the development of a model that is able to generate some residuals or observations of the states or of the parameters. Now it is assumed that parameter estimation methods reconstruct non-measurable parameters from the input and output signals while state observers and Kalman filters estimates non-measurable state variables.

The presented methodologies differ for few details. For example, an input excitation is needed for a better identification of the model while using the parameter estimation approach. Instead, state estimation and parity equations can work well in steady-state conditions. Moreover, the high dynamic of a process may lead to the choice of a state estimation instead of parity equations approach. Some factors that could led to the choice of the parameter estimation approach can be the knowledge of the model parameters, noise, MIMO vs SISO systems, the presence of multiplicative faults, the robustness of parameter change and the computational effort as well. All this is well described in Figure 2.14 and explained in section 2.6.

All these considerations will be useful to create a mathematical model, that is, by its nature, the closest and most accurate method to describe the knowledge that human have of a certain system. Yet, complex systems may be the result of linear and nonlinear dynamics, that may be hard to describe mathematically. Moreover, in certain applications, the knowledge of the system physics may limited or totally void, so that other FDI approaches such as the signal-based one could be more effective. Now that the model-based approach has been investigated, next, signal-based approach is described.

2.3 Signal-based approach method

For large-scale or complex processes, it is not always possible to develop an efficient model of the system. Also, when the available process measurements are highly correlated but only severe faults have an effect on the usual patterns of the system (identified in healthy conditions), signal-based methods may be helpful. The

idea is that the faults are somehow reflected in the measurements and that it is possible to extract some features that are useful to detect and identify eventual anomalies. This happens especially when the monitored process is characterized by an oscillating or cyclic time behavior. If a cycle is present in the measured signal, then a period can be identified and together with it, some basic characteristics of such signal (such as frequency and phase modulation) can be extracted [7]. The overall signal-based procedure is depicted in Figure 2.12, in which Y_0, S_{yy} and R_{yy} are example of features extracted by the measurements. Such features are

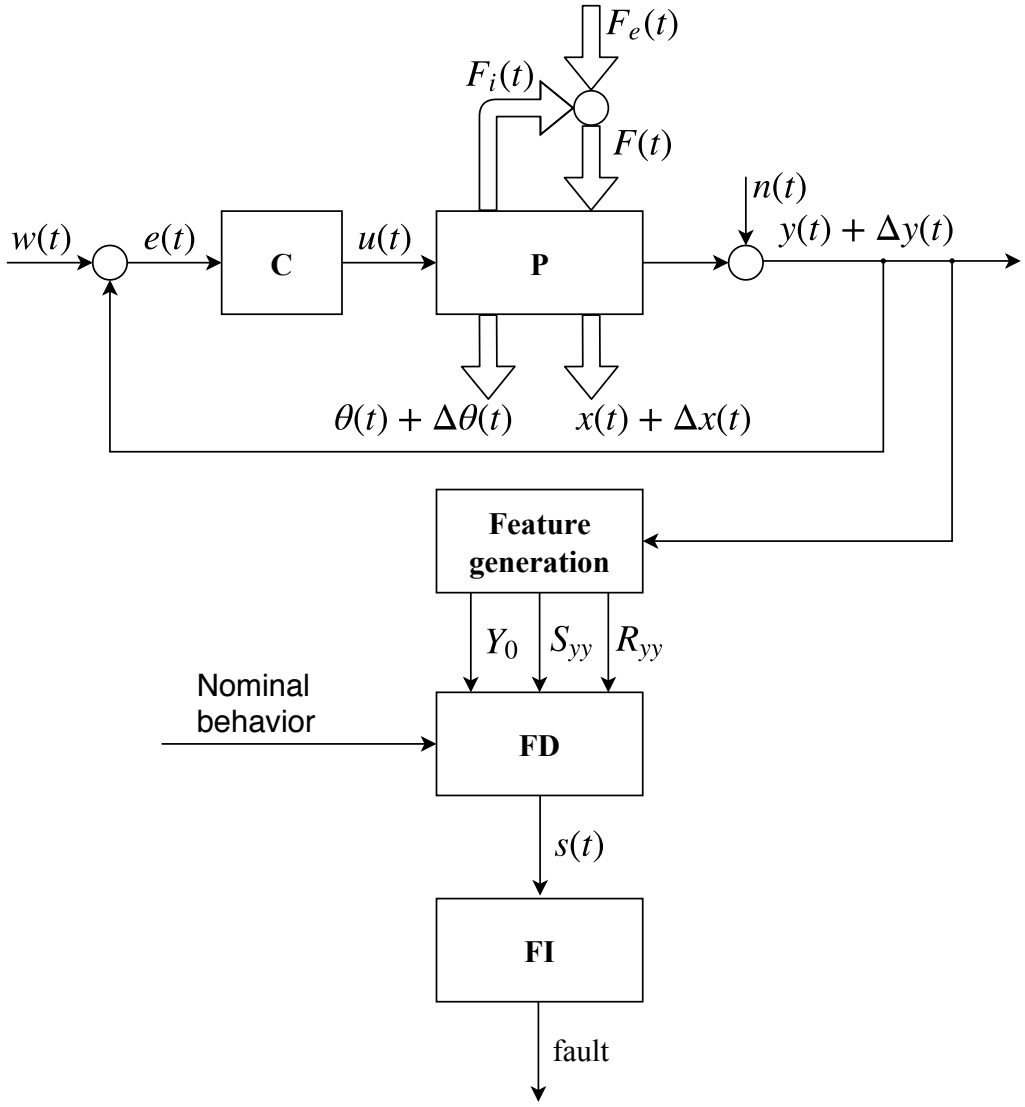

Figure 2.12: General scheme of signal-based FDI methods

then compared with the nominal behavior of the system in healthy conditions and, eventually, symptoms are highlighted and analyzed for the detection phase of the FDI process. Of course, in fact, this approach needs a solid prior knowledge

of the system and its behavior in healthy conditions. To manage such a priori knowledge, two main strategies can be adopted [37]:

- *classification* [38]: it involves building classes from the database either in a supervised way (i.e., with the help of an expert - see section 2.4 for further details on human interaction with FDI approaches), in an unsupervised manner (i.e., collecting elements of the database that are close to one another) [39] [40] or in a semi-supervised learning process [41]. A classifier is then trained with respect to these classes to perform the classification of the newly measured variables as representative of a healthy or faulty behavior
- *regression* [42]: it builds a statistical model that uses the redundancy of the process history in order to predict the values of the new variables and generate residuals by comparing predictions to measured values

In a sense, both aim at interpolating the new measured point based on the available data. In other words, the model-free diagnosis is based on the algorithm experience with the system: a mapping of behaviors of the system efficiently associates the observations to the corresponding diagnoses.

However, the first step of the signal-based approach is to provide features that contain information about faults. There exist plenty of approaches to extract features directly from the measurements, some of them in the time domain, some in the frequency domain, some others in the time-frequency domain [6]. Next, all the three methods are reported.

2.3.1 Time-Domain Signal-Based methods

The time-domain methods aims at extracting features from time-domain measurements. These methods are usually employed for continuous dynamical processes. Next, some features are listed, together with reference of the study that generated them:

- on sensors, the covariance of the signals in [43]
- on measured signals, the Dynamic Time Wraping (DTW) and the correlated kurtosis (CK) in [44]
- on electrical motors applications:
  - the Root Mean Square (RMS) of currents in [45]
  - the induction current slope [46]

  - the comparison between measured and reference current signals in [47]
  - the absolute value of the derivative of Park's vector phase angle in [48]
  - the magnitude of the negative and zero-sequence currents in [49]
  - the Crest Factor (CF) of currents in [50]

Also, other features can be employed, for example, in HOLMES project (presented in chapter 4.1), which is the predecessor of the REPRISE project, the following features have been considered:

- Signals ratio: ratio between two measured signals
- Kurtosis of measured signals
- Skewness of measured signals
- Peak-to-valley of measured signals
- Energy operator of measured signals
- Shape factor of measured signals

Next, the frequency-domain methods are reported.

2.3.2 Frequency-Domain Signal-Based methods

The frequency-domain methods aims at extracting features from frequency-domain of the measurements. As before, some features are listed together with reference of the study that employed them:

- on vibrations:
  - the Fourier spectrum in [51]
  - the characteristics of acoustic measurements in [52]
- on electrical motor applications:
  - the Motor Current Signature Analysis (MCSA) in [53] [54]
  - the current-based spectrum in [55] [56]

Also, other features can be employed, for example, in HOLMES project (see chapter 4.1) the following features have been considered:

- Mean frequency of measured signals

- Frequency center of measured signals
- Root Mean Square frequency of measured signals
- Standard deviation frequency of measured signals
- Sixth central moment of measured signals

However, there exists some applications in which both time-domain and frequency-domain signal-based methods fail in their tasks. This could happen because of varying conditions in the system or dynamic behavior of some measured signals [6]. Thus, especially in real-time case studies, a time-frequency-domain Signal-Based method is introduced and presented next.

2.3.3 Time-Frequency-Domain Signal-Based methods

The time-frequency-domain method is used to extract features where the previous methods fail or do not accomplish well. The idea is that the information of the fault is included in nonstationary signals [57], and thus features are extracted from the listed techniques:

- on electrical motor applications: Short-Time Fourier Transform (STFT) in [58]
- Wavelet Transform (WT) in [59]
- Hilbert-Huang Transform (HHT) in [60]
- Wigner-Ville Distribution (WVD) in [61]

However, no matter which method is employed, most of the features obtained may not bring along useful information about the anomalies that the system is facing. Also, some of the extracted features may be linear dependent one from another. For this reason a feature selection phase is needed with the aim of obtaining a dimensionality reduction [62] [63] [64]. To do so, there exist linear and non linear methods. To name some:

- Linear: Principal Component Analysis (PCA) [65]
- Linear: Local Linear Embedding (LLE) [66]
- Nonlinear: Kernel Independent Component Analysis [67]
- Nonlinear: Spectral Clustering [68]

- Nonlinear: Generalized Discriminant Analysis (GDA) [69]

Next, as representative case, the functionality of the PCA is described.

2.3.4 Principal component analysis

The PCA approach is usually used when large amount of information are present and consists in reducing the dimensionality of the set of data by the transformation of measured signals into a new set of variables, named *principal components* [70] [71]. Principal components must be uncorrelated. The idea is to employ orthogonal vectors in the direction where most of the data variation occurs. This leads to the generation of a set of reduced number of variables containing most of the significant information of the system. At this point, after a training process, several approaches can be exploited in order to evaluate the presence of abnormal patterns or to estimate the state of degradation of the system. To name one, PCA can be pursued by clustering based on k-means [72] [73] is a well-known technique that has proved its simplicity and efficacy over the years [74]. In the end, corrected data can even be reconstructed via back-transformation with principal component variances.

Now that the signal-based approach has been investigated, next, knowledge-based approach is described.

2.4 Knowledge-based approach method

The knowledge-based approach (known also as Data-driven approach) relies on both analytical and heuristic knowledge [7] and it is useful when no mathematical models of the system can be obtained (in a model-based approach) or no information in the signals can be extracted (in a signal-based approach). Data driven methods employ only the available measurable signals from the system instead of an input-output model [75]. For this reason, the knowledge-based approach needs a large quantity of historic data, comprising data on faulty states of the system. Having a look at Figure 2.13, it is possible to follow the diagram from the fault occurrence to the fault diagnosis. The fault occurs in the considered process and has an effect on both measured and observed variables. Then, a phase of symptom generation is achieved by means of analytical and heuristic methods in parallel. The analytical symptom generation, that presents similarities to the signal-based method, manipulates the measured variables through data processing based on analytical knowledge on the system via

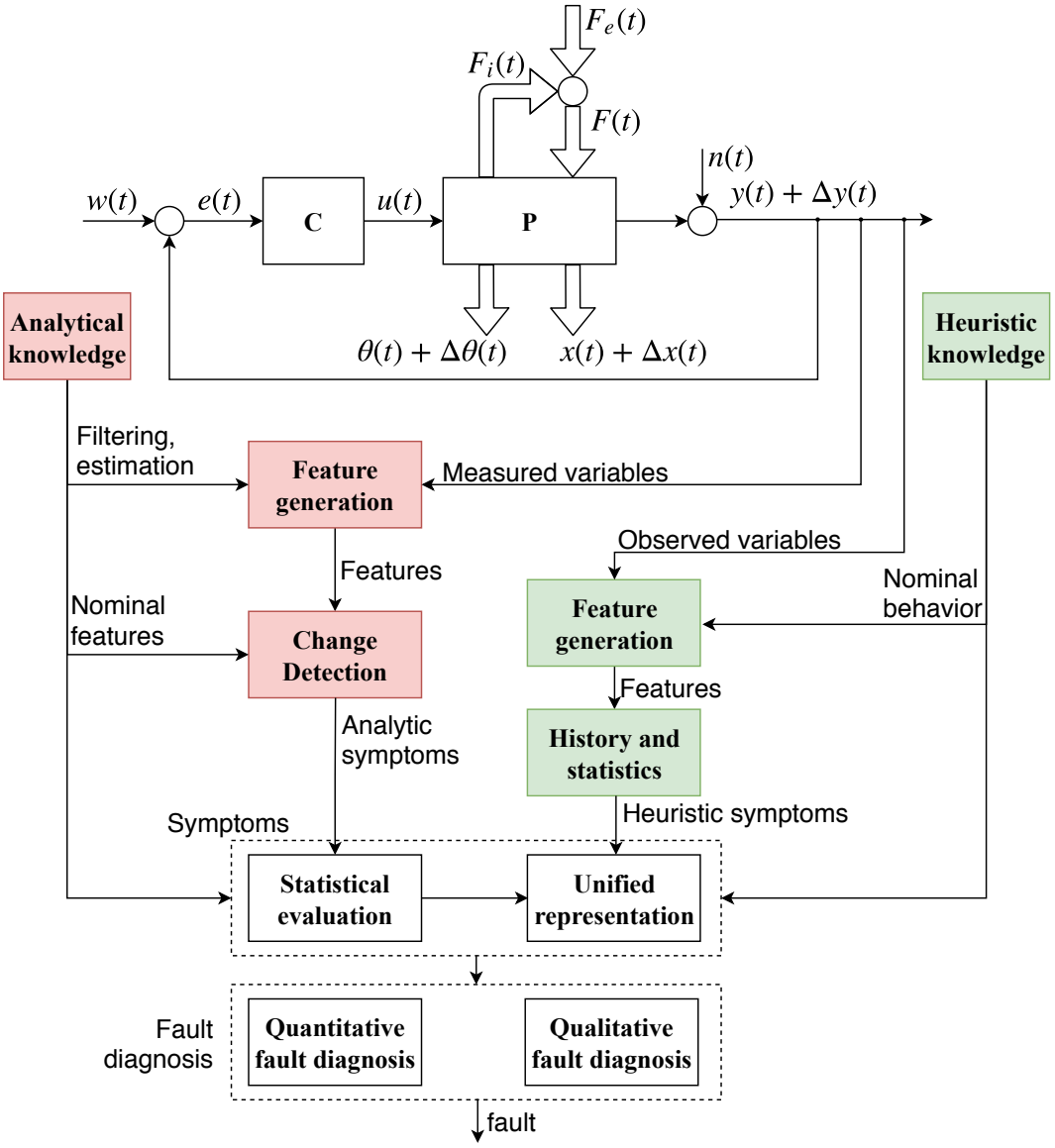

Figure 2.13: Overall scheme of knowledge-based FDI

analytical process model and filtering estimation. The latter, once obtained the characteristic values, is employed during the features extraction. In the end, a change detection with respect to normal system conditions is achieved in order to highlights any symptom. On the other side, in parallel, the first step of the heuristic symptom generation is based on the heuristic operator observations. As well as for the analytical symptom generation, a features extraction is achieved on qualitative information from experience. In the end, process history and statistics lead to the heuristic symptoms generation, considering the fault-symptom causalities and the weighting of symptoms and events. At this point, if analytical and heuristic symptoms are detected, they have to be unified and integrated with all the knowledge of the system in order to reach the fault identification via two approaches [6]:

- qualitative knowledge-based fault diagnosis: inferencing and ruled-based algorithms (the fault decision happens through forward/backward chaining)
- quantitative knowledge-based fault diagnosis: pattern-based algorithms (classification and clustering)

2.4.1 Qualitative fault diagnosis

The most common qualitative fault diagnosis methods relies on expert systems, that are considered a branch of the artificial intelligence, in a human expertise representation structure. The human experience on a system is based on rules, learned from the historic data of human experts on the system, as proposed in [76] and [77]. Usually, such approach is seamlessly deployable through logic reasoning, even under uncertainty. However, considering also the great amount of historic data needed, the implemented solutions are usually hardly expandable and remain specific for the application, with lacking possibilities of being adapting to other applications. An object-oriented approach may help and can be taken as a generalization to the matter, as presented in [78] and [79]. Other qualitative methods rely on the idea that the identified processes from noisy data contain information about the fault trend (Qualitative Trend Analysis [80] [81] [82]).

A similar approach, but based on patterns, is named quantitative fault diagnosis method, as described in the next section.

2.4.2 Quantitative fault diagnosis

The quantitative fault diagnosis methods are based on the same conceptions of the qualitative ones, but employing pattern recognition techniques. Quantitative

information are presented in the form of features, generated via both statistical and non-statistical methods. The statistical approach to this method can rely on several techniques, to name some:

- Principal Component Analysis (PCA) (presented in section 2.3.4)
- Partial Least Squares (PLS)
- Independent Component Analysis (ICA)
- Support Vector Machine (SVM)

The non-statistical methods rely instead to Fuzzy Logic (FL) [21] or Artificial Neutral Network (ANN) [4], that can be:

- Radial Basis Networks
- Recurrent Dynamic Networks
- Self-Organizing-Maps
- Back-Propagation Networks
- Extension Networks

2.5 Hybrid approach method

This chapter has presented a general methodological overview of the most employed FDI techniques. Of course, each of the presented approach, shows advantages and limitations that may be stringent for specific applications. The next section is to compare all pros and cons of each methodology. However, in the last years, some hybrid FDI methods have been implemented. The aim of hybrid approaches is to seamlessly integrate different methodologies in order to benefit from their advantages and prevent their limitations. The hybrid approaches also increase the overall diagnostic capabilities. For example, features can be extracted with multiple approaches and then combined together to increase the entropy, or a model can be identified via both model and signal-based methods. Thus, the hybrid method can be model + signal-based, or model + knowledge-based, etcetera. As example, some applications are referenced next:

- hybrid signal + knowledge-based in [83] [84] [85] and on electrical motor in [86]

- hybrid model + knowledge-based in [87]
- hybrid model + signal-based in [88]

2.6 Comparison and conclusive overview

The previous sections presented the state of the art of the most used FDI techniques with details on implementation, advantages and peculiarities of each approach. Just as a remind, this thesis focused on those cases where no additional HW should be employed for FDI purposes However, the addition of external HW may rely on the safety level required or may be dictated by the necessity to measure signals that cannot be estimated otherwise. In some cases, it is possible to employ signal-based approaches which are able to estimate unknown variables. In some others, if the system dynamic is known, model-based approaches could help in this sense.

Sometimes the choice of the method to employ is dictated by some physical or data requirements or limitations. However, in some cases, it is possible to achieve different FDI techniques and it may be not easy to establish which one will be more effective. Depending on the monitored system and on the specification of the application, one approach may be better than others. Based on [89] and following the author's analysis, a comparative summary has been reported in Table 2.1. The columns display the approaches that have been presented previously:

- Model-based parity equations approach
- Model-based state/output estimation approach
- Model-based parameter estimation approach
- Signal-based approach
- Knowledge-based approach

In this table some assumptions are made, following the idea of a general methodological approach to the matter. First, the grade of knowledge of the system structure is taken into account: of course, M.B. approaches necessitate a good awareness of the system processes and physics, while K.B and S.B. approaches operate without a priori knowledge. Although, K.B. approach strongly relies on historical data and S.B. approach necessitates a set of data of the system during

Table 2.1: Comparative summary of FDI approaches

Assumption	**M.B. par. eq.**	**M.B. st./outp. estim.**	**M.B. param. estim.**	**S.B.**	**K.B.**
Model structure	Exactly known	Exactly known	Partially known	Not known	Heuristically known
Historical data necessity	Smaller	Smaller	Smaller	Larger	Medium
Computational effort	Smaller	Medium	Larger	Maximum	Maximum
Noise rejection	Very small	Very small	Medium	Good	Maximum
Incipient fault detection	Not suitable	Fairly suitable	Very suitable	Fairly suitable	Very suitable
Abrupt fault detection	Very suitable	Very suitable	Fairly suitable	Very suitable	Very suitable

the nominal healthy operation condition. Instead, M.B. methods do not rely on historical data. Also for this reason, M.B. approaches imply a minor computational effort with respect to the others. However, observers in M.B. methods may slow the operations. The noise rejection depends on several factors, however it is possible to generalize and affirm that K.B. and S.B. approaches perform better in presence of disturbances and noise. In the end, the ability of detecting two different types of fault is considered. Incipient faults (including slowly devloping faults) are better detected by S.B. and M.B. via parameter estimation approaches, while are not easily detected by M.B via parity equations. Abrupt faults (including both permanent and intermittent faults) are of course less complicated to detect by all approaches, however M.B. via parameter estimation could be significantly slower.

In the end, after the previous considerations, a general methodological approach is proposed by the author, comparing the type of background knowledge on the system, on the type of eventual fault and on other parameters, in Figure 2.14. The aim is to help the reader exploring the best approach to employ for a specific case study.

The first aspect to take into account is the grade of knowledge of the structure and the physics of the system. If nothing is known about the system, then the choice is redirected only on the signal and knowledge-base approaches, depending on the amount of historical data (both analytical and heuristic) available. If, instead, the structure and the physics of the system is exactly or partially known,

then other aspects may be important in the decision of the method to employ. Of course, signal and knowledge-base approaches may be employed simply neglecting the knowledge over the system structure, however, they are usually less robust than model-based methods, especially when noise is present or parameters change (as in the case of the parameter estimation approach). Model-based methods are usually more complex to implement and their performances depend on the accuracy of the model. However, when the model is implemented, they can rely on small computational efforts (as in the case of parity equations). In the end, model-based methods can employ the state and output estimation with moderate computational effort and perform well when the process is non-static.

To conclude, it is worth remembering that more and more often, different methodologies are employed together in the previously presented hybrid approach form. Also, the final choice of the technique to employ, beyond the limitation of the system and the measured variables, depends on the final aim of the case study. In fact, as described in section 2.1, there exist some differences between the mere fault detection and the sequent phase of fault isolation and health monitoring tasks.

2.6.1 Considerations on HM and CA tasks

This chapter has given an exhaustive overview on fault detection and isolation methods. Furthermore, information can be continuously obtained by a system, also in real-time. The continuous monitoring of the health of a system by means of FDI methods could lead to highlight a gradual deterioration of performances. This task is called Condition Assessment (CA) (see chapter 1). The idea is that symptoms and faults can develop gradually and systematically, so that a correspondence between the grade of severity and the direct or indirect effect on the system variables can be found. CA techniques can be useful in those environment where the safety is a must or in those application in which a frequent maintenance is scheduled. For example, in the aerospace environment, great attention is naturally given to the health condition of the system and all of its components. The employment of a HM supervision system by means of CA techniques brings along significant advantages in terms of safety and maintenance costs savings. For example, this is the case of Electro-Mechanical Actuators (EMAs) [90].

The next two chapters are to present an overview of FDI approaches, with attention to CA techniques, in the aerospace environment (chapter 3) and specifically on EMAs (chapter 4).

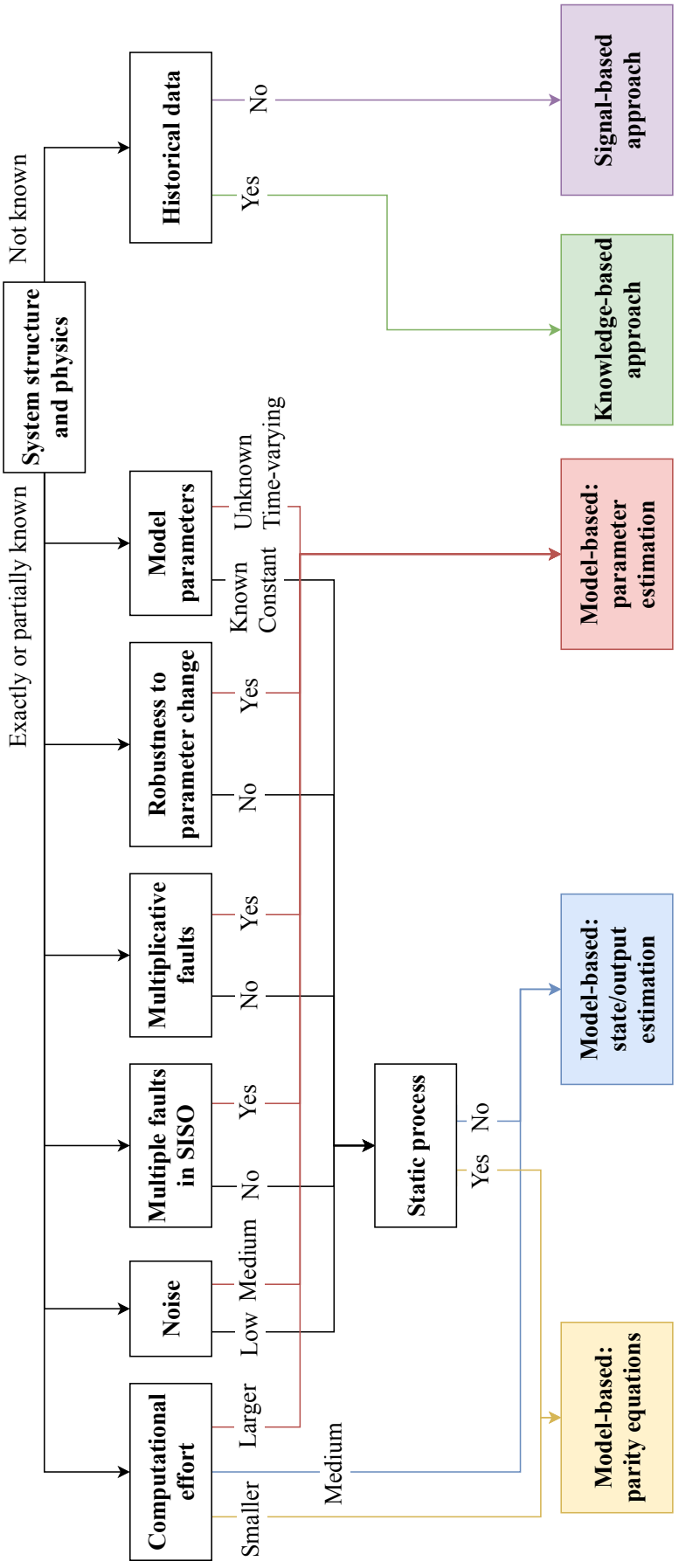

Figure 2.14: Methodological FDI flowchart

CHAPTER 3

FDI in aerospace environment

Methods to perform risk and reliability assessment originated in US aerospace and missile programs in the early 1960s [91]. Early in the Apollo project the question was asked about the probability of successfully sending astronauts to the moon and returning them safely to Earth: the risk (or reliability) calculation result was a mission success probability that was unacceptably low. Despite such result, history was made and NASA successfully accomplished important space missions: at that time, further quantitative risk or reliability analysis was discouraged. No trust was given to the topic of Health Monitoring (HM) until the Challenger accident occurred in 1986. Therefore, NASA decided to rely on the use of methods for system safety assessments. Several methods for system safety assessment were developed, specifically for the aerospace environment. To name some, Failure Modes and Effects Critical Analysis (FMECA) [92] [93] and Probabilistic Risk Assessment (PRA) [94], Fault Tree Analysis (FTA) [95] in systems risk and reliability became key topics and approaches in aerospace fault diagnosis around 1980. An analysis of such methods in aerospace environment can be found in [96] [97] [2] and are briefly presented in the next sections.

3.1 FMECA

The FMECA is a bottom-up technique used to prioritize and identify potential failures based on experience with similar products and processes or on common physics of failure logic. The FMECA has the aim to identify all the applicable

failure modes and analyze them in term of their effect, their Severity and Criticality. Its operation is to develop a ranked list of potential failure modes, establishing a priority system for corrective action considerations. The provided FMECA can also give an evidence of the effectiveness of the monitoring system with respect to the analyzed failures.

The FMECA procedure is divided into three phases:

1. identification of possible failures

2. analysis of the probability of failure along with its consequences, calculus of the Risk Priority Number (RPN) (see next section)

3. elimination of the occurrence (or at least reduction of consequences severity)

Point two includes further details on Probability, Severity, Detectability indexes and the calculus of the RPN number.

3.1.1 Risk priority number

As introduced, a phase of the FMECA consists of the calculus of the RPN number, which is obtained by the following three factors:

P The probability of an occurrence of an event can be predicted on the documented past experience along with physical considerations. A failure cause is looked upon as a design weakness: all the potential causes for a failure mode should be identified and documented.

S The severity of an occurrence is strongly related to the safety of the whole system (or part of it). Generally, the worst-case scenario evaluating a failure is taken into account

D The detectability of a failure comprehends the method by which a failure is detected, isolated and the time it may take.

To each of these indexes a factor is assigned.

The risk priority number is the product of the indexes:

$$RPN = P \cdot S \cdot D \tag{3.1}$$

However, this number is useful in case of improving actions over the system, in order to identify components whit higher priorities. An example of FMECA result can be found in section 4.1.

FMECA and FTA present some differences in their approaches [91]:

- FMEA, is an inductive, bottom-up analysis method aimed at analyzing the effects of single component or function failures on equipment or subsystems; FTA, instead, is a deductive, top-down method aimed at analyzing the effects of initiating faults and events on a complex system
- while FMECA is intended at finding all the possible initiating faults, FTA is very good at showing how resistant a system is to such single or multiple initiating faults
- while FMECA is good at exhaustively cataloging initiating faults and identifying their local effects, it is not good at examining multiple failures or their effects at a system level as FTA
- FMEA does not consider external events, while FCA does

The Fault Tree Analysis (FTA) could take into account the results of the FMECA analysis. This is presented in the next section.

3.2 FTA

FTA is a top-down failure-based deductive approach. It is an analytical technique, whereby an undesired state of the system is specified (usually a state that is critical from a safety or reliability standpoint), and then determines (deduces) its causes using a systematic backward-stepping process, in order to find all realistic ways in which the undesired event can occur. In determining the causes, a Fault Tree (FT) is constructed as a logical illustration (and model) of the various parallel and sequential combinations of faults that will result in the occurrence of the predefined undesired event (top event). The faults can be events that are associated with component hardware failures, human errors, software errors, or any other pertinent events which can lead to the undesired event. A fault tree is not a model of all possible system failures or all possible causes for system failure, but instead, it is tailored to its top event, and thus includes only those faults that contribute to this top event. The considered faults are not exhaustive, they cover only those that are assessed to be realistic by the analysts. The data flow in a FT is regulated by Logic Gates representing the status of a part and/or other factor being included in the analysis, such things as training, tools, safety equipment, supervision etc (see Figure 3.1).

FTA can be applied to both an existing system and to a system that is being designed. When it is applied to a system being designed for which specific

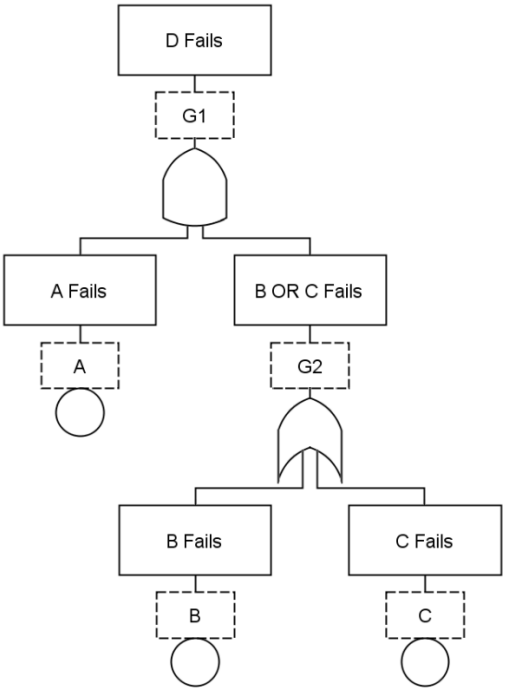

Figure 3.1: Example of simplified fault tree

data do not exist, it can provide an estimate of the failure probability and the important contributors using generic data to bracket the design components or concepts. Also, it may be used as an important element in the development of a performance-based design. When applied to an existing system, FTA can be used to identify weaknesses and to evaluate possible upgrades. In the end, it can also be used to monitor and predict behavior, as in this project interest. In fact, FTA provides critical information that can be used to prioritize the importance of the contributors to the undesired event. The contributor importances provided vividly show the causes that are dominant and that should be the focus of any safety or reliability activity.

The FTA procedure is described:

1. assume a system state and identify and clearly document the top level undesired events
2. develop the upper levels of the trees via a top down process
3. continue the top down process until the root causes for each branch is identified and/or until further decomposition is not considered necessary
4. assign probabilities of failure to the lowest level event in each branch of the tree

5. establish a Boolean equation for the tree and evaluate the probability of the undesired top level event

6. compare to the system level requirement

The calculation of risk likelihood originated from equipment failure during its mission is performed with the following formula:

$$Q_Y = 1 - R(t) = 1 - e^{-\lambda_O \cdot t} \tag{3.2}$$

where t is the operation time and λ_O is the operative failure rate.

All the procedures described in this chapter have been employed in the this thesis project and in a past project as well. The following chapter considers aerospace applications related to Electro-mechanical Actuators (EMA) diagnosis and condition assessment, presenting also some results of FMECA an FTA on an EMA prototype.

CHAPTER 4

FDI on EMAs

Even though there is a strong economic motivation for the addition of HM in aeronautical actuators and even though it has gained interest within the last decades [98], its development is still in the early stages, also due to the fact that there is a lack of knowledge, especially about EMAs [99]. In order to develop HM algorithms on EMAs, information on the behavior of the actuators in case of incipient faults must be known. In particular, this work focuses on the mechanical transmission components of and EMA (bearings) and does not take into account eventual faults regarding the electronic elements and sensors of the actuator. Similarly, this chapter gives attention to such types of faults. Thus, experimental tests have to be achieved in different conditions:

- healthy condition
- single fault condition (one fault at each time)
- multiple fault condition (more than one fault together)

This implies an extensive experimental effort. Experimental activities, conducted in [100], indicate that is very difficult to identify a failure precursor for all of the components and failures tested. Although the good repeatability observed in the test program, an adequate coverage of high probability failures may lead to unreasonable sensor requirements.

Moreover, it is necessary to take into account that an amount of incipient faults greater than the considerable ones can occur. For this reasons, a phase of

simulation can be helpful for the early detection and identification of eventual faults through the development of a model of the actuator and its transmission. There exist applications in which an EMA model has been carried out and via simulations a health monitoring system has been developed, as in [101], in which a Kalman filter has been included and therefore a combination of signal filtering and frequency analysis has been achieved. In [102] a model-based approach to prognostics and health management was developed and validated for actuator fault detection and failure progression. Such a system was able to successfully simulate the actual operation of the EMA but for limited given failure modes. Similar approaches are used in [103] for the health monitoring of the EMA motor and bearings. In [104] the authors approach the health monitoring for bearing and screws. With regards of bearings, main failures are lubrication fault (no lubricating grease or degraded grease), race or ball/roller mechanical jam and an overloading failure. The analyzed solution is based on accelerometers and the detection of the failure results easy and robust. The fault diagnosis method is implemented using short Fourier transform. Relative to screw/nut assembly, the mechanical jam due to severe heating of components over the operation ranges defined by the supplier is the typical event. The temperature increment could be produced by lubrication failure, recirculating jam of rotating elements, degradation of races / rolling element surfaces due to wear. In this study, both direct (accelerometers, thermocouples, position, sensors) and indirect (current sensors) measurements have been used. The lubrication and recirculation jam failures appear as a sudden increment of the friction torque (detected with the current); meanwhile the fatigue failure appears as a gradual increment of the backlash (detected comparing the input position with the lineal position).

Also, there exists methods to predict the remaining useful life (RUL) of single components of the EMAs. For example, a nonlinear model is built together with an extended Kalman filter for RUL prediction of bearings, depending on their degradation, in [105]. A similar study has been introduced also during the Health On Line Monitoring for Electromechanical actuator (HOLMES) project, in which a Particle filter has been tested on a nonlinear model of the system, as described in the next section.

4.1 HOLMES project

Recently, the HOLMES project, involving the author and some of her colleagues in the Control and Automation Laboratory of University of Study of Bergamo, has

Table 4.1: Failure Mode Effect Summary of EMA

End effect	**Failure per milion hours [fmph]**
Actuator jam	$3.647 \cdot 10^{-2}$
Actuator runaway	$6.000 \cdot 10^{-6}$
False Alarm Signal	$7.859 \cdot 10^{-2}$
Loss of actuator	6.152
Loss of capability to engage the static brake	$3.664 \cdot 10^{-1}$
Loss of service communication	$5.748 \cdot 10^{-2}$
No Functional Effect	$1.039 \cdot 10^{1}$
No functional effect. The failure could become critical in presence of other failures	$1.777 \cdot 10^{-1}$
No significant effect	$4.366 \cdot 10^{-2}$
Possible loss of actuator	$1.550 \cdot 10^{-4}$
Static brake always engaged	$6.660 \cdot 10^{-2}$

started a deep analysis of the possible failure reasons based on massive experimental activity which aimed to evaluate both different electro-mechanical configurations and different approaches for HM [106] [107]. The fault analysis was focused on mechanical faults with the aim of detecting them by means of measurements available on the system without additional sensors. More specifically, the HOLMES project, which is the predecessor of the REPRISE project, was focused on the study of eventual EMA faults and symptoms that may be evidenced.

Also, Fault Tree Analysis (FTA) and a Fault Mode Effect Criticality Analysis (FMECA) have been performed. Thanks to the analysis the failure modes for each component have been identified and have been classified depending on their effect on the system operation. Thanks also to the knowledge developed during HOLMES project, the FMECA during the REPRISE project has produced the results reported in Table 4.1. According to the FMECA analysis, there are no failure "NOT detectable" within the ones taken into account in the FTA. For each FTA basic event, that represents a specific component failure mode, the relevant failure mode rate (expressed in fpmh) has been used, in accordance with FMECA.

Based on this analysis, faults have been injected by artificially damaging the actuator components, e.g. ball spalling, teeth cracking etc. A large and intensive experimental activity has produced data collected on the system in healthy and faulty conditions. New algorithms for fault diagnosis have been designed and tested. The results of the project were strongly encouraging and showed a clear track for the definition of a stable and robust health monitoring system. However, some issues are still open. Among these, one of the most important is the concept

of "minimum detectable fault", e.g. which is the minimum fault that causes a change of behavior of the system that cannot be rapidly detected, since the closed loop control system is compensating (and hiding) the effects. A second important issue is the estimation of the RUL, that cannot be easily computed without bringing to failure and collapse the components.

4.2 Conclusions

The research in the development of health monitoring systems for EMAs for airplanes is in progress and a definitive solution to this issue has not yet been identified. Due to the highly stochastic environment and to the complexity of this issue, the theme of the health monitoring is still open and field of improvements. In particular, there are very few activities based on experimental activity and none of them considers bringing the actuators to a complete failure.

Recent studies [108] report that existing current and position/speed sensors equipping aerospace EMA are a promising tool for health monitoring of electromechanical actuators based on screw systems. It is also evident that additional sensor for acceleration/vibration and temperature mapping of the actuator are a recognized instrument to tune the approach of fault diagnosis, even in a model-free method, in which, by definition, the complete insight of the physical aspects of the degradation of the system is not strictly needed. Based on the experience of the HOLMES project, it is known that fault diagnosis can rely on sensors and components that are standard equipment on an EMA, like electric motors sensors, motor commutation devices etc. Therefore, the reliability and safety of the EMA will be improved without any penalty in terms of weight and envelope.

As the basic rationale of the REPRISE project, the idea for future HM development on EMAs is the simplification of the hardware measurement layout, moving complexity in the software and algorithm design.

Part II

Experimental setup

During the development of the REPRISE project, a continuous and intensive experimental activity has been carried out in order to obtain data, that were collected from a dedicated test rig. The purpose of the experimental activity was to bring an aeronautical EMA prototype from its healthy nominal condition to a gradual progressive deterioration of the mechanical parts through a continuous operation, acquiring as much information as possible during its degradation.

CHAPTER 5

Test rig

Small transport aircrafts entrust the management of the flight control to few surfaces. Some surfaces are cataloged as the ones for the primary flight control (in blue in Figure 5.1), while others are slats and flaps (in orange in Figure 5.1).

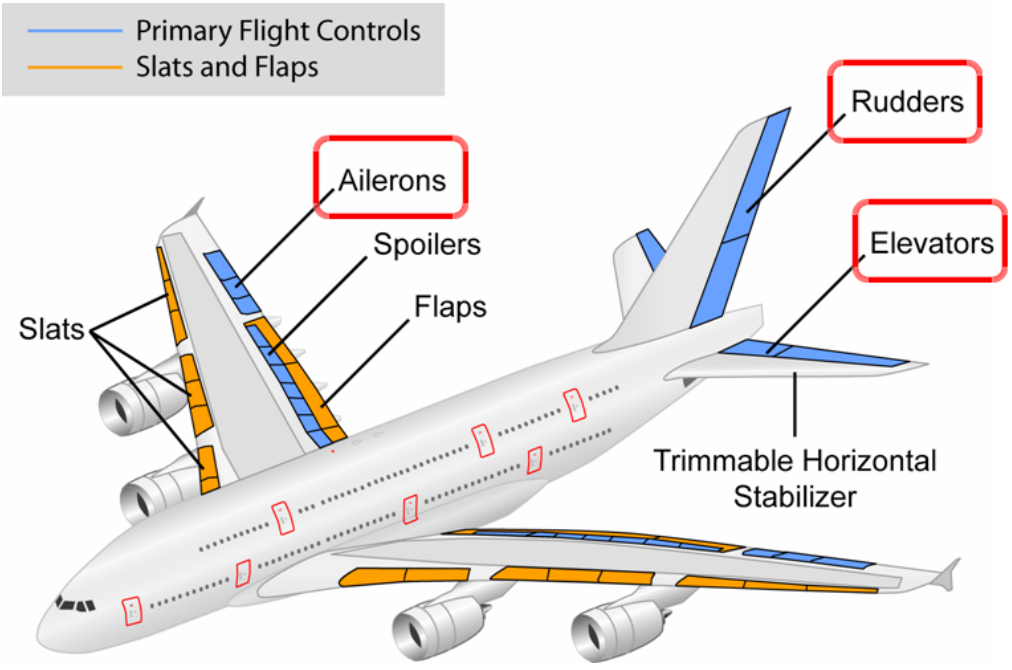

Figure 5.1: Flight surfaces of a small transport aircraft

This project focuses in particular on three primary flight control surfaces that are:

- Ailerons
- Rudders
- Elevators

Such surfaces serve for the control of the airplane, especially during take off and landing procedures. It is easy to imagine that such surfaces are subjected to a non negligible aerodynamic counteracting force.

For this reason and because of the lack of knowledge regarding aerospace EMAs (as stated in chapter 4), a test rig has been designed and built to test the EMA prototype. Next, the test bench is presented in terms of mechanical, electronic systems and control architecture. The front view illustration of the test rig is shown in Figure 5.2.

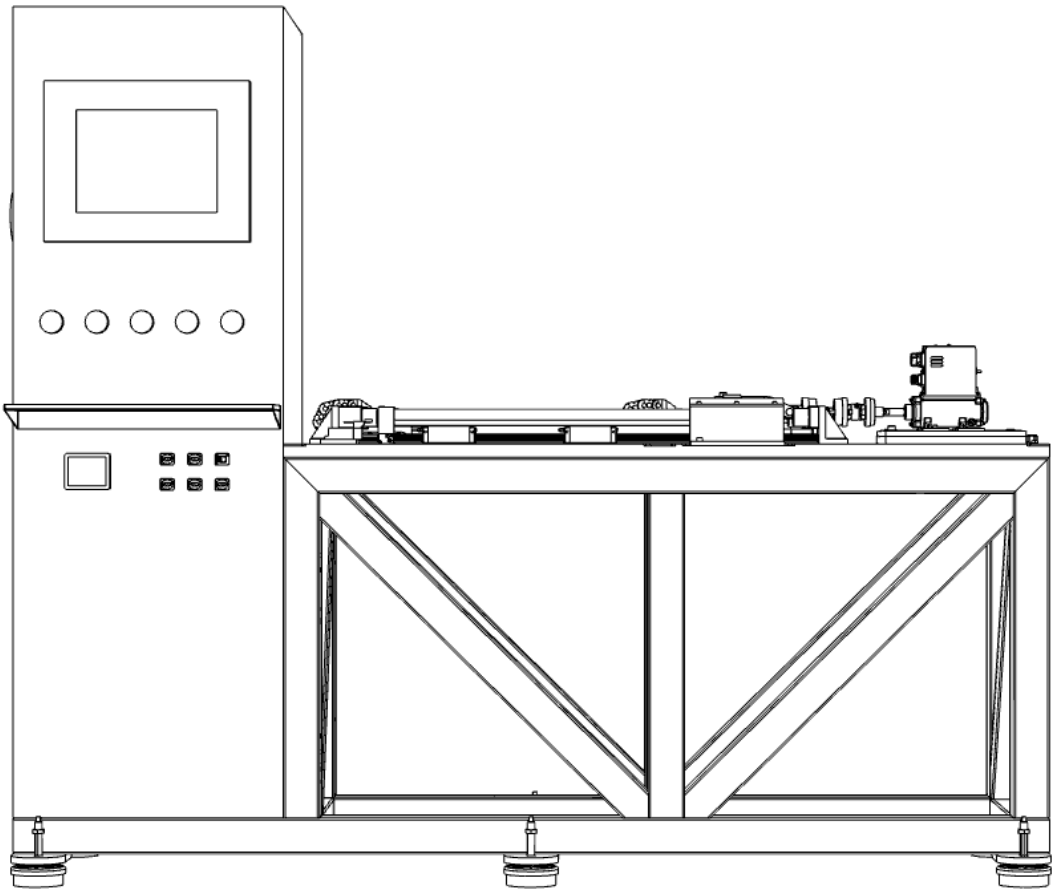

Figure 5.2: Front view illustration of the test rig

All the tests are devoted to the analysis of the EMA prototype which realizes the imposed kinematic profile of aerodynamic surfaces, e.g. airplanes flaps. The

load force, simulating the resistance that the surfaces might encounter during flight, is generated by a electric linear motor. The EMA, with a ballscrew transmission, is connected to the linear motor via a rigid joint. More in details, the supplied bench system, as depicted in Figure 5.3, is composed of three main components:

- an EMA prototype (in red) with ballscrew transmission, the actuation system
- a linear motor (in green), opposed to the EMA, for the simulation of the load resistance
- a control panel (in gray), for the control and synchronization of the parts, that acts also as user interface

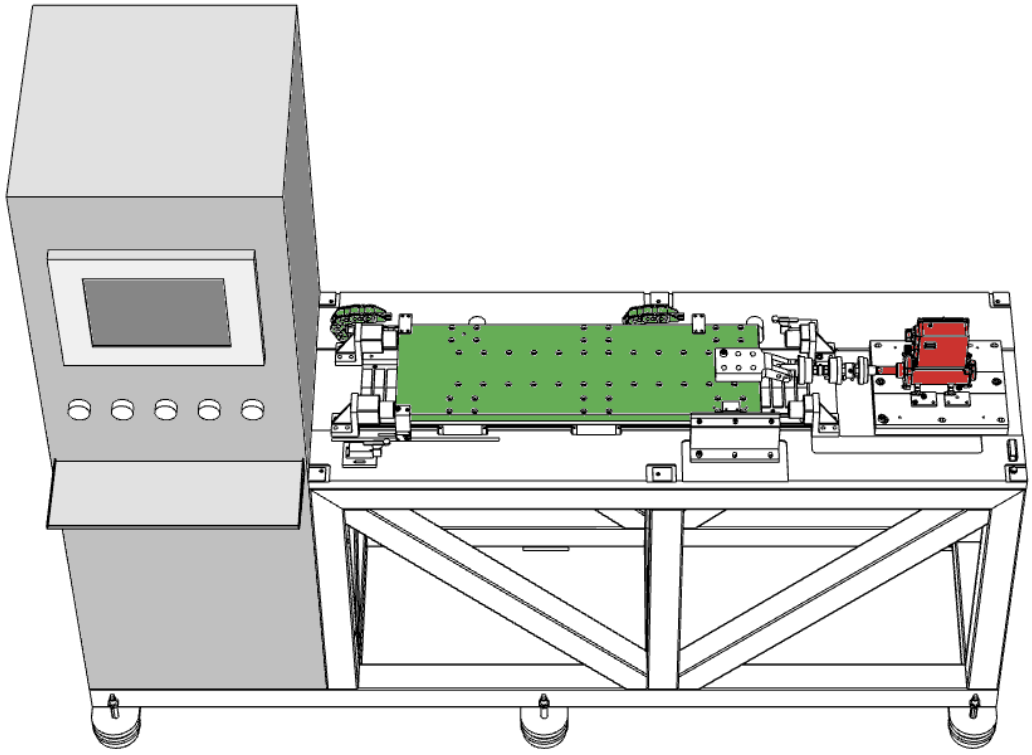

Figure 5.3: Front-up view of the test rig

The responsibility of the motion is thus given to the EMA and the linear motor. Referring to Figure 5.4, in which the test area is shown without the control panel, the EMA (in red) is anchored to the test bench and actuates the kinematic profile imposed by controller, encountering the resistance of the linear motor (in green). The latter moves forward and backward, maintaining a certain load profile reference as demanded by the controller, with the feedback of a load cell (in blue)

positioned between the EMA ballscrew and the linear motor itself. The EMA has an internal position sensor, however, on the linear motor, a linear absolute encoder is mounted (in yellow).

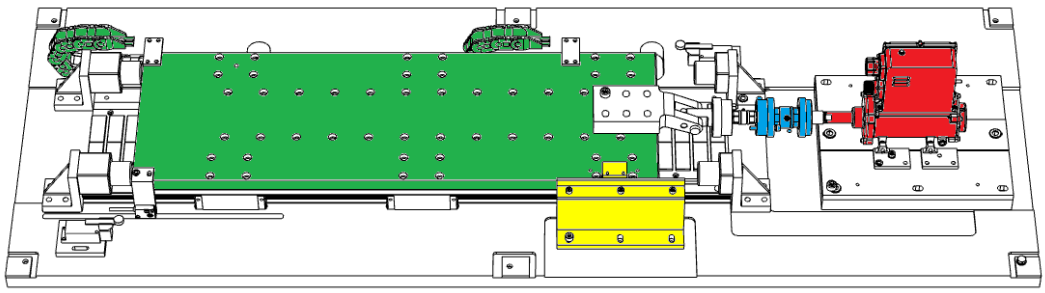

Figure 5.4: Front-up view illustration of the test area with higlighted components

The next sections are to describe all the test rig components and the measurement system in details.

5.1 Electro-Mechanical Actuator

The part of most interest of the bench system is embodied by the EMA, highlighted in red in Figure 5.4. A detail of the EMA is depicted in Figure 5.5.

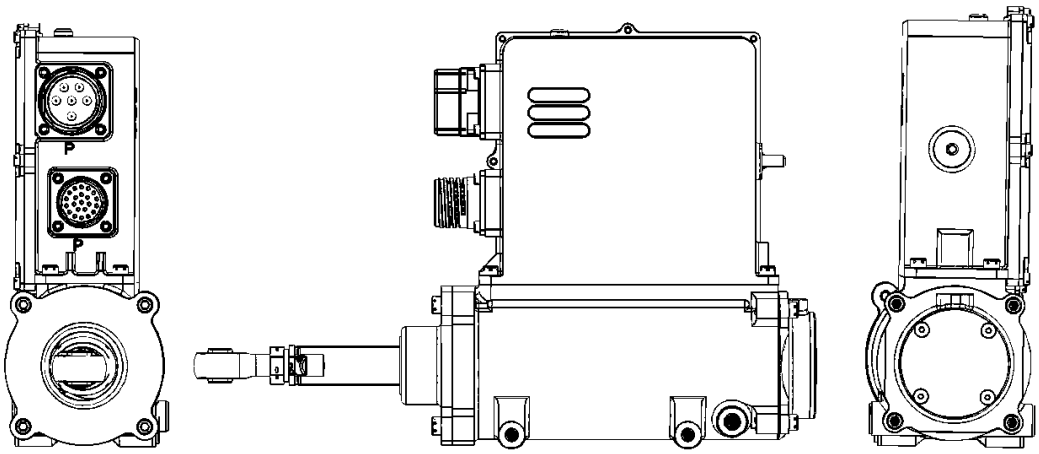

Figure 5.5: EMA illustration: multiple sides

The system therefore consists of a Mechanical Actuator (MA) with an incorporated Electrical Control Unit (ECU). Installing requirements have led to the choice of a compact design, with the ECU directly assembled on MA housing,

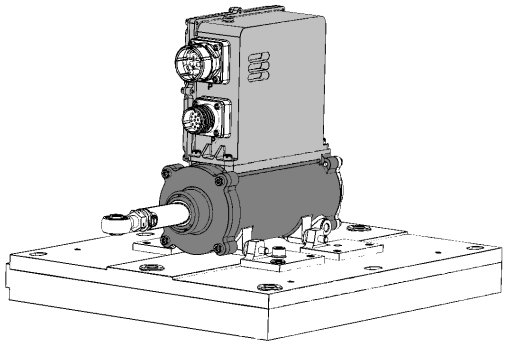

Figure 5.6: EMA detail

as visible in Figure 5.6, in which it is possible to distinguish the actuator (in dark gray) from the ECU (in light gray).

The ECU is dedicated to the control of the actuator and runs the control software. The EMA, instead, is composed of several parts, which are designed as follows:

1. Ballscrew design (see section 5.1.1)
2. Motor design:
    - three-phase brushless DC motor
    - phase commutation provided by three Hall Effect Sensor elements
    - motor stator + housing sub-assy: use of epoxy resin for better thermal performances
3. Integration:
    - permanent magnets directly assembled on ballnut outer surface
    - angular contact bearing inner rings directly machined on ballnut outer surface
    - elliptical anti-rotation directly machined on screwshaft rod
    - simplex LVDT totally inside the screwshaft (see section 5.4 for details)
    - Hall Effect Sensor elements embedded in the stator winding
4. Bearings:
    - isostatic arrangement; no preload change due to temperature variations
5. Electro-mechanical brake design:

- teeth design
- power-on type: with no current/voltage applied to the brake (normal operating condition), the rotating teethed flange is free to rotate; with current/voltage applied (fail-safe condition) the magnetic field of the solenoid attracts the teethed flange, overcoming the elastic force of the spring, causing the engage of the teeth on the brake housing and locking the ballnut, hence no linear actuation is allowed
- continuous service thermal design for solenoid
- optimized spring geometry for force vs. stroke characteristic

Next, the ballscrew will be presented in details.

5.1.1 Ballscrew

The ballscrew is the component responsible of the transformation of the rotational motion generated by the EMA into a linear motion, allowing the movimentation of the linear motor backward and forward. In Figure 5.7, a picture of a sectioned ballscrew is shown, with detail on the recirculating balls.

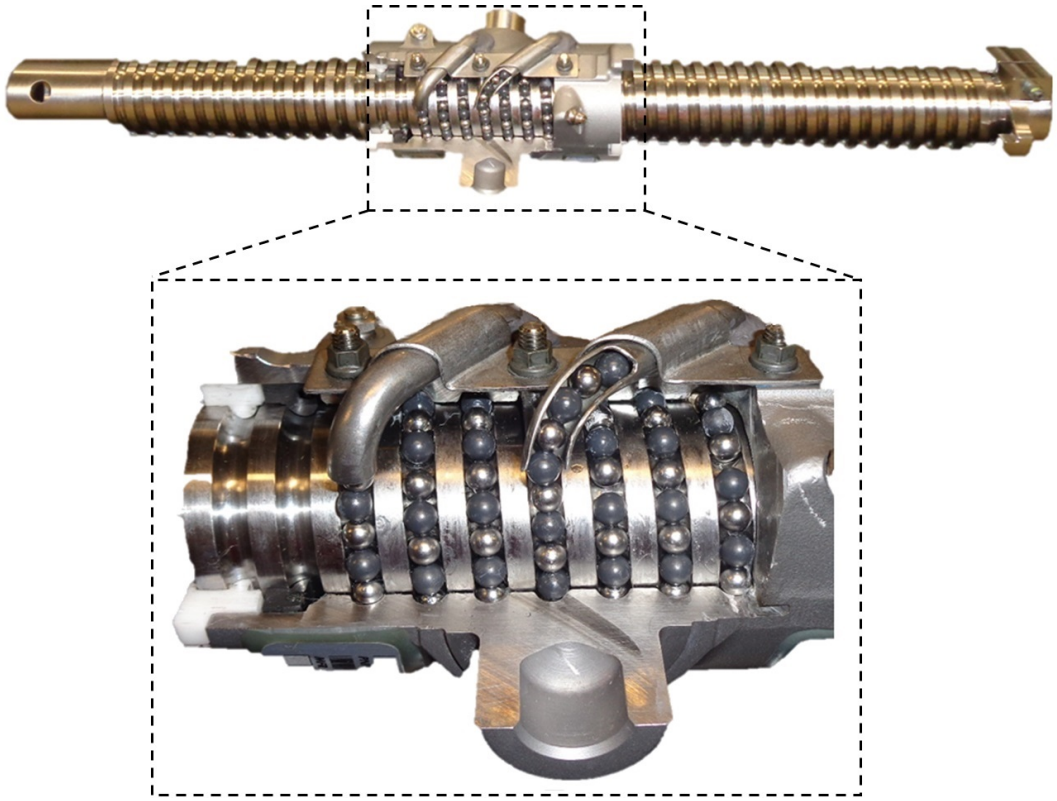

Figure 5.7: Ballscrew detail

The ballscrew is designed as follows:

- rotating nut – translating screwshaft
- recirculation is provided by suitable paths on the screwshaft itself
- standard ball configuration: all steel balls carrying the loads (configuration led by high load conditions)
- 8 turns

A lubricant is present in the recirculation and is responsible of the healthy functioning of the ballscrew.

5.2 Linear motor

The part of responsible of the simulation of the load force includes a linear motor Parker model *Ironcore R16-3A-HS* (highlighted in green Figure 5.4 and showed in Figure 5.8), which is controlled in force through the servo drive Parker model *Compax3*. The linear motor is capable of delivering a constant load of 2230N and

Figure 5.8: Linear motor Parker Ironcore R16-3A-HS

a peak (for time $<$ 5s) of approximately 7400N. Nevertheless, with associated drive, the linear motor is able to deliver a peak force of about 4100N.

The piezoelectric load cell, described in the following section 5.4.1, returns the load feedback to the S100V2 drive, allowing to control the operation of the linear motor through the force loop.

5.3 Test bench supervision system

The *NI CompactRIO 9030* controller that is installed on the bench includes the NI Real-Time Linux operating system OS. This allows the implementation of a local Human Machine Interface (HMI) to simplify application development. Therefore a Host PC is not needed to operate the software. In Figure 5.9, the software

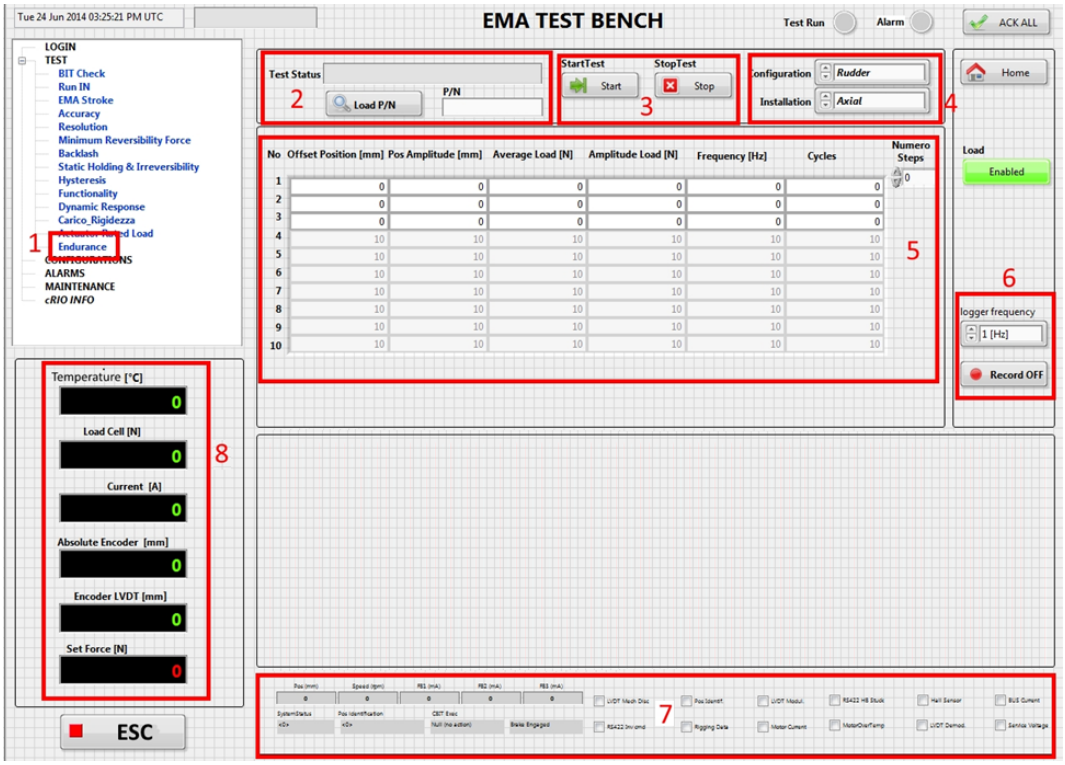

Figure 5.9: Human Machine Interface

interface is shown and the following sections can be identified:

1. Test type selection (in the figure the endurance one is highlighted)
2. EMA Part Number field and test status display
3. Test start and stop buttons
4. Selection of the test configuration in reference to the EMA (Rudder, Aileron and Elevator) and type of load to be applied (axial/radial)

5. Test parameters:
    - EMA offset from zero position
    - EMA amplitude in case of oscillating movement
    - Average load applied to the EMA
    - Load amplitude in function of EMA displacement
    - Movement frequency
    - Cycles to be performed
6. Selection of the data acquisition frequency and button for starting the saving
7. Main parameters detected via BUS RS-422
8. Real time display of the following variables:
    - Temperature measured within the EMA containment box
    - Load applied to the actuator (load cell)
    - Current supplied to EMA
    - EMA linear position (optical encoder)
    - Set-point force commanded to the linear motor

Concerning the test bench control, all the commands and signals are elaborated by a programmable controller National Instruments model *CompactRIO 9030* that is a 4-slot controller with 1.33 GHz Intel Atom dual-core processor, a Xilinx Kintex-7 FPGA, and four slots for C Series I/O modules. A LabVIEW software has been created, debugged, and deployed on the onboard FPGA and on the processor in which the NI Linux Real-Time OS runs. The controller is provided with following I/O modules:

- A National Instruments NI 9203 C Series DAQ module with 8 analog current input channels, +/-20mA, 16-Bit, 200kS/s; this module is foreseen to acquire the following variables:
    - Linear actuator feedback load
    - Temperature measured within the EMA containment box
    - Current supplied to EMA
- A National Instruments NI 9263 4-channel analog output module, with 100kS/s simultaneously updating and ±10V output range, 16-bit resolution. The following signals are generated with this module:

  - Set-point force commanded to the linear motor
  - EMA position reference

- A National Instruments NI-9375 digital input and digital output module. It is equipped with 16-channel, 7μs sinking digital inputs and 16-channel, 500μs sourcing digital outputs. This module is employed for the test rig automation process
- A SEA 9521 BiSS Interface Module with 3 BiSS interfaces used to connect the absolute digital position encoder to the National Instruments CompactRIO system

Moreover, there are other measurements that can be externally acquired. For this reason, an external measurement system has been provided for such acquisitions, as described in the next section.

5.4 Measures acquisition system

As stated, there are measures other than the ones already acquired by the control unit that can be observed. For this reason a *National Instruments cDAQ-9188*, CompactDAQ chassis (8 Slot ENET), equipped with:

- NI 9203 Screw Term, +/-20mA, 16-Bit, 200kS/s, 8-Ch AI module
- NI 9215 Screw Term, +/-10V, 16-Bit, 100kS/s/ch, 4-Ch AI module
- NI 9401 Digital I/O TTL 8 channels, 100ns module

has been employed as well.

Figure 5.10 shows a sketch of the measurement chain of all acquired measures. The signals directly managed by the test bench control system are shown in green, whereas the variables acquired through the external acquisition system are in red.

Variables acquired directly from the test rig are listed hereunder:

1. EMA linear position (optical encoder)
2. Load applied to the actuator (load cell)
3. EMA position reference
4. Linear motor load reference

The external acquisition system allows the acquisition of the following signals:

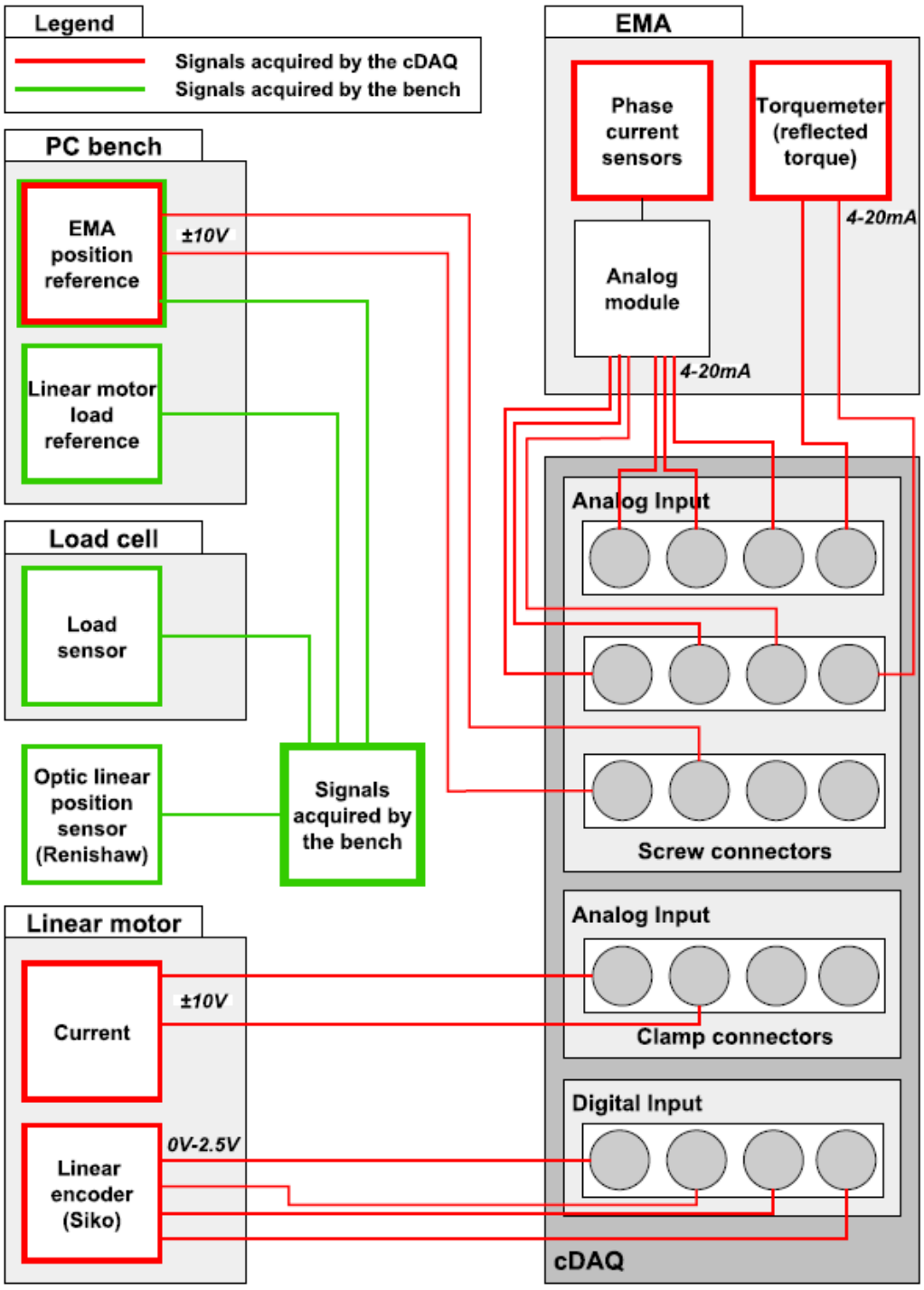

Figure 5.10: External acquisition system

1. Linear motor current
2. Linear motor position
3. EMA position reference
4. EMA motor phase currents
5. EMA reflected torque (when applicable, see chapter 6)

The EMA position reference measure is acquired twice from both acquisition systems in order to synchronize the measurements. However, a trigger was provided for a perfect synchronization.

Some measures are also the feedback of some control loops, e.g. the load cell, described in the next section, provides the feedback to the linear motor.

5.4.1 Load cell

A piezoelectric load cell *Kistler 9321BU* (highlighted in blue in Figure 5.4 and shown in Figure 5.11) is used to measure tensile and compression forces. It has

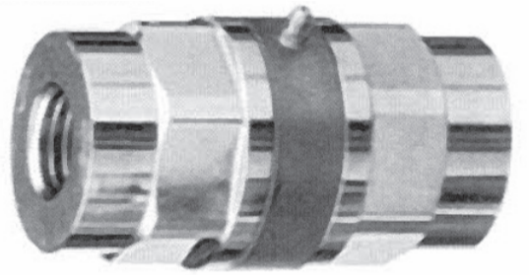

Figure 5.11: Load cell

a high rigidity and thus a high natural frequency. The high resolution allows to measure low dynamical changes of large forces. As a result of its great rigidity, the load cell is particularly suitable both for the measure of rapid changing tensile and compression forces and also quasi-static forces

5.4.2 Linear encoder

An absolute linear optical encoder *Renishaw Resolute Biss* (highlighted in yellow in Figure 5.4 and shown in Figure 5.12) is foreseen to externally measure the EMA position and installed on the linear motor side on the bench. This encoder has 50nm and 26-bit resolution and supports BiSS C (unidirectional) that is a high-speed

Figure 5.12: Linear encoder

serial open protocol. This protocol is suitable for dynamic measures that require high acceleration, silky-smooth velocity control, bi-directional repeatability and positional stability. The encoder scale tape, adopted for the rig, is characterized by a high accuracy ($\pm 5 \mu$m/m).

CHAPTER 6

Test procedure

The test procedure defines the tests and concerning activities which have been carried out in order to verify if and how mechanical degradation on transmission components (like ball screws and bearings) of an EMA can be monitored, in real time, through a condition assessment process, using both electrical and mechanical variables (mainly currents, voltages, position and speed) measured by the test bench and via an external acquisition hardware (see chapter 5), and specific algorithms developed ad hoc. The final scope of the test is to bring the EMA to failure. To bring the EMA to a status of severe degradation or breakage, as the employed components are conceived to be extremely robust and durable, some procedures to accelerate deterioration of the mechanical parts have been adopted as described in this chapter. The breakage of the EMA could happen because of several factors. Thanks to the results obtained by a FMECA (see in Table 4.1), a list of typical and more frequent mechanical faults on EMAs have been analyzed and the most significant failure modes with hazardous effects have been identified.

It was likely that the degradation of the components and thus the breakage of the actuation system would have gone toward one or more of the identified failure modes. The tests has been performed in order to gradually drive the system into one of those modes, accelerating the process of deterioration of the mechanical parts. Continuous data acquisitions was performed, in order to maintain a constant monitoring to allow a precise characterization of the status of degradation of the system. Sensor faults and electrical faults of the EMA, instead, are excluded from the present project, thus they are not taken into account.

All the tests were executed at common conditions, described next.

6.1 Test conditions

The tests have be performed at the following environmental conditions:

- Temperature: 21 ± 11°C (70 ± 20°F)
- Humidity: 10 to 90% RH
- Atmospheric Pressure: 650mm Hg to 775mm Hg

The EMA surface temperature has been maintained constantly under 40°C by means of an air cooling system constantly turned on while the actuator was running.

The specimen has been initially tested in "healthy" condition, that is the "should build" configuration, and, as a natural process of degradation, the specimen reached the "faulty" condition at the end of the phase of tests. Due to the fact that the specimen has been designed and built to be extremely robust and fault-tolerant, it was not feasible to wait for failures to occur by themselves with simple nominal usage of the EMA. To induce the acceleration of the degradation of the mechanical parts, some expedients were needed since the start of the phase of tests. In order to reach a gradual deterioration of the mechanical parts, no abrupt faults were injected appositely on the EMA. Although, the process of degradation was accelerated through the following actions:

- Reduction of the number of ball circuits of the ballscrew from 8 to 3: this increased the contact pressure on the balls and on the ball tracks of the installed circuits, allowing a faster degradation of the parts
- Gradual removal of the lubricant: this increased the friction and the probability of mechanical part degradations (see section 6.2.3)

Moreover, the RUDDER configuration, which is the worst case condition, has been used as the test condition. In fact, RUDDER configuration requires the highest axial force. Furthermore, not only an axial load has been applied, but also a radial load. This resulted in an even higher pressures, above design allowable, on a certain number of balls in the ballscrew, which could lead to an accelerated degradation of the mechanical parts.

All the tests have been performed with a sampling frequency of:

- 4800Hz for the EMA phase currents acquired by the cDAQ
- 500Hz for the mechanical measures acquired by the cDAQ
- 100Hz for the measures acquired by the cRIO

Moreover, all the tests, have been executed with sinusoidal position reference inputs given to the EMA (with varying amplitude between 5 and 30mm and varying frequencies between 0.1 and 10Hz), as the tests aimed at simulating the real work cycle of an actuator during flight, which is pull-back and deflection of the primary flight control surfaces. An exemplifying plot of the position signal reference is shown in Figure 6.1.

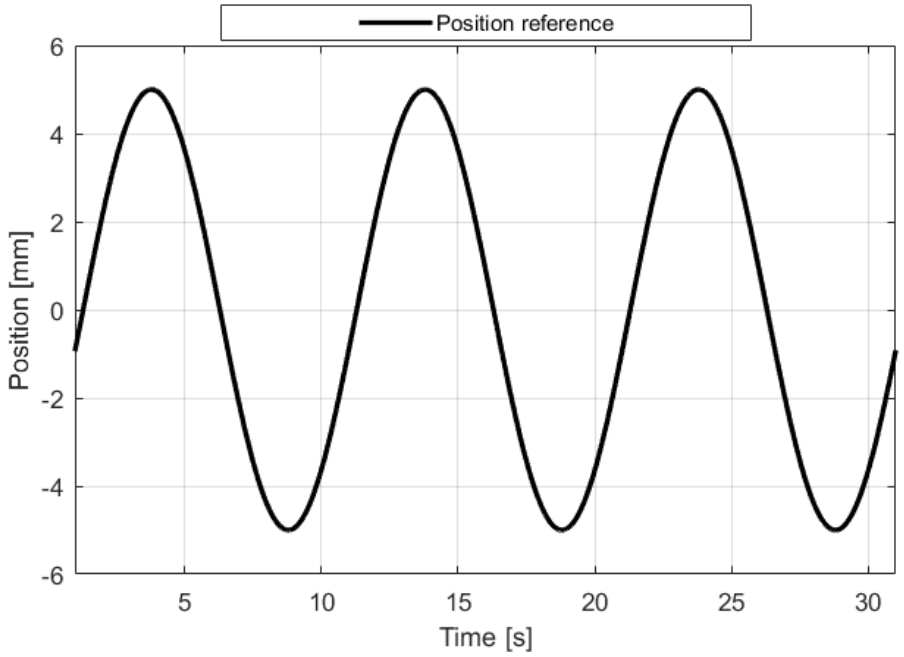

Figure 6.1: EMA position reference (amplitude: 5mm, frequency: 0.1Hz) example

A constant load, reached by means of a ramp in 5 seconds, has been applied during all the first endurance test phase. The value of the constant load, however, changed depending on the test type as explained in the next section. An exemplifying plot of the load signal reference is shown in Figure 6.2

Next, all the executed tests are reported.

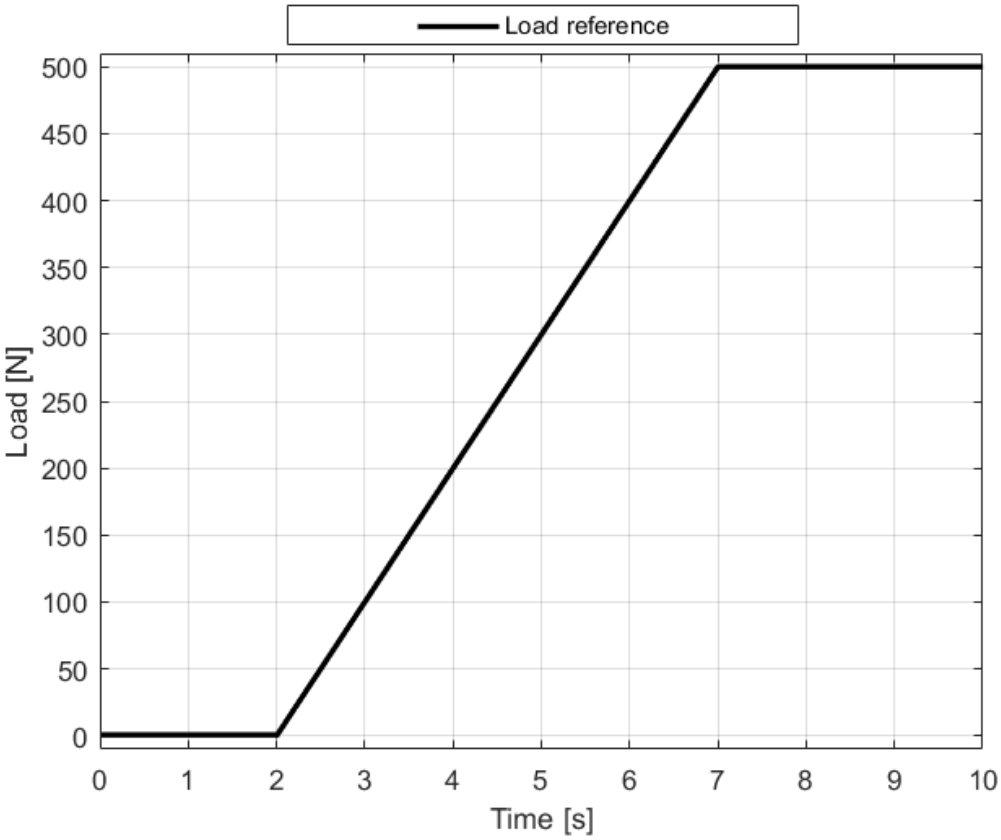

Figure 6.2: Load reference (500N) example

6.2 Test report

During the test phase, different configurations for different types of tests have been employed. Some tests were planned to fatigue the actuator with numerous test cycles while monitoring its deterioration process (endurance tests, presented in section 6.2.2); others, instead, had the only purpose to characterize the status of degradation of the system and evaluate the EMA performances (performance evaluation tests, presented in section 6.2.1). Performance evaluation tests and endurance tests have been periodically alternated. The complete chronological tests procedure is described in section 6.2.3.

The difference between performance evaluation tests and endurance tests resides in a different combination of the sinusoidal EMA position reference characteristics and in a different load reference profile provided to the linear motor.

6.2.1 Performance evaluation tests

The performance evaluation tests are those tests achieved with no counteracting load force. In fact, the reduced or no load condition helps to avoid the introduction of further noise or disturbance in the system, allowing a better characterization of the specimen, also with the passage of time.

The performance evaluation tests are characterized by a null load applied from the linear motor. The frequencies of the sinusoidal position references given to the EMA varied densely between 0.1 and 10Hz, for a better evaluation of the state of degradation of the prototype.

Such condition is thought considering that this kind of test could be easily performed on small aircrafts during ground maintenance operations.

6.2.2 Endurance tests

The endurance tests are those tests achieved with a constant counteracting load force and are meant to stress the actuator. Nevertheless, these tests provide useful information on the state of degradation of the EMA and will thus be employed in the development of the HM system (see part III).

The endurance tests are characterized by a counteracting load force varying between 300 and 800N, with the increase of the grade of stress to be applied to the EMA. The frequencies of the sinusoidal position references given to the EMA varied less densely than the performance evaluation tests between 0.1 and 4Hz.

Next, a chronology of the tests is reported.

6.2.3 Chronology of the tests

The considered test phase started on the 6^{th} of September 2017 and lasted until the 13^{th} of October 2017. However, other tests (that are not reported in this thesis) have been performed from April 2017 to date. In Table 6.1, all the tests performed in the considered period are reported (*perf.* is the abbreviation for performance evaluation test and *end.* is the abbreviation for endurance test). The tests interchanging between endurance and performance evaluation tests was dictated by a constant data analysis, suggesting the level of degradation of the components. The tests have been achieved with the following status of lubricant:

- Normal lubricant, at the start of the tests
- Poor lubricant (lubricant *partially* removed), after about one third of the tests were achieved
- No lubrication (lubricant *completely* removed), for the last third part of the test phase

The lubricant has been manually removed by unmounting the ballscrew.

Moreover, during the tests, several visual inspections have been performed (see chapter 7 for details).

To conclude this chapter, a summary of the executed tests on the specimen at the end of the test phase is reported in Table 6.2 (considering also other tests that were not included in the considered test phase). The summary includes:

- the total work time for each type of test
- the total distance traveled during each type of test
- the toal number of revolutions of the screw in each condition, computed using the formula:

$$screw\_revolution = \frac{distance}{screw\_step} \tag{6.1}$$

Table 6.1: Performed tests (perf.=performance evaluation, end.=endurance)

Date (2017)	**Type of test**	**Counteracting load force [N]**
01 September	Visual inspection	
06 September	perf.	0
06 September	end.	300
08 September	perf.	0
11 September	end.	300
12 September	perf.	0
12 September	end.	800
15 September	perf.	0
18 September	end.	300
18 September	Visual inspection	
Lubrication removal: poor lubricant condition		
19 September	end.	300
21 September	perf.	0
21 September	end.	300
25 September	perf.	0
25 September	end.	300
26 September	Visual inspection	
Lubrication removal: no lubricant condition		
02 October	perf.	0
02 October	end.	300
03 October	end.	300
04 October	end.	300
05 October	perf.	0
09 October	perf.	0
09 October	end.	300
10 October	end.	800
11 October	end.	300
12 October	end.	300
12 October	end.	800
13 October	perf.	0
13 October	Visual inspection	

Table 6.2: Summary of the executed tests on the specimen

Type of test	**Work time [h]**	**Distance [km]**	**Number of revolutions**
Endurance 300N	164.88	8.20	2582939
Endurance 800N	324.74	16.29	5130369
Others	166.68	17.72	5582805

CHAPTER 7

EMA performance evaluation

Chapter 6 presented all the executed tests and their procedure. This led to the acquirement of an enormous quantity of data describing the status of degradation of the EMA. Besides the HM algorithm that has been implemented (see part III), other two analysis were carried out during all the tests execution for a sudden evaluation of the EMA performances:

- *EMA functionality evaluation*: frequency response models of the position closed-loop behavior of the actuator have been estimated using the data obtained by performance evaluation tests. In this way, it was possible to check if the position tracking, which is the main function of the device, was performed correctly over time. This is presented in section 7.1.
- *Visual inspection* of the mechanical components: the balls and the screw thread were inspected to understand if there was a correspondence between the EMA functionality evaluation results and the physical status of the mechanical parts. This is presented in section 7.2.

7.1 Functionality evaluation of the EMA

The functionality evaluation of the EMA was achieved by analyzing the position tracking performance of the actuator. Since the reference signals were sinusoids at different frequencies (and different amplitudes - see chapter 6), a frequency response model (one for each amplitude) of the position closed loop [109] [110]

has been estimated using the measured feedback position with respect to the sinusoidal reference position.

The control system has a position tracking bandwidth of about 1.5Hz. Thus, the density of the sinusoid input frequencies was major around such cut-off frequency. Once the frequency response models were obtained, they were compared together. The result can be seen in Figure 7.1, in which all the magnitude $|F(j\omega)|$ (in dB) and phase $\angle F(j\omega)$ (in deg) Bode diagrams have been compared at each acquired frequency (in rad/s), one for each test date (in the legend, during year 2017).

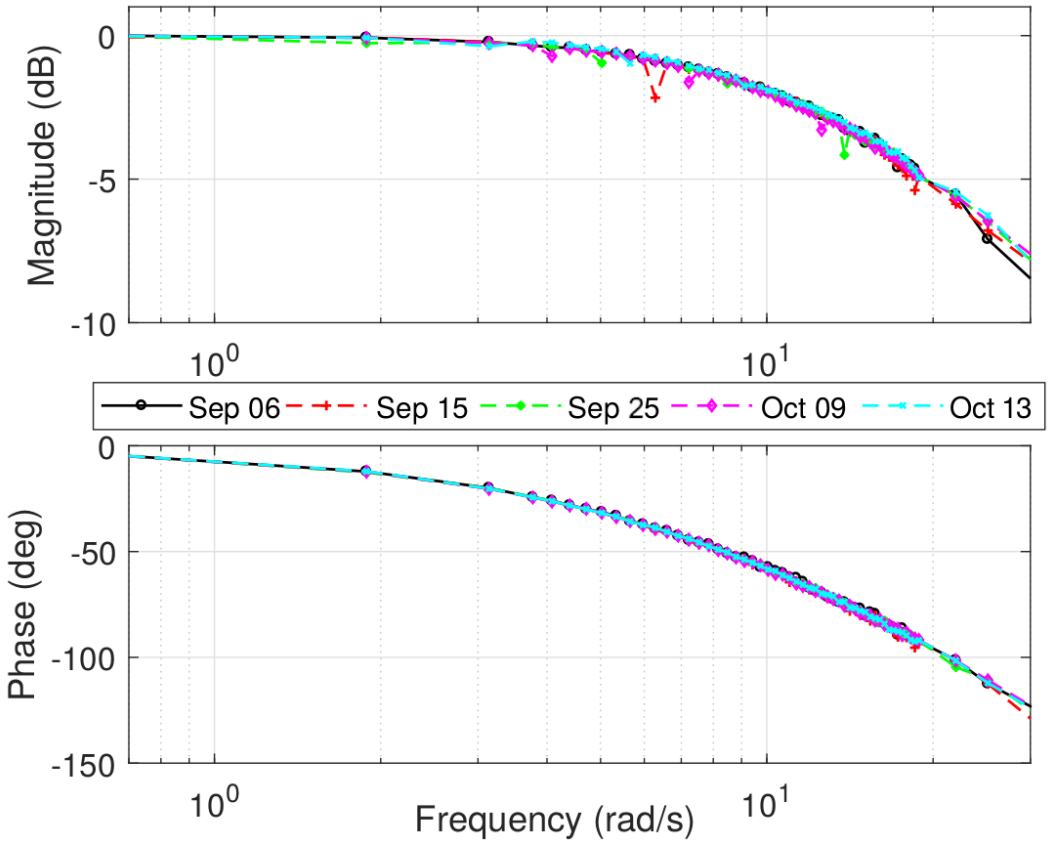

Figure 7.1: EMA frequency response models comparison (amplitude: 5mm)

It is possible to visually notice that no position tracking degradation happened during the test phase, as all the diagrams were perfectly overlapping. This has been confirmed also by the calculus of the Relative Squared Error (RSE) E for the frequency response $F(j\omega)$, both for the magnitude and the phase, with respect to the first considered test (at the start of September). Thus, named $F_S(j\omega)$ the response considered as the reference, the RSE for the magnitude and the phase in

each date i are, respectively:

$$E_{mag,i} = \left(\frac{\sum_{\omega=\omega_{min}}^{\omega_{max}} \left(|F_i(j\omega)| - |F_S(j\omega)| \right)^2}{\sum_{\omega=\omega_{min}}^{\omega_{max}} |F_S(j\omega)|^2} \right)^{\frac{1}{2}} \tag{7.1}$$

$$E_{pha,i} = \left(\frac{\sum_{\omega=\omega_{min}}^{\omega_{max}} \left(\angle F_i(j\omega) - \angle F_S(j\omega) \right)^2}{\sum_{\omega=\omega_{min}}^{\omega_{max}} \angle F_S(j\omega)^2} \right)^{\frac{1}{2}} \tag{7.2}$$

where $[\omega_{min}, \omega_{max}]$ is the frequency interval covered by the input frequencies (which is [0.1Hz,10Hz], as stated in chapter 6). To conclude, such indexes indicate the distance of one test from the reference test. All the results show a variation of such indexes of about $\pm 5\%$. Such result confirms that the EMA was able to maintain its performances intact from the start to the end of the test phase. This happened thanks to the fault-tolerant control implemented in the ECU, that is able to counteract any ongoing incipient fault. In fact, visual inspection revealed a strong physical degradation ongoing during the test phase. The next section presents the results of such visual inspection.

7.2 Visual inspections

In this section, the results of the four visual inspections are summarized.

1 - 01 September: before tests start The first visual inspection does not show any particular signs. Of course, balls (in Figure 7.2) and screw (in Figure 7.3) shaft were found in healthy state. A small quantity of metallic particulate was found in the grease.

Figure 7.2: Balls after visual inspection 1

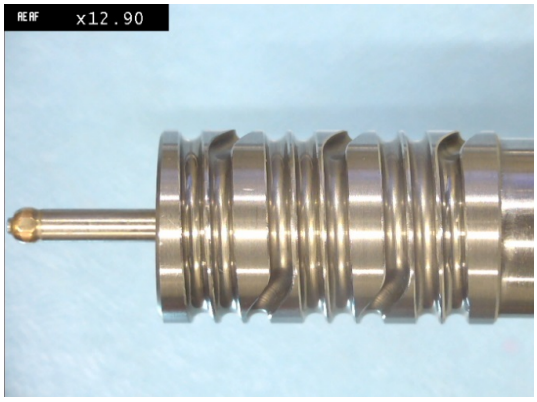

Figure 7.3: Screwshaft after visual inspection 1

2 - 15 September: tests with normal lubricant The visual inspection of check 2 showed that the surface color of balls of circuit 1 and 2 have changed (in Figure 7.4); those circuits were carrying the biggest amount of load. However, no significant signs were noticed on the screwshaft (in Figure 7.5).

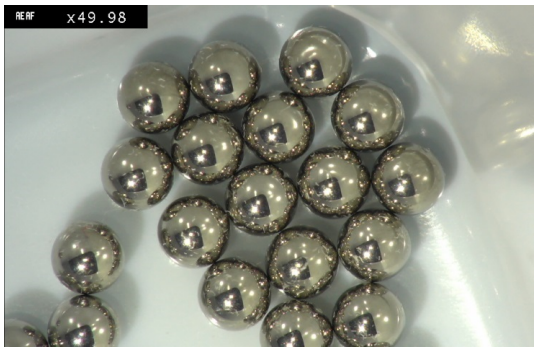

Figure 7.4: Balls after visual inspection 2

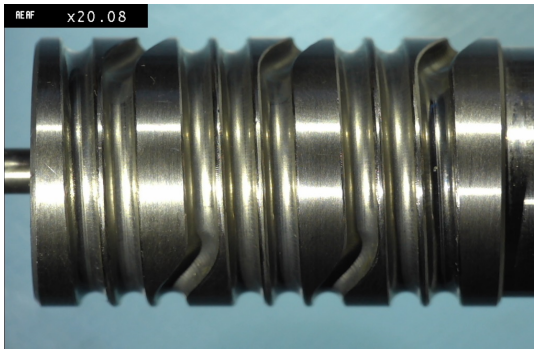

Figure 7.5: Screwshaft after visual inspection 2

3 - 26 September: tests with partial removal of lubricant During check 3 all parts of ballscrew assy were disassembled, in order to verify the condition of all mechanical components after the test performed with poor lubrication. Check 3 confirmed the considerations already made after the check 2; in addition, the balls of the bearing installed on the opposite side of the motor were found less shiny than those of the bearing installed on the motor side (in Figure 7.6). The ball tracks of the screw were starting to show some signs in the areas of balls passage under higher loads (in Figure 7.7).

Figure 7.6: Balls after visual inspection 3

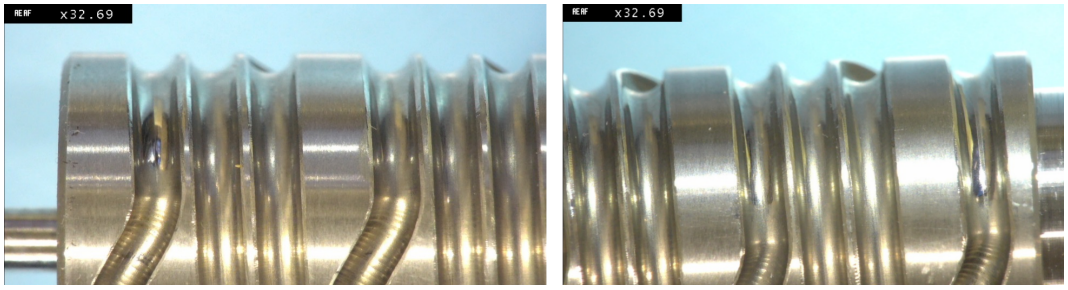

Figure 7.7: Screwshaft after visual inspection 3

4 - 13 October: tests with total removal of lubricant Check 4 was carried out after the test without lubricant. The balls appeared like after the previous check (in Figure 7.8) while the recirculation zones showed a change in color (in Figure 7.9). After a qualitative consideration, this color could be caused by the oxidized lubricant particles. In addition, a small quantity of mechanical particulate was found.

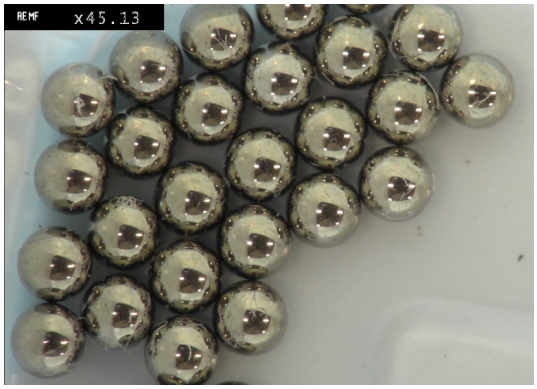

Figure 7.8: Balls after visual inspection 4

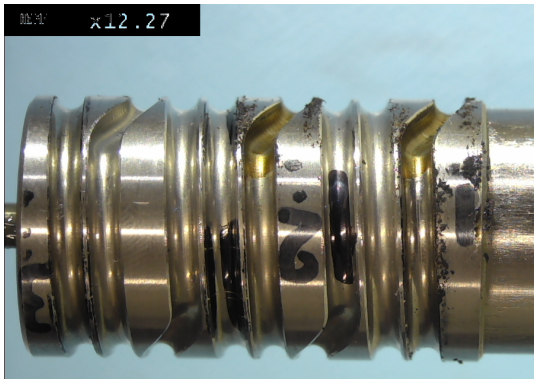

Figure 7.9: Screwshaft after visual inspection 4

7.3 Conclusions

In conclusion, in a preliminary analysis, no significant differences can be appreciated in time and frequency domain, while considering the position reference and measure of the EMA (see section 7.1). However, considering the results of the visual inspections (in section 7.2), it is possible to affirm that during the test phase some incipient faults were taking place, even without showing any effects on the overall functionality of the actuator. This led to the idea that the mechanical components degradation could result in a loss of efficiency of the system. This hypothesis was at the base of the HM algorithm that has been developed and tested, as described in part III.

Part III

Health Monitoring based on Change Detection algorithms

The Health Monitoring algorithm was carried out based on the assumption that mechanical components degradation results in a loss of efficiency of the system. Thus, in order to obtain a correct position tracking, the EMA drains more current in certain situations such as in case of incipient faults happening. So, a statistically robust feature has been conceived and computed. The continuous monitoring of such feature led the bases for the HM algorithm, that is presented and described in this part, which is structured as follows:

- Chapter 8 presents the concepts and the theory behind the developed HM algorithm
- Chapter 9 implements the HM system in MATLAB environment
- Chapter 10 discuss the testing and the results of the HM system on the measurements of the experimental tests

CHAPTER 8

Health Monitoring System of EMA for aerospace

The Health Monitoring (HM) strategy proposed in this work is based on the assumption that the mechanical components degradation, that comes along with usage and increase in case of incipient faults, results in a loss of efficiency of the system. The loss of efficiency implies the employment of major resources (power and current) for achieving the same actions. Thus, for example, in order to obtain a correct position tracking, the Electro-Mechanical Actuator (EMA) would drain more current to perform the same duty in a situation of degradation or incipient faults. A plot of the measured phase currents is reported in Figure 8.1.

The measured phase currents contain disturbances that deviate the overall sum of the three from zero. For this reason, it has been decided to consider all the currents singularly. Following this assumptions, two indicators (features) are computed on measured phase currents data, with no need of additional sensors (see section 8.1):

- the Root Mean Square (RMS), see section 8.1.1
- the Crest Factor (CF), see section 8.1.2

Other features were considered during the implementation phase, but these two showed the best results, as presented in chapter 10.

These two features are used by the Change Detection (CD) algorithm (see section 8.2) to assess the health state of the EMA regardless of its performances. In fact, as demonstrated in the previous chapter, in section 7.1, the EMA is intrinsically fault tolerant: until the power supply can provide enough energy and

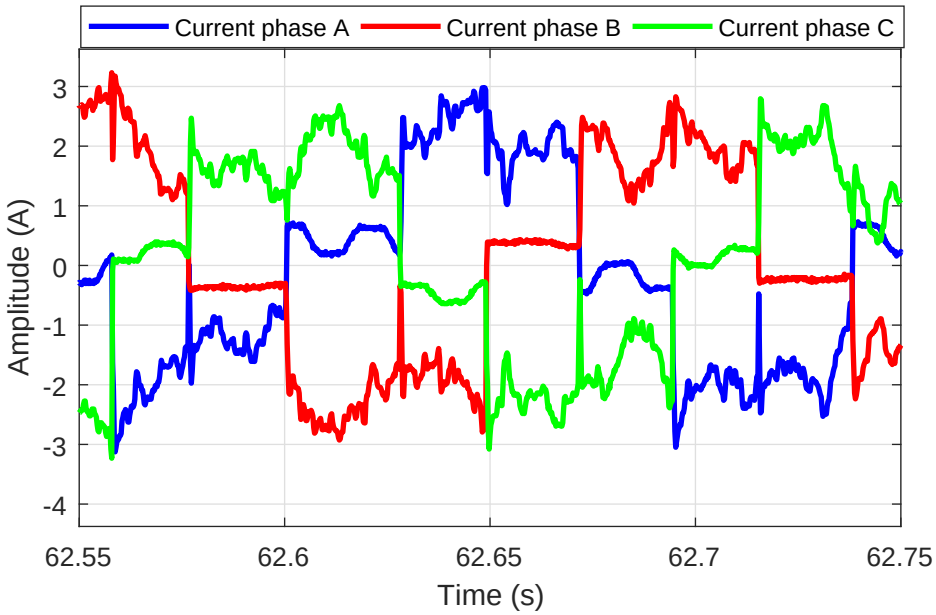

Figure 8.1: Phase currents measurement example

the system does not undergo a critical failure, it could not be possible to see any degradation in its performance, for example in the position tracking task. On the contrary, monitoring the control actions, such as the phase currents, allows to identify EMA degradation, as confirmed also by the visual inspection of the mechanical components of the EMA (see section 7.2).

8.1 Features extraction

The considered features are extracted from the three phase currents of the EMA, $i_a(t)$, $i_b(t)$ and $i_c(t)$, measured during the experimental tests. Since the measured position is a sinusoid (in the test phase, the EMA has always been tested in position tracking experiments using sinusoids with different amplitude and frequency as a reference signal, see section 6.1) with period $T = 2\pi/\omega$, with ω being the frequency of the sinusoid measured in rad/s, it is possible to write the current signal of the x-th phase as:

$$i_x(t), \quad (\tau - 1)T \leq t \leq \tau T \tag{8.1}$$

where $x = a, b, c$ and $\tau = 1, ..., N_p$ being N_p the total number of periods T in the considered experiment.

Thus, features are extracted as explained next.

8.1.1 RMS

The Root Mean Square (RMS) of a signal is defined as the squared root of the arithmetic mean of the squared value of the signal at each sampling time. In this work, for each phase current $i_x(t)$ with $x = a, b, c$, the RMS $\sigma_x(t)$ is computed over a single period τ as:

$$\sigma_x(\tau) = \sqrt{\frac{1}{T} \sum_{t=(\tau-1)T}^{\tau T} i_x^2(t)}. \tag{8.2}$$

with $\tau = 1, ..., N_p$.

For each experiment, it is possible to compute a mean RMS value at every period $\tau = 1, ..., N_p$ over the three phase currents as:

$$\Sigma(\tau) = \frac{1}{3}\Big(\sigma_a(\tau) + \sigma_b(\tau) + \sigma_c(\tau)\Big) \in \mathbb{R} \tag{8.3}$$

Thus, the first extracted feature is the RMS $\Sigma(\tau)$. This feature has also a strong physical meaning. In fact, since it is measured in Ampere, $\sigma_x^2(\tau)$ is related to the mean square current and $\Sigma(\tau)$ to the mean electrical power. Considering, again, the assumption that the mechanical components degradation results in a loss of efficiency of the system, and that the efficiency is related to the electrical power, this feature is the perfect candidate for being the most explicative one.

However, also another feature has proved to be informative: the Crest Factor of phase currents, as presented in the next section.

8.1.2 CF

The Crest Factor (CF) is defined as the ratio between the absolute value of the maximum of a signal, over a given time interval, and the standard deviation value of the same signal, computed in the same time interval. In this project, the CF of the three phase currents $i_x(t)$ with $x = a, b, c$ is computed. Similarly as for the RMS feature, since the measured positions are sinusoidal with period T, the computation is made over every single period of the considered measurement.

Thus, the CF $\gamma_x(\tau)$ is extracted for each phase current $i_x(t)$, as:

$$\gamma_x(\tau) = \frac{\max\left(|i_x(t)|\right)}{std_x\left(\tau\right)}, \quad (\tau - 1)\, T \leq t \leq \tau T \tag{8.4}$$

with $\tau = 1, ..., N_p$ and being $std_x\left(\tau\right)$ the standard deviation of $i_x(t)$ over the τ-th

period. The standard deviation $std_x(\tau)$ is computed as:

$$std_x(\tau) = \sqrt{\frac{\sum_{N_{i=1}}^{N}(i_{xi} - \overline{i_x})^2}{N-1}} \tag{8.5}$$

where $\overline{i_x}$ is the mean value of the observed phase current and N the number of observations in the experiment.

So, for each experiment measurement, it is possible to compute a mean CF value of the three phase currents at every period $\tau = 1, ..., N_p$:

$$\Gamma(\tau) = \frac{1}{3}\Big(\gamma_a(\tau) + \gamma_b(\tau) + \gamma_c(\tau)\Big) \in \mathbb{R} \tag{8.6}$$

Thus, the second extracted feature is the CF $\Gamma(\tau)$. This feature is a dimensionless quantity and is a positive real number. In real applications, in some cases, it could happen that two identical EMAs, one perfectly healthy and one degraded, may drain the same amount of true power. However, in the healthy case the crest factor may be different from the case in which a fault is happening. For this reason, the CF is an important feature that could contain information about the fault.

These two presented features will be used by the Change Detection (CD) algorithm that looks for changes in the sampling distribution of the features.

8.2 Change Detection algorithm

The aim of the HM algorithm is to compute the features to be used for evaluating how they evolve in time. Following the idea presented in chapter 2, when a change is detected, there is a symptom that the system health state is deteriorating. In order to establish the importance of changes in the features, a density-ratio estimation method known as Relative unconstrained Least-Squares Importance Fitting (RuLSIF) [111] [112] has been employed.

8.2.1 RuLSIF

The Relative unconstrained Least-Squares Importance Fitting (RuLSIF) algorithm is built assuming that the estimation of the ratio of two probability densities is somehow easier than estimating the two densities separately [113]. In this work setting, the two densities represent kernel estimates of the time series data distribution, before and after a certain time instant. Once these densities (or, as

stated, their ratio) have been estimated, by using suitable divergence measures, it is possible to assess how much they differ. Density ratio estimation is a tool largely employed in both statistical community and machine learning as well. However, because of the unbounded nature of density ratio, the estimation procedure can be vulnerable to corrupted data points, which often pushes the estimated ratio toward infinity. Thus, a bounded (relative) density-ratio estimator was presented in [112] and employed also in this work.

Let $y(t) \in \mathbb{R}^{d\times 1}$ be a d-dimensional time-series sample at time t. Let:

$$\mathbf{Y}(t) \equiv [\mathbf{y}(T)^T, \mathbf{y}(t+1)^T, ..., \mathbf{y}(t+k-1)^T]^T \in \mathbb{R}^{d\cdot k\times 1} \tag{8.7}$$

be a "subsequence" of time series of length k, at time t. The subsequence $\mathbf{Y}(t)$ is treated as a single data sample. The quantity $\mathcal{Y}(t)$ is defined as the matrix composed by n of the $d \cdot k$-th dimensional samples $\mathbf{Y}(t)$, starting from t:

$$\mathcal{Y}(t) \equiv [\mathbf{Y}(T)^T, \mathbf{Y}(t+1)^T, ..., \mathbf{Y}(t+n-1)] \in \mathbb{R}^{d\cdot k\times n} \tag{8.8}$$

The matrix $\mathcal{Y}(t)$ forms a *Hankel matrix*, playing a key role in change-point detection based on subspace learning [114].

Consider now two consecutive segments $\mathcal{Y}(t)$ and $\mathcal{Y}(t+n)$. The change-detection problem is then solved by computing a certain dissimilarity measure between such consecutive segments. The higher the dissimilarity measure is, the more likely the two distributions differ. The entire notations are depicted schematically in Figure 8.2, in which, as illustrative settings, d = 1, t = 1, n = 5 and k = 3.

Divergence measures

Denote now the probability distributions of the samples in $\mathcal{Y}(t)$ and $\mathcal{Y}(t+n)$ as P and P', respectively. The Pearson divergence is defined as [115]:

$$\mathrm{PE}\left(P \,\|\, P'\right) \equiv \frac{1}{2}\int p'(\mathbf{X}) \cdot \left(\frac{p(\mathbf{X})}{p'(\mathbf{X})} - 1\right)^2 d\mathbf{X} \tag{8.9}$$

where $p(\mathbf{X})$, $p'(\mathbf{X})$ are the probability density functions of P and P', respectively and $\mathbf{X}$ denotes the generic dk-th dimensional random variable.

Let now $\{\mathbf{Y}_i\}_{i=1}^n$ and $\left\{\mathbf{Y}'_j\right\}_{j=1}^n$ be a set of samples drawn from $p(\mathbf{X})$ and $p'(\mathbf{X})$. In order to compute (8.9),an *estimate* of the density-ratio $\frac{p(\mathbf{X})}{p'(\mathbf{X})}$ is employed, using proper sets of samples which are representative of the two distributions. The

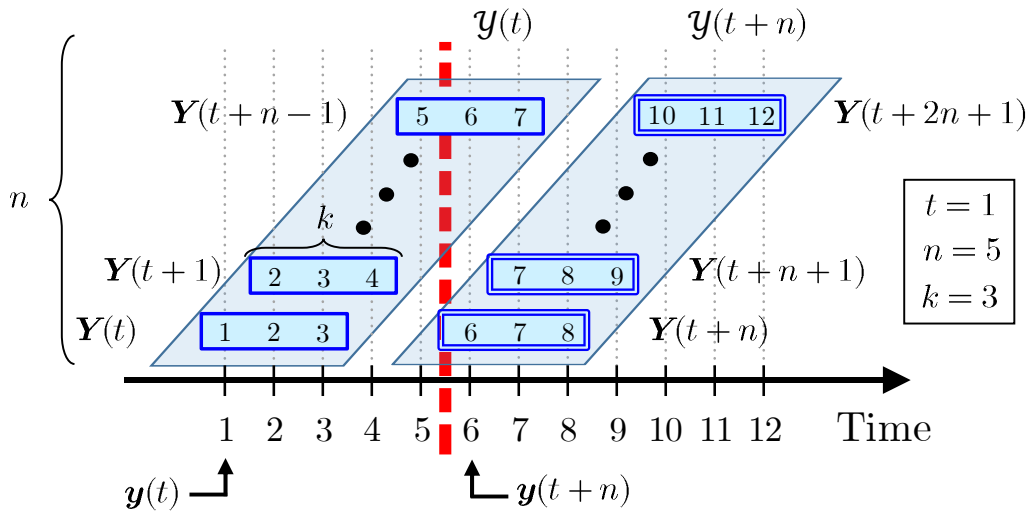

Figure 8.2: Schematic representation of the notation for a one-dimensional time series

samples $\{\mathbf{Y}_i\}_{i=1}^{n}$ are those belonging to $\mathcal{Y}(t)$. The samples $\left\{\mathbf{Y}'_j\right\}_{j=1}^{n}$, instead, are those belonging to $\mathcal{Y}(t+n)$. The density-ratio value $\frac{p(\mathbf{X})}{p'(\mathbf{X})}$ in (8.9) could be unbounded, depending on the condition of the denominator density $p'(\mathbf{X})$. To overcome this problem, the α-relative Pearson divergence measure was introduced in [112], for $0 \leq \alpha < 1$, as:

$$\mathrm{PE}_\alpha\left(P\|P'\right) \equiv PE\left(P\|\alpha P + (1-\alpha)P'\right) = \frac{1}{2}\int p'_\alpha(\mathbf{X}) \cdot \left(\frac{p(\mathbf{X})}{p'_\alpha(\mathbf{X})} - 1\right)^2 d\mathbf{X} \tag{8.10}$$

where $p'_\alpha(\mathbf{X}) = \alpha p(\mathbf{X}) + (1-\alpha)\,p'(\mathbf{X})$ is the *α-mixture density*. The *α-relative density-ratio* is then defined as:

$$r_\alpha(\mathbf{X}) = \frac{p(\mathbf{X})}{p'_\alpha(\mathbf{X})} = \frac{p(\mathbf{X})}{\alpha p(\mathbf{X}) + (1-\alpha)\,p'(\mathbf{X})} \tag{8.11}$$

which reduces to plain density-ratio when $\alpha = 0$, and it is bounded above by $1/\alpha$ for $\alpha > 0$, even when the plain density-ratio $\frac{p(\mathbf{X})}{p'(\mathbf{X})}$ is unbounded.

It is important to notice that neither (8.9) nor (8.10) are metrics, since they are not symmetric and the triangular inequality does not hold. To cope with the first problem, authors in [112] proposed to use the symmetrical divergence:

$$\mathrm{PE}_\alpha\left(P\|P'\right) + \mathrm{PE}_\alpha\left(P'\|P\right) \tag{8.12}$$

where each term is estimated separately.

The aim now is to estimate the quantity in (8.11) by a suitable model.

Learning algorithm

The α-*relative density-ratio* is modeled as:

$$g\left(\mathbf{X};\boldsymbol{\theta}\right) \equiv \sum_{l=1}^{n} \theta_l \cdot K\left(\mathbf{X}, \mathbf{Y}_l\right) \tag{8.13}$$

where $\boldsymbol{\theta} = \left[\theta_1, \ldots, \theta_n\right]^{\mathrm{T}} \in \mathbb{R}^{n\times 1}$ are unknown parameters, $K\left(\cdot,\cdot\right)$ is a kernel basis function, and $\mathbf{Y}_l$ refers to the l-th data sample in $\mathcal{Y}(t)$. In the experiments, the Gaussian kernel has been employed:

$$K\left(\mathbf{Y}_1, \mathbf{Y}_2\right) = \exp\left(-\frac{\|\mathbf{Y}_1 - \mathbf{Y}_2\|^2}{2\delta^2}\right) \tag{8.14}$$

where $\delta > 0$ is the kernel width. The parameters vector $\boldsymbol{\theta}$ is learned by minimizing the squared loss:

$$\begin{aligned} J(\boldsymbol{\theta}) &= \frac{1}{2}\int p'_\alpha(\mathbf{X})\Big(r_\alpha(\mathbf{X}) - g(\mathbf{X};\boldsymbol{\theta})\Big)^2\, d\mathbf{X} \\ &= \frac{1}{2}\int p'_\alpha(\mathbf{X}) r^2_\alpha(\mathbf{X})\, d\mathbf{X} - \int p(\mathbf{X}) g(\mathbf{X};\boldsymbol{\theta})\, d\mathbf{X} \\ &\quad + \frac{\alpha}{2}\int p(\mathbf{X}) g(\mathbf{X};\boldsymbol{\theta})^2\, d\mathbf{X} + \frac{1-\alpha}{2}\int p'(\mathbf{X}) g(\mathbf{X};\boldsymbol{\theta})^2\, d\mathbf{X} \end{aligned} \tag{8.15}$$

where the computations were made by expanding the square and employing the definition of $p'_\alpha(\mathbf{X})$.

The first term of (8.15) can be discarded since it does not depend on the unknown parameters. By substituting $g(\mathbf{X};\boldsymbol{\theta})$ with the definition (8.13), and approximating the expectations with empirical averages, it is possible to obtain the following minimization problem (with the addition of a Ridge regularization term $\frac{\lambda}{2}\boldsymbol{\theta}^{\mathrm{T}}\boldsymbol{\theta}$):

$$\widehat{\boldsymbol{\theta}} = \underset{\boldsymbol{\theta}\in\mathbb{R}^n}{\arg\min}\left[\frac{1}{2}\boldsymbol{\theta}^{\mathrm{T}}\widehat{\boldsymbol{H}}\boldsymbol{\theta} - \widehat{\boldsymbol{h}}^{\mathrm{T}}\boldsymbol{\theta} + \frac{\lambda}{2}\boldsymbol{\theta}^{\mathrm{T}}\boldsymbol{\theta}\right] \tag{8.16}$$

where $\widehat{\boldsymbol{H}} \in \mathbb{R}^{n\times n}$, $\widehat{\boldsymbol{h}} \in \mathbb{R}^{n\times 1}$ and $\lambda > 0$ controls the regularization strength.

The element in position (l,m) of $\widehat{\boldsymbol{H}}$ is given by:

$$\widehat{H}_{(l,m)} = \frac{\alpha}{n}\sum_{i=1}^{n} K(\mathbf{Y}_i, \mathbf{Y}_l)\cdot K(\mathbf{Y}_l, \mathbf{Y}_m) + \frac{1-\alpha}{n}\sum_{j=1}^{n} K(\mathbf{Y}'_j, \mathbf{Y}_l)\cdot K(\mathbf{Y}'_j, \mathbf{Y}_m) \tag{8.17}$$

The element in position l of $\widehat{\boldsymbol{h}}$ is given by:

$$\widehat{h}_{(l)} = \frac{1}{n}\sum_{i=1}^{n} K(\mathbf{Y}_i, \mathbf{Y}_l) \tag{8.18}$$

The solution to problem (8.16) can expressed as:

$$\widehat{\boldsymbol{\theta}} = \left(\widehat{\mathbf{H}} + \lambda \boldsymbol{I}_n\right)^{-1} \cdot \widehat{\boldsymbol{h}} \tag{8.19}$$

where $\boldsymbol{I}_n$ is n-th dimensional identity matrix. The density ratio estimator assumes thus the form of:

$$\widehat{g}\left(\mathbf{X}\right) = \sum_{l=1}^{n} \widehat{\theta}_l \cdot K(\mathbf{X}, \mathbf{Y}_l) \tag{8.20}$$

Computing the divergence

In order to use (8.20), it is first necessary to rewrite the Pearson divergence (8.10) as:

$$\begin{aligned}
\mathrm{PE}_\alpha\left(P \,\|\, P'\right) &= \tfrac{1}{2}\int p'_\alpha(\mathbf{X}) \cdot \left(\frac{p(\mathbf{X})}{p'_\alpha(\mathbf{X})} - 1\right)^2 d\mathbf{X} \\
&= \frac{1}{2}\int p'_\alpha(\mathbf{X}) \cdot \left(\tfrac{p(\mathbf{X})^2}{p'_\alpha(\mathbf{X})^2} - 2\tfrac{p(\mathbf{X})}{p'_\alpha(\mathbf{X})} + 1\right) d\mathbf{X} \\
&= \frac{1}{2}\int \left(\tfrac{p(\mathbf{X})^2}{p'_\alpha(\mathbf{X})} - 2p(\mathbf{X}) + p'_\alpha(\mathbf{X})\right) d\mathbf{X} \\
&= \frac{1}{2}\int \left(\frac{p(\mathbf{X})}{p'_\alpha\left(\mathbf{X}\right)}\right) \cdot p(\mathbf{X})\; d\mathbf{X} - \frac{1}{2}
\end{aligned} \tag{8.21}$$

where the simplification in the last step follows since probability distributions integrate to one. Replacing the estimator (8.20) in (8.21), and approximating the integrals with empirical averages, leads to the following approximation of the α-relative divergence:

$$\widehat{\mathrm{PE}}_\alpha = \frac{1}{2n}\sum_{i=1}^{n} \widehat{g}\left(\mathbf{Y}_i\right) - \frac{1}{2} \tag{8.22}$$

The final computed score is then, as reported by (8.12), the quantity:

$$\Pi \equiv \widehat{\mathrm{PE}}_\alpha(P \,\|\, P') + \widehat{\mathrm{PE}}_\alpha(P' \,\|\, P) \tag{8.23}$$

8.2.2 Assessment of the HM algorithm as CD problem

Condition monitoring approaches for EMAs already faced in the literature were presented in section 4. The work presented in this thesis differs from the previously cited ones, since it relies on an *unsupervised nonparametric knowledge-based*

method, using only features computed from phase-current measurements. As stated, the method employed is a CD algorithm based on density-ratio estimation [14]. The rationale of the method consists into assessing if a change occurred between the probability distributions of data samples over past and present intervals. The assumption is to relate the motor degradation to a distributional change in its measured data. Change-point detection methods are usually classified into:

- real-time [116]
- retrospective detection [117]

The difference lies in the immediate response of the former methodologies, with respect to the greater accuracy and higher computation times of the latter ones. Other change detection methods relies instead on ideas from subspace methods, usually employed in system identification [114]. In its basic form, the algorithm employed in this work belongs to the retrospective category. However,the method has been proposed in a batch manner, with respect to the on-line fashion. This is possible by planning regular checks of the mechanical component, and comparing the previously measurements with the currently performed ones. If the system detects that the data distribution is changed between the two known time instants, than we can suspect a degradation of the motor functionalities in the meantime. By comparing measured data with a "gold standard" set of measures (for example a healthy dataset at the beginning of actuator's life), it would be also possible to detect small changes that, with the standard on-line methods, would be more difficult to recognize.

Thus, the proposed algorithm compares the features computed on the new experiment with past ones, as highlighted in Figure 8.3, in which, as example, d=1, k=3, n_1=2 and n_2=7.

The rationale of applying a batch procedure is mainly due to the certainty that external conditions at which the experiments are made can be set to remain the same every time this procedure is carried on. As an example, it is difficult to reliably estimate the load when the EMA operates in flight. Variations in load conditions can alter the decision of an on-line condition monitoring algorithm, that was designed to work on controlled test conditions. Another factor of variation can be the temperature, that can reach very low values at high altitudes. Obviously, the method requires a policy to chose the "reference measures" to be compared with the new acquired ones. In the following, three different rationales are compared, that is:

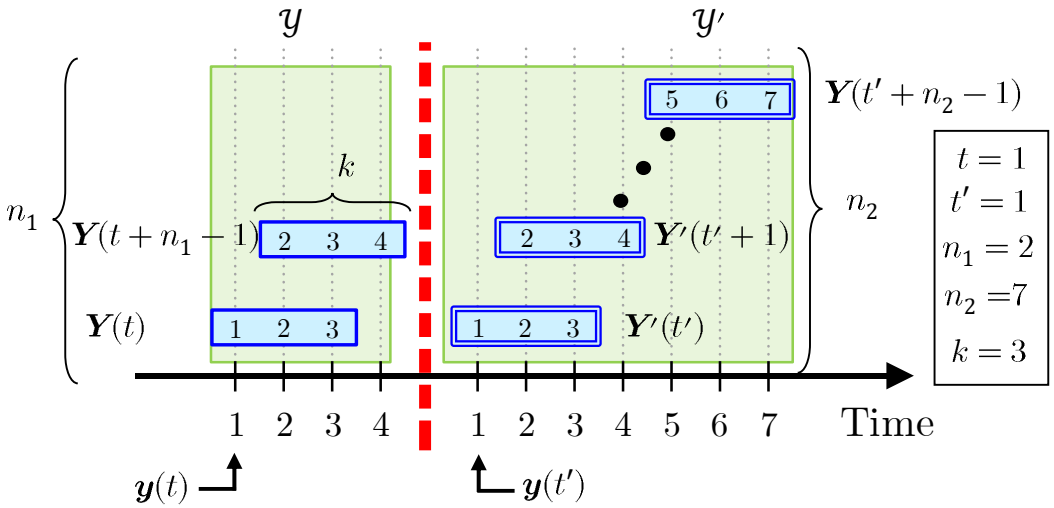

Figure 8.3: Health monitoring via batch RuLSIF method, with a one-dimensional time series

- **Always Healthy (AH)**: always compare with the healthy dataset
- **Always Previous (AP)**: always compare with the most recent dataset
- **Last Change (LC)**: always compare to the last dataset that triggered a predetermined threshold. The method generates a score, defined as the number of threshold violations.

Differently from the standard method, the proposed approach applies the algorithm not with a sliding window, but directly comparing the measurements of one test with the measurements of a different test.

Here there is not a continuous progression of the time series, since the data are considered in a separate way, and not as a continuous stream of information. Thus, even the time indexes t and t' are different. The parameter k maintain its previous role. The first dataset is denoted as $\mathcal{Y}$, and the second one with $\mathcal{Y}'$. Thus, $\mathcal{Y}$ and $\mathcal{Y}'$ do not depend on the time anymore. The number of observations in the two datasets, that depend on k, can be different. The number of observations in $\mathcal{Y}$ is denoted with n_1, and the number of observations in $\mathcal{Y}'$ with n_2. Apart from these considerations, the method computes the divergence between $\mathcal{Y}$ and $\mathcal{Y}'$ as previously described.

The considered time series has dimensionality $d = 2$. Each sample $\boldsymbol{y}(\tau) \in \mathbb{R}^{2\times 1}$ is a vector which elements are $\Sigma(\tau)$ and $\Gamma(\tau)$. The same reasoning can be done with the data from $\mathcal{Y}'$. The parameter k plays the role of a "memory" which usually

appears in dynamic systems. Since we computed the value of the considered time series as independent indicators at each period τ, we choose to set $k = 1$. Thus:

$$\boldsymbol{Y}(t) = \boldsymbol{y}(t) \in \mathbb{R}^{2\cdot 1\times 1}; \quad \boldsymbol{Y'}(t') = \boldsymbol{y'}(t') \in \mathbb{R}^{2\cdot 1\times 1} \tag{8.24}$$

The hyperparameters δ and λ are chosen via κ-fold cross-validation. Since following the heuristic rule to have at least $10 \cdot m$ data points, where m is the number of parameters to tune, it follows that at least 20 samples per fold are needed. For this reason, κ has been chosen to be equal to 5. Also, to the default value $\alpha = 0.5$ has been selected as in [112].

In the next chapter the implementation and results of the HM algorithm are presented.

CHAPTER 9

Implementation of the Health Monitoring System

The Change Detection (CD) algorithm has been presented in chapter 8 and has applied to the features $\Sigma(\tau)$ and $\Gamma(\tau)$, discussed in section 8.1. The implementation of the algorithm is presented in this chapter in MATLAB environment. The implementation of the HM algorithm has been divided in three phases:

- Phase I: data pre-processing phase, in which all the informative tests are collected
- Phase II: data loading and features extraction, in which all the data and are loaded into the workspace and features are extracted in a structured way (the logic is implemented in a file named *load_data.m*)
- Phase III: change detection, in which the HM algorithm is in fact implemented (the logic is implemented in a file named *CD_algorithm.m*)

This is represented in Figure 9.1

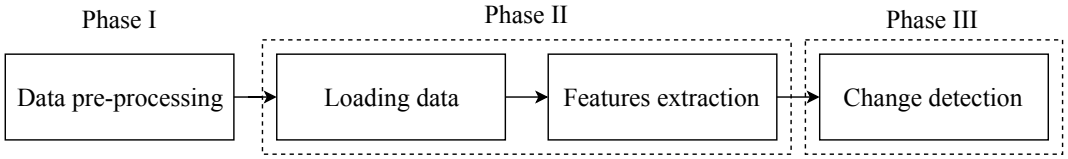

Figure 9.1: Representation of the three algorithm implementation phases

9.1 Phase I: data pre-processing

The considered features have been computed for a discrete range of operating frequencies: 0.1Hz, 0.3Hz, 0.5Hz, 0.8Hz, 0.9Hz and 1Hz (see section 6). This range of frequencies is that for which the EMA has been designed. In the present work, the CD method to measurements at the frequency of 1Hz is reported as explicative example. The frequency value is not a critical parameter and similar results can be obtained also using data from experiments at different frequencies. Similar reasonings can be achieved for the reference sinusoid input amplitude, thus only the 10mm amplitude has been considered.

The data pre-processing phase only consisted in providing to the environment the experimental data. All the considered tests are included in subfolders, which are contained in a parent folder named "Acquisitions". All the measurements were stored in the form of a data table, named *data_table*, saved inside MATLAB files named *test.mat*. This is better represented in Figure 9.2, in which the environment comprises two .m files, *load_data.m* and *CD_algorithm.m* and two folders, the library folder, in which the RulSIF implementation is included in *RulSIF.m* script, and the acquisition folder, in which all the tests are stored, as explained.

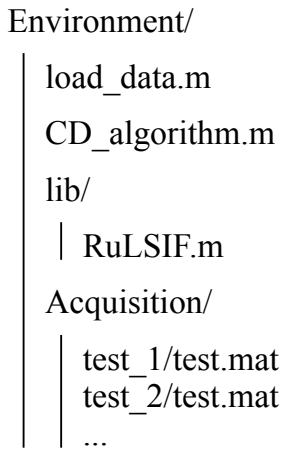

Figure 9.2: Representation of the three algorithm implementation phases

9.2 Phase II: Data loading and features extraction

The second phase of the implementation consists of loading the data and preparing them for the features extraction. Next, the code and the pseudocode are reported to illustrate the implementation of the algorithm.

9.2.1 Data loading

First, the paths of all folders are defined, as follows:

```
%% Path definition
path{1} = '\Acquisitions\test_1\';
path{2} = '\Acquisitions\test_2\';
% ...
```

Then, the phase of data loading and features extraction starts. A for loop is employed to load all data and extract the measurement. This phase comprise the loading of the files and the feature computation, as shown in the following pseudocode:

```
>> Path definition

% Loop over all the tests
for tt = 1 : length(path)
  >> Loading tests and initialization
  >> Features computation
end
```

Only the employed measurements are considered (compare with section 5.4). Thus, the loading tests and initialization is composed of:

- a loading phase
- an initialization phase for the features matrix
- a retrieval of the measurements

This is reported in the code below:

```
%% Loading tests and initialization
% Loading test
load([path{tt}, 'test.mat']);

% Features matrix initialization
X = cell(1,1);

% Retrieving signals from saved data format: data_table
phase_A = data_table.get('phase_A');
phase_B = data_table.get('phase_B');
```

```
phase_C = data_table.get('phase_C');
EMA_pos_LVDT = data_table.get('EMA_pos_LVDT');
t = 0:1/ff:length(phase_A)
```

where phase_A, phase_B and phase_C are the three phase currents measurements, EMA_pos_LVDT is the position measurement of the EMA from the LVDT sensor that is later employed for zero crossing and t is the time vector.

9.2.2 Features extraction

The features are extracted on the phase currents after a zero crossing procedure to identify when the sinusoids are equal to zero, in order to equally divide periods. The CF feature is stored in the first row of the features vector, the RMS, instead, in the second one. CF and RMS are calculated with the function $peak2rms$ and rms provided by MATLAB libraries. The features vector contain a mean of the features computed of each phase:

$$features(k,i) = \frac{features\_A(k,i) + features\_B(k,i) + features\_C(k,i)}{3} \tag{9.1}$$

where k = 1 if computing the CF or k = 2 if computing the RMS, i is the i-th considered period. All this is implemented next:

```
%% Features computation
% Zero crossing
zci = @(v) find(v(:).*circshift(v(:), [-1 0]) <= 0);
zx = zci(EMA_pos_LVDT)';
% Removal of final zero crosses
zx = zx(1:end-1);
t_zero = find(EMA_pos_LVDT == 0);
% Removal of zero crosses when the method has not started
zx = setdiff(zx, t_zero);
% Taking the periods of the sinusoid
zx = zx(1:2:end);
ss = size(EMA_pos_ref_cDAQ);

% Vectors initialization
num_features = 2;
features_A = zeros(num_features, length(zx)-1);
features_B = zeros(num_features, length(zx)-1);
features_C = zeros(num_features, length(zx)-1);
features = zeros(num_features, length(zx)-1);

```

```
% Computation of the two features
for i=1:length(zx)-1
  % Indexes of zero crossing
  t_feat_1 = find(phase_A.Time>t(zx(i)), 1);
  t_feat_2 = find(phase_A.Time>t(zx(i+1)), 1);

  % CF
  features_A(1,i) = peak2rms(phase_A.Data(t_feat_1:t_feat_2));
  features_B(1,i) = peak2rms(phase_B.Data(t_feat_1:t_feat_2));
  features_C(1,i) = peak2rms(phase_C.Data(t_feat_1:t_feat_2));
  features(1,i) = (features_A(1,i) ...
    + features_B(1,i) + features_C(1,i)) / 3;

  %% RMS
  features_A(2,i) = rms(phase_A.Data(t_feat_1:t_feat_2));
  features_B(2,i) = rms(phase_B.Data(t_feat_1:t_feat_2));
  features_C(2,i) = rms(phase_C.Data(t_feat_1:t_feat_2));
  features(2,i) = (features_A(2,i) ...
    + features_B(2,i) + features_C(2,i)) / 3;
end
```

In the end, the *features* vector contains the CF feature, period per period, in the first line and the RMS feature, period per period, in the second line.

At this point, the CD algorithm can be applied.

9.3 Phase III: Change detection

The CD algorithm is applied to the extracted features. Each experiment is performed in a different date and in the same (nominal) condition. Then, the final scores $\Pi(q)$ (see 8.23) were computed for each dataset comparison q. Different implementations are necessary depending on the type of the comparison to be achieved. As stated in section 8.2.2, there are three different comparison policies: always healthy, always previous and always last change. Three subsections are devoted to the implementation of each policy, at the end of this section. However, first, a common phase of CD initialization is needed, following the logic described in 8.2.2. Then, the RuLSIF method is implemented as a function, taking as inputs the reference feature *exp_1*, the current feature to compare *exp_2*, *dlt* is the kernel width δ, *lmb* is λ and controls the regularization strength, and the alpha and k parameters, returning rPE the α-relative Pearson divergence PE_α. As stated, the hyperparameters δ and λ are chosen via κ-fold cross-validation.

Here follows the code, that is simplified for a better understanding:

```
function[rPE] = RuLSIF(exp_1,exp_2,alpha,k)

%% Parameter Initialization Section
[¬,n_1] = size(exp_1);
[¬,n_2] = size(exp_2);
% Max 100 samples for computational reasons
b = min(100, n_nu);
idx = randperm(n_nu);
% Data permutation
x_ce = x_2(:, idx(1:b));
% Gaussian centers construction
[¬, n_ce] = size(x_ce);
% Getting dlt candidates
x = [exp_1, exp_2];
% Median distance between samples
med = comp_med(x);
dlt_list = med * [.6, .8, 1.0, 1.2, 1.4];
% Lambda candidates
lmb_list = 10.^[-3:1:1];
% Distance computation
[dist2_1] = comp_dist(x_1, x_ce);
[dist2_2] = comp_dist(x_2, x_ce);

%% Cross validation
score = zeros(length(dlt_list),length(lmb_list));
for i = 1:length(dlt_list)
    k_1 = kernel_gau(dist2_1, dlt_list(i));
    k_2 = kernel_gau(dist2_2, dlt_list(i));
    for j = 1:length(lmb_list)
        cv_index_1 = randperm(n_2);
        cv_split_1 = floor([0:n_2-1]*fold./n_2)+1;
        cv_index_2 = randperm(n_1);
        cv_split_2 = floor([0:n_1-1]*fold./n_1)+1;
        sum = 0;
        for kk = 1:k
            k_1_k = k_1(cv_index_1(cv_split_1≠kk),:)';
            k_2_k = k_2(cv_index_2(cv_split_2≠kk),:)';
            H_k = ((1-alpha)/size(k_1_k,2)) * (k_1_k * k_1_k') ...
                  + (alpha/size(k_2_k,2)) * (k_2_k * k_2_k');
            h_k = mean(k_2_k,2);
            theta = (H_k + eye(n_ce)*lmb_list(j))\h_k;
            k_1_test = k_1(cv_index_1(cv_split_1==kk),:)';
            k_2_test = k_2(cv_index_2(cv_split_2==kk),:)';
            % Objective function value
```

```
45              J = alpha/2 * mean((theta' * k_2_test).^2) ...
46                  + (1-alpha)/2*mean((theta' * k_1_test).^2) ...
47                  - mean(theta' * k_2_test);
48              sum = sum + J;
49          end
50          score(i,j) = sum/k;
51      end
52  end
53  % Find the chosen dlt and lambda
54  [i_min,j_min] = find(score==min(score(:)));
55  dlt_chosen = dlt_list(i_min);
56  lmb_chosen = lmb_list(j_min);
57
58  %% Final score computation
59  k_1 = kernel_gau(dist2_1', dlt_chosen);
60  k_2 = kernel_gau(dist2_2', dlt_chosen);
61  H = ((1-alpha)/n_1)* (k_1 * k_1') + (alpha/n_2) * (k_2 * k_2');
62  h = mean(k_2, 2);
63  theta = (H + eye(n_ce)*lmb_chosen)\h;
64  g_2 = theta'*k_2;
65  g_1 = theta'*k_1;
66  g_re = [];
67  if not isempty(x_re)
68      dist2_re = comp_dist(x_re, x_ce);
69      k_re = kernel_gau(dist2_re', sigma_chosen);
70      g_re = theta' * k_re;
71  end
72  rPE = 1/2 * mean(g_2) - 1/2;
73
74  end
```

where *comp_med*, *comp_dist* and *kernel_gau* compute, respectively, the median, the distance and the gaussian kernel and are functions implemented as follows:

```
1  function [med] = comp_med(x)
2
3  [d,n] = size(x);
4  G = sum(x.*x,1);
5  T = repmat(G,n,1);
6  dist = T - 2*x'*x + T';
7  dist = dist - tril(dist);
8  R = dist(:);
9  med = sqrt(.5 * median(R(R>0)));
10 end
```

```
function [dist] = comp_dist(x,y)

[d, nx] = size(x);
[d, ny] = size(y);
G = sum(x.*x,1);
T = repmat(G,ny,1);
G = sum(y.*y,1);
R = repmat(G,nx,1);
dist = T' + R - 2.*x'*y;
end
```

```
function [k] = kernel_gau(dist, sigma)

k = exp(-dist/(2*sigma^2));
end
```

Now that all the functions have been explained, the main functionality of the CD algorithm is presented in the next sections, depending on the adopted policy.

9.3.1 Always healthy policy

In the Always Healthy (AH) policy the reference features are extracted from the system in healthy state and remains the same for all the CD algorithm execution. In other words, the new extracted features are compared always with the first extracted features in nominal conditions. The final score, thus, is obtained from the comparison of tests q, where $q = 2, ..., Q$ (being Q the total number of experimental tests), with the test having $q = 1$, as implemented below:

```
%% Change Detection parameters initialization
% Hyperparameter of the method
alpha = 0.5;
% Number of cross validation folds
k = 5;

%% AH policy
% Initialization
score_AH = nan(Q,1);
for tt = 2 : 1 : Q
  exp_1 = features{1}; % features from experiment 1
  exp_2 = features{tt}; % features from experiment tt
  % Compute score in both directions
```

```
14    s1 = RuLSIF(exp_1,exp_2,alpha,k);
15    s2 = RuLSIF(exp_2,exp_1,alpha,k);
16    % Final score computation
17    score_AH(tt) = s1 + s2;
18    % Set to zero negative results
19    if score_AH(tt) ≤ 0
20      score_AH(tt) = 0;
21    end
22  end
```

where $score\_AH(tt)$ is the final score $\Pi(q)$. The final score is set to zero at each cycle in case it is negative.

It is easily demonstrable that this policy can be effective in evidencing deviations from the nominal behavior, but do not perform well in assessing the grade of deterioration or the severity of the faults. In fact, the score computed with the AH policy rapidly reaches a high value at the first evidence of deterioration, but it does not increase anymore even in case of an increase of the actuators degradation.

9.3.2 Always previous policy

The policy Always Previous (AP) compares each dataset with the previous one. In other words, the AP works similarly to the AH policy but updating the reference features at each cycle. The new extracted features are thus compared always with the previous extracted features, as implemented next:

```
1  %% Change Detection parameters initialization
2  % Hyperparameter of the method
3  alpha = 0.5;
4  % Number of cross validation folds
5  k = 5;
6
7  %% AH policy
8  % Initialization
9  score_AP = nan(Q,1);
10 for tt = 2 : 1 : Q
11   exp_1 = features{tt};
12   exp_2 = features{tt-1};
13   % Compute score in both directions
14   s1 = RuLSIF(exp_1,exp_2,alpha,k);
15   s2 = RuLSIF(exp_1,exp_2,alpha,k);
16   % Final score computation
```

```
17    score_AP(tt) = s1 + s2;
18    % Set to zero negative results
19    if score_AP(tt) ≤ 0
20      score_AP(tt) = 0;
21    end
22  end
```

where Q is the number of the experimental tests and $score\_AP(tt)$ is the final score $\Pi(q)$, that is set to zero if negative during each cycle.

This approach can track better the general trend of degradation of the actuator but is less sensitive to slow changes in the motor degradation. In fact, by always comparing the current experiment to the previous one, the actual data can show a small deviation from the previous data even though both datasets are referred to a deteriorated condition. As a consequence, the AP policy can produce smaller scores.

9.3.3 Last change policy

The Last Change (LC) strategy compares each new experiment with the last one that gave a *large* value of the score $\Pi(q)$. A $\Pi(q)$ score is defined *large* if it exceeds a threshold η at a value that is two times larger than the first score computed, which is the computed difference between the first two consecutive healthy datasets (in this case $thr = 0.81$). This threshold can be refined in various ways, for instance averaging more scores from different healthy datasets. Then, a degradation counter $\rho(q)$ (cum_LC in the code) is defined, which counts the tests that produced a score $\Pi(q)$ greater than the threshold η. All this is implemented:

```
1  %% Change Detection parameters initialization
2  % Hyperparameter of the method
3  alpha = 0.5;
4  % Number of cross validation folds
5  k = 5;
6
7  %% LC policy
8  % Initialization
9  score_LC = nan(n_test,1);
10 cum_LC = zeros(n_test,1);
11 thr = 0.81;
12 exp_to_compare = features{1};
13 for tt = 2 : 1 : n_test
14   exp_2 = features{tt};
```

```
15    s1 = RuLSIF(exp_1,exp_2,alpha,k);
16    s2 = RuLSIF(exp_1,exp_2,alpha,k);
17    score_LC(tt) = s1 + s2;
18    if score_LC(tt) ≤ 0
19      score_LC(tt) = 0;
20    end
21    if score_LC(tt) > thr
22      exp_to_compare = features{tt};
23      cum_LC(tt) = 1;
24    end
25  end
26  cum_LC = cumsum(cum_LC);
```

This counter gives an information coherent with the status of degradation of the actuator, as explained also in the next section, in which the results of the CD algorithm are presented.

CHAPTER 10

Testing and results of the Health Monitoring System

This chapter discuss the testing and results of the HM system based on CD algorithms. The CD algorithm has been applied on a total of 11 experimental tests of the endurance type, which have been executed from September to October 2017 (see section 6 and 6.2.3), with degrading condition of the actuator (from health, through low lubricant, to the absence of lubricant in the ballscrew). Only the measurements obtained by the input reference sinusoids at 10mm and the input reference load at 300N have been considered as exemplification.

A resumption with all the considered tests has been reported in table 10.1.

First, the trends of the considered features, RMS and CF, are analyzed. Then, the results of the CD application to such feature are illustrated.

Table 10.1: Considered tests during the CD algorithm application

Test number (q)	Date (2017)	Lubricant status
1	11 September	Normal lubrication
2	18 September	Normal lubrication
3	21 September	Poor lubrication
4	25 September	Poor lubrication
5	02 October	No lubrication
6	02 October	No lubrication
7	03 October	No lubrication
8	04 October	No lubrication
9	09 October	No lubrication
10	11 October	No lubrication
11	12 October	No lubrication

10.1 Experimental assessment results: RMS

Figure 10.1 depicts the distribution of the RMS feature $\Sigma(\tau)$ computed using measurements at the input frequency of 1Hz. Each element of the time series is a value of $\Sigma(\tau)$. Light gray vertical lines indicate the end of one experiment and the beginning of another one. There are in total 11 sections in the plots, corresponding to the 11 experiments performed. The 11 tests are depicted in chronological order (from the first, on the left, to the last, on the right). Results of Figure 10.1 show that the increasing of harshness conditions is responsible for the damaging of the actuator, causing a higher current drain to perform the same duty, that ends into higher RMS mean values.

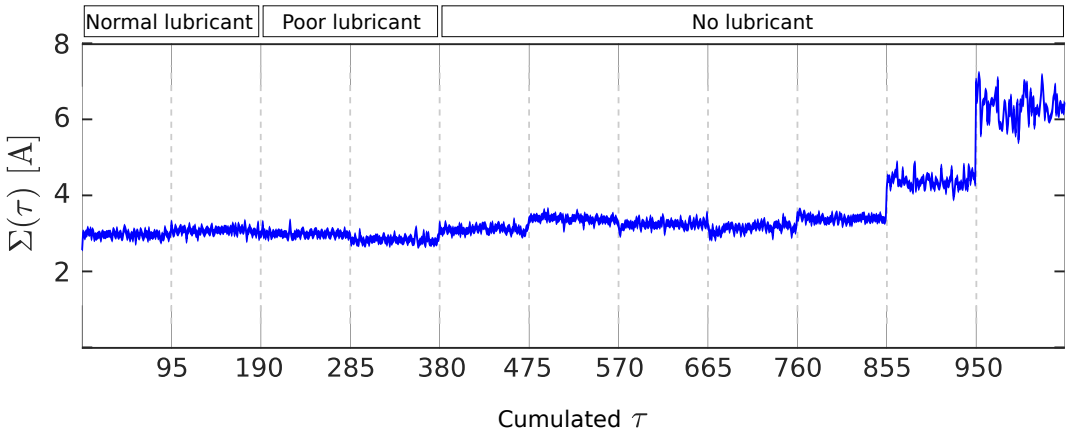

Figure 10.1: Time evolution of the RMS feature Σ at 1Hz

In Figure 10.1, the sensitivity of the RMS feature to the measurement

frequency is shown. Instead of plotting the computed RMS feature over time, box plots in Figure 10.2 are used to represent the sampling distribution of the RMS feature obtained in each different test. There are 6 groups of box plots, one for each considered frequency: 0.1Hz, 0.3Hz, 0.5Hz, 0.8Hz, 0.9Hz, 1Hz, which is basically the design bandwidth of the actuator. Each group is made by 11 boxplots, one for each experimental test (2 in normal lubricant condition, 2 in poor lubricant condition and 7 in no lubricant condition). The 11 tests are depicted in chronological order (from the first, the number 1 in green on the left, to the last, the number 11 in black on the right in each boxplot). Figure 10.2, therefore, compares the sampling distribution of $\Sigma(\tau)$ at different measurement frequencies and at the different test dates.

Figure 10.2 represents a zoom of the information displayed in Figure 10.2, at the frequency of 0.8Hz. In this picture, at first an initial decrease in RMS value is given probably due to the actuator break-in but then it is strongly evident that the RMS feature is able to detect the effects of the actuator absence of lubrication. In fact, the mean value of the computed RMS feature is significantly increasing and, also, the dispersion is similarly increasing.

The effect of the incipient fault is better visible at higher frequencies. This can be determined by a series of factors related to the functioning of the EMA [118]. It is possible to observe characteristic frequencies for each fault (and incipient fault) that may not be directly related to the frequency under consideration. However, the information displayed in Figures 10.1, 10.2 and 10.3 show that the RMS feature $\Sigma(\tau)$ is sensitive to changes of the actuator health state, and thus could be used as an input information for the HM algorithm.

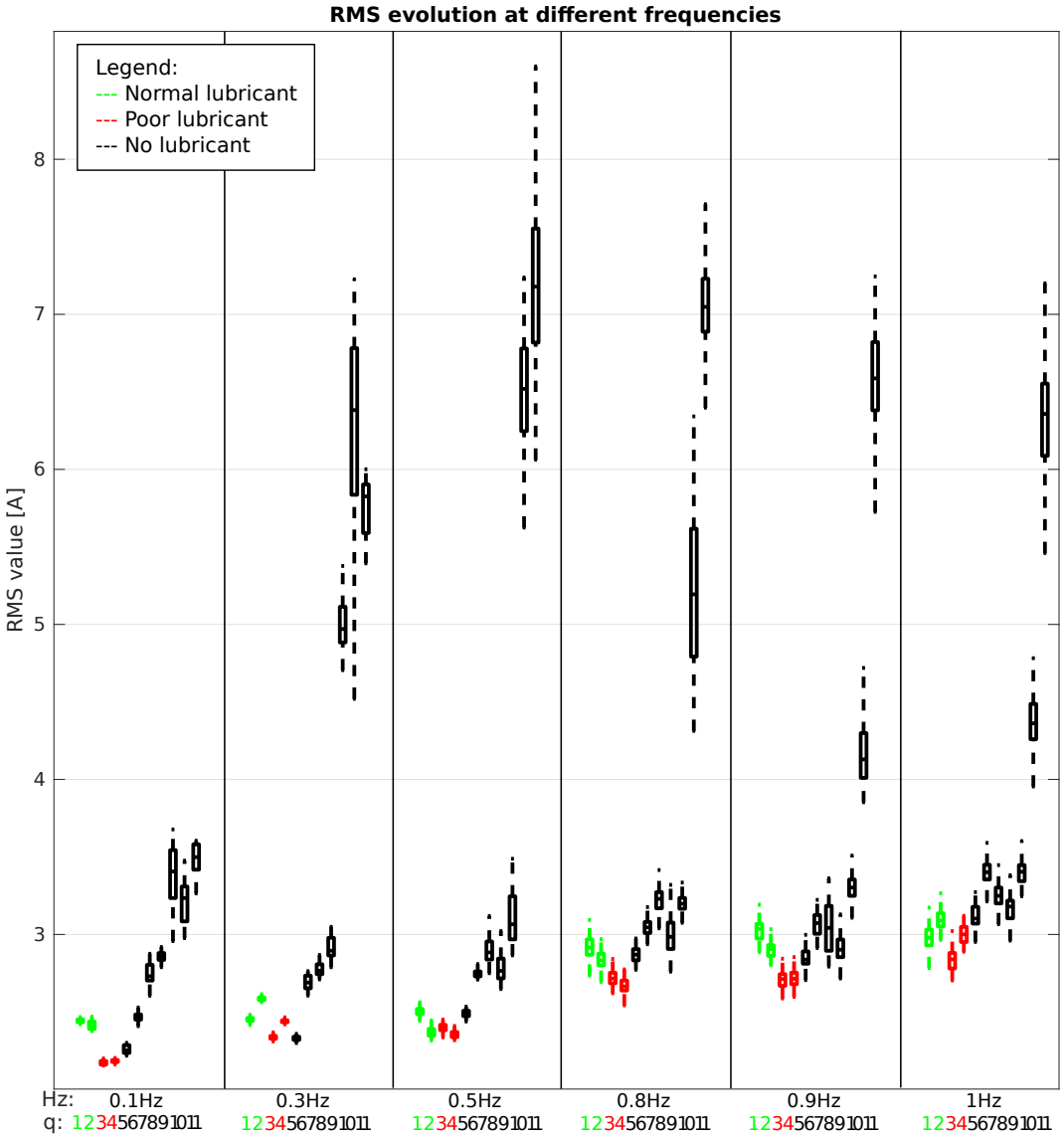

Figure 10.2: RMS evolution in time at different frequencies

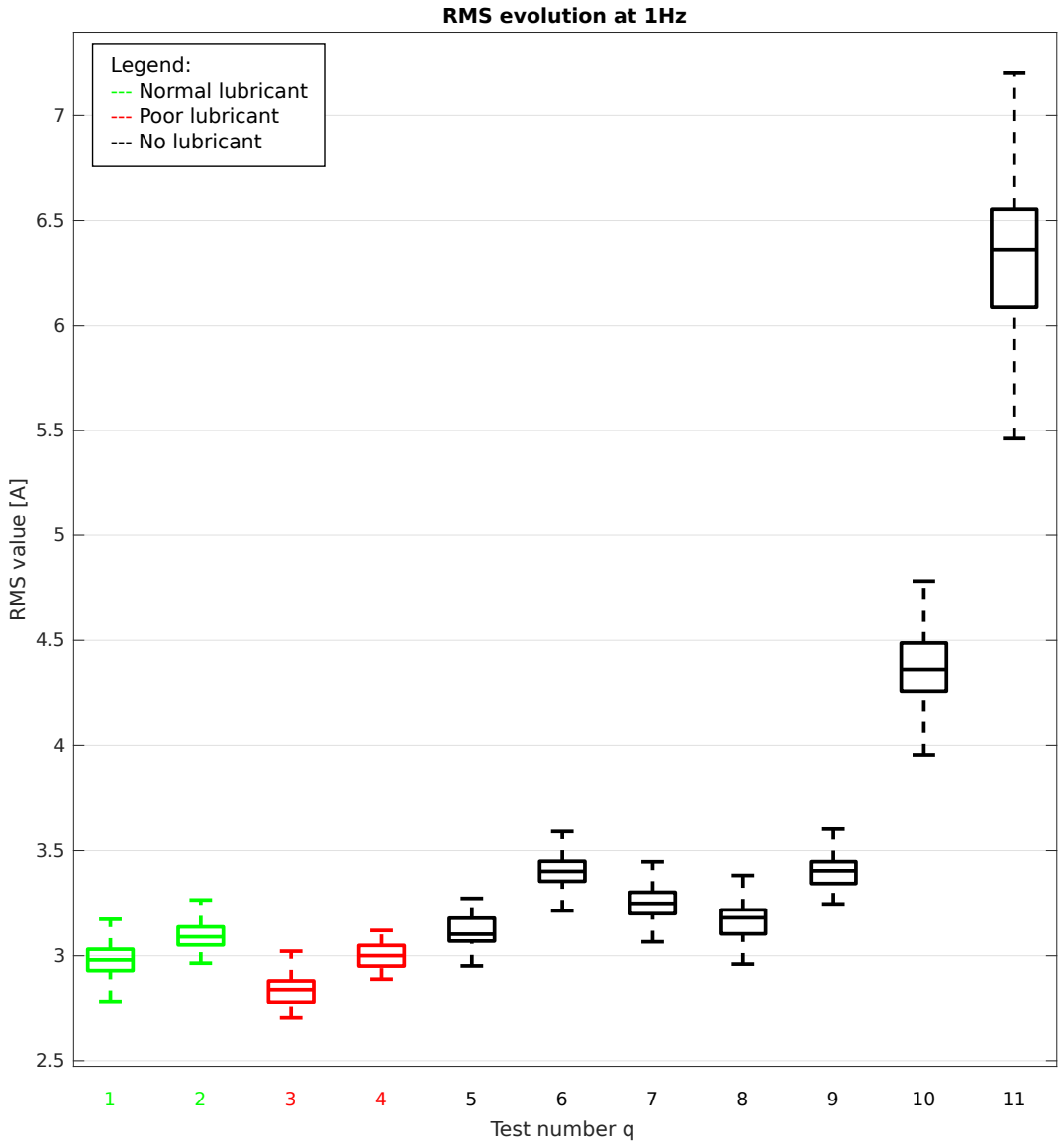

Figure 10.3: RMS evolution in time at 1Hz (zoom of the previous Figure)

10.2 Experimental assessment results: CF

The CF feature $\Gamma(\tau)$ has been computed using the same measurements used to compute the RMS features (in the same 11 different test dates). Figure 10.4, similarly as Figure 10.1 for the RMS feature, represents the time evolution of the CF feature, computed using all the measurements at 1Hz. Light gray vertical lines indicate the end of one experiment and the beginning of another one. In this case as well, there are in total 11 sections in the plot, corresponding to the 11 experiments performed in the aforementioned dates. The 11 tests are depicted in chronological order (from the first, on the left, to the last, on the right). Results show a progressive decrease in the value of the CF feature. It is worth noting that the CF feature is less reactive than the RMS feature and the change of its value is gradual as the health of the EMA deteriorate.

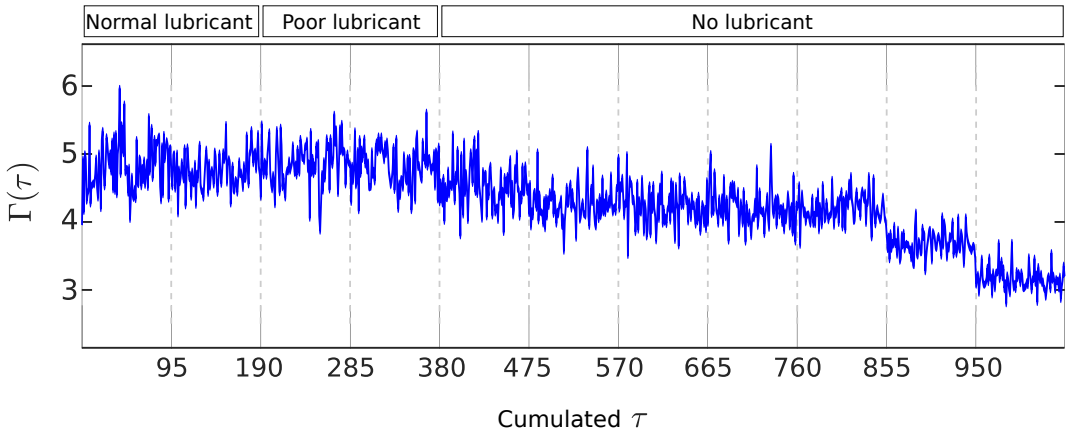

Figure 10.4: Time evolution of the CF feature Γ at 1Hz

Similarly as for the RMS feature, Figure 10.5 represents the variation over time and over frequency of the statistical distribution of the CF feature using a box plot representation. There are 6 groups of box plots, one for each considered frequency: 0.1Hz, 0.3Hz, 0.5Hz, 0.8Hz, 0.9Hz, 1Hz. Each group is made by 11 boxplots, one for each experimental test (2 in normal lubricant condition, 2 in poor lubricant condition and 7 in no lubricant condition). The 11 tests are depicted in chronological order (from the first, the number 1 in green on the left, to the last, the number 11 in black on the right in each boxplot). Correlation of this indicator with the actuator degradation is less evident with respect to the RMS feature (compare Figure 10.5 with Figure 10.2). However, especially at higher frequencies, the CF feature shows a clear decreasing trend correlated with the actuator degradation.

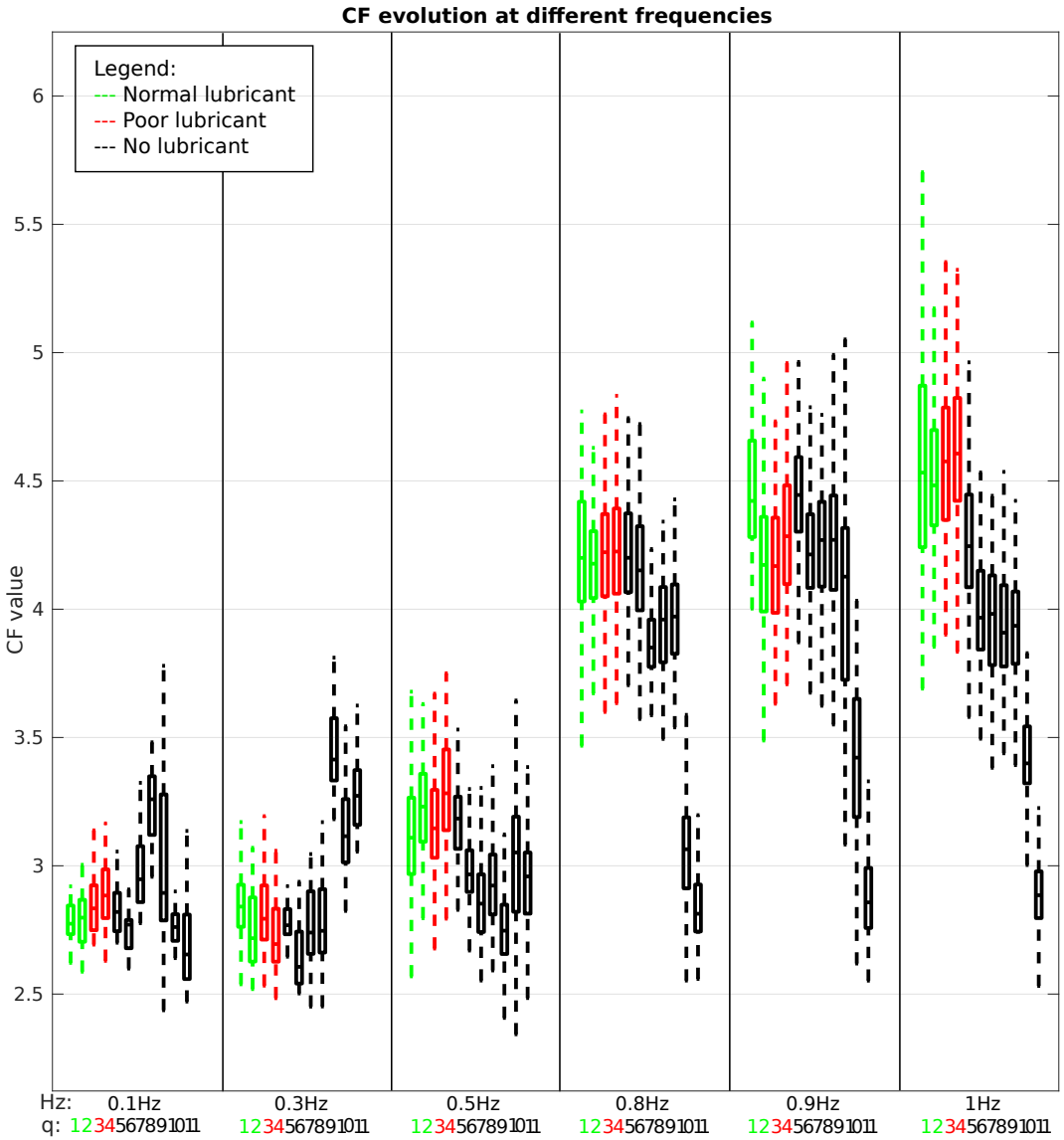

Figure 10.5: CF evolution in time at different frequencies

Figure 10.6 depicts a detail of Figure 10.5, at the frequency of 1Hz. Notice that there is a significant decrease of the mean value of the distribution, but its dispersion is not changing, contrary to the RMS feature.

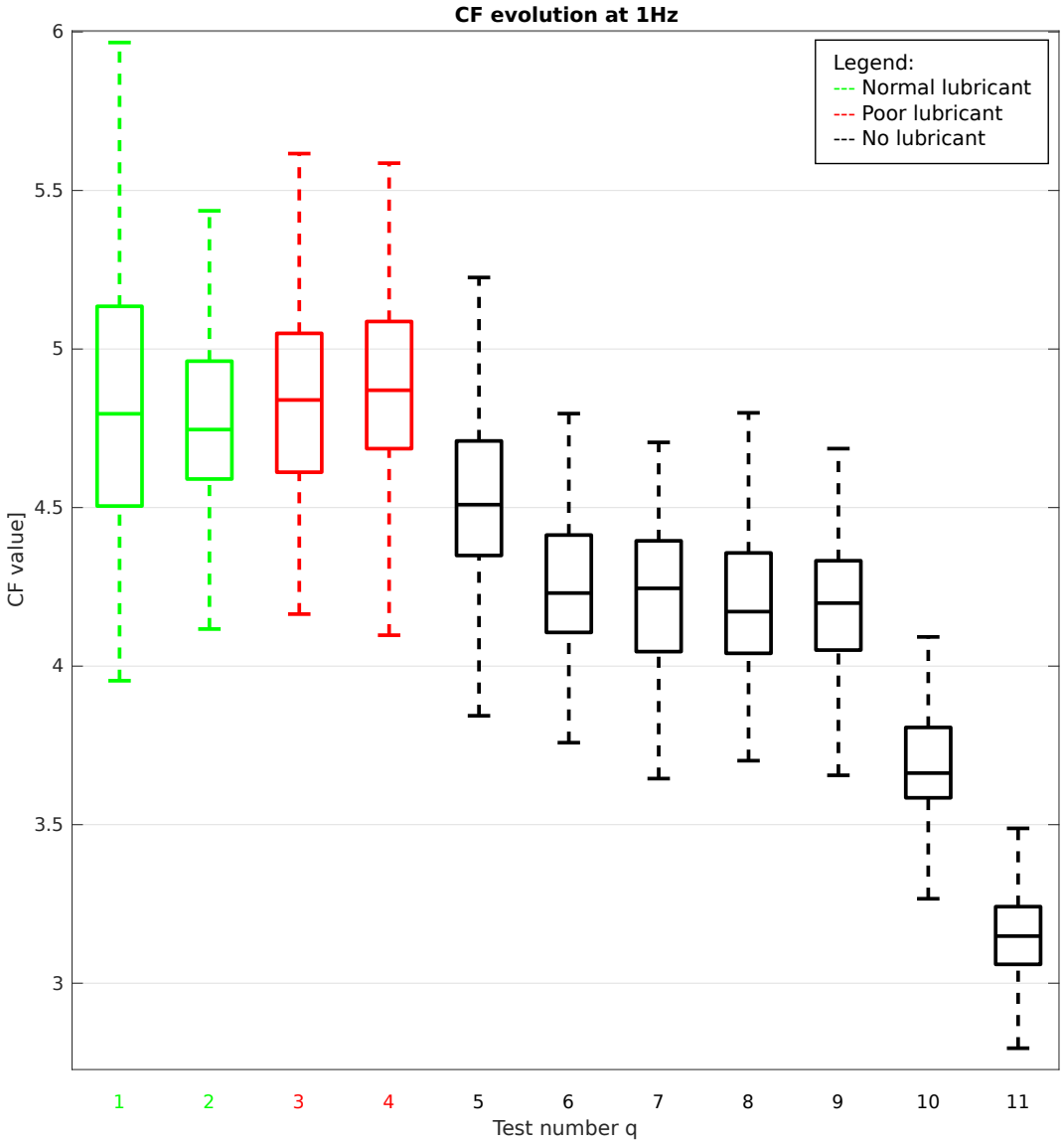

Figure 10.6: CF evolution in time at 1Hz (zoom of the previous Figure)

Results show that this indicator could be used for HM since it changes significantly its value when the actuator undergoes stressing operating conditions. The HM system relies on a CD algorithm, as discussed in this and in the previous chapters. Next, the final results are presented and discussed.

10.3 Experimental assessment: CD algorithm

The CD algorithm has been applied to the features $\Sigma(\tau)$ and $\Gamma(\tau)$, that have been computed for a discrete range of operating frequencies: 0.1Hz, 0.3Hz, 0.5Hz, 0.8Hz, 0.9Hz and 1Hz. This range of frequencies is that for which the EMA has been designed. In the present work, the application of the CD method to measurements at the frequency of 1Hz is reported as exemplification. The frequency value is not a critical parameter and similar results can be obtained also using data from experiments at different frequencies. For the purpose of the project, we applied the change detection algorithm in a batch modality (see section 8.2.2). Thus, the algorithm compares the features computed on the new experiment with the past ones. The rationale of applying a batch procedure is mainly due to the certainty that the experiments are performed in the same external conditions since the algorithm is designed to work in controlled test conditions. As stated, the method requires a policy to choose the reference measures to be compared with the newly acquired ones. In the following, all three different policies are compared (Always Healthy (AH), Always Previous (AP) and Last Change (LC)).

For the application of the proposed methodology, we consider a total of $Q = 11$ test experiments. The first 2 of these tests can be considered as healthy state experiments. Tests 3 and 4 have been performed after endurance sessions with poor lubricant. The remaining tests have been performed after endurance sessions with no lubricant at all.

In Figure 10.7 the results of the HM system via three different CD strategies, using a 1Hz sinusoidal position reference are depicted. Vertical light gray bars represent the different experiments. The last plot depicts also the threshold η (dashed horizontal gray line) and the degradation score $\rho(q)$. This counter is represented in the last plot of Figure 10.7 (red diamonds), and gives an information coherent with the degradation of the actuator. In fact, it is monotone increasing and reactive also to slow changes in the features.

The proposed solution has been tested at other frequencies with respect to the 1Hz frequency of Figure 10.7. The results are in line with what expected. In Figure 10.8, the described policies are tested on current measurement acquired with a 0.8Hz sinusoidal position profile. Results are in line with those reported in Figure 10.7. It is possible to observe a clear degradation detected by the indicators in the last two tests with no lubricant. The algorithm correctly detects the changes.

Figure 10.9 shows the proposed strategies tested with current measurements acquired with a 0.1Hz sinusoidal position reference profile. Although the changes

in RMS and CF are less evident at low frequencies (due to a less demanding duty for the actuator) the algorithm is able to detect changes in experimental condition. The score $\rho(q)$ reaches a level similar to those of Figure 10.7 and Figure 10.8. This observation suggests that, even if the algorithm is able to perform correctly at lower frequencies, higher ones are more likely to enhance the detection of a degradation.

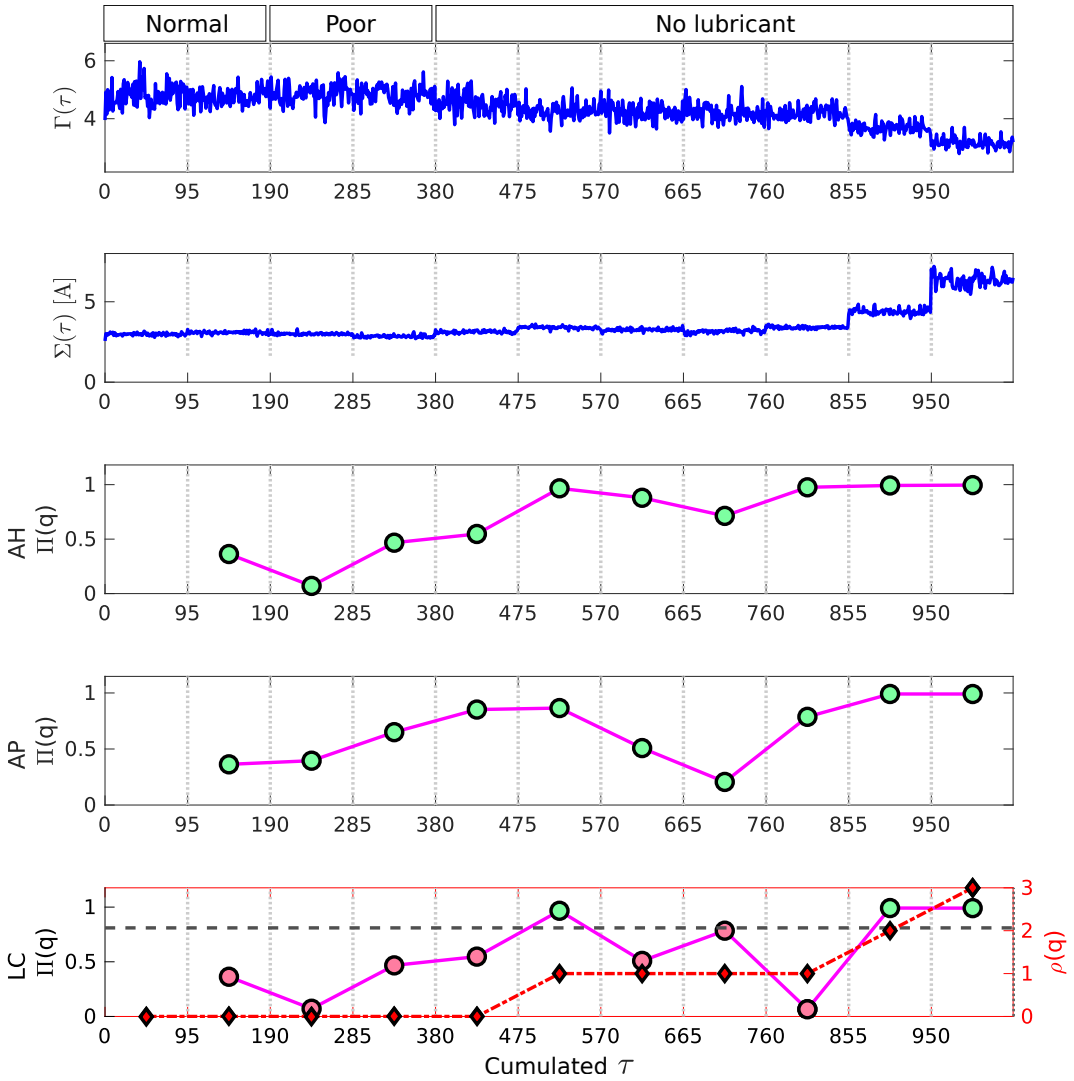

Figure 10.7: Results of the HM via three CD strategies with 1Hz input reference

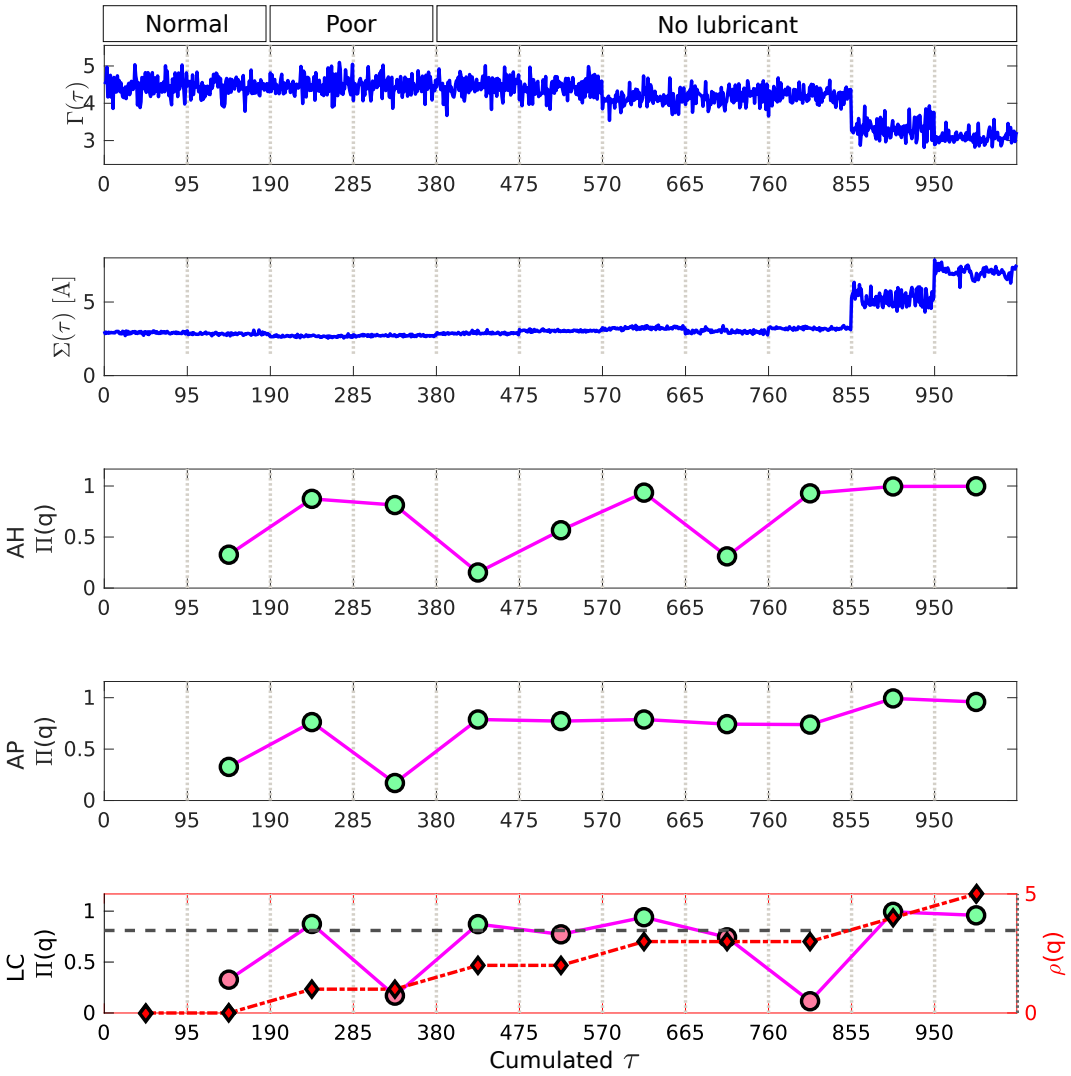

Figure 10.8: Results of the HM via three CD strategies with 0.8Hz input reference

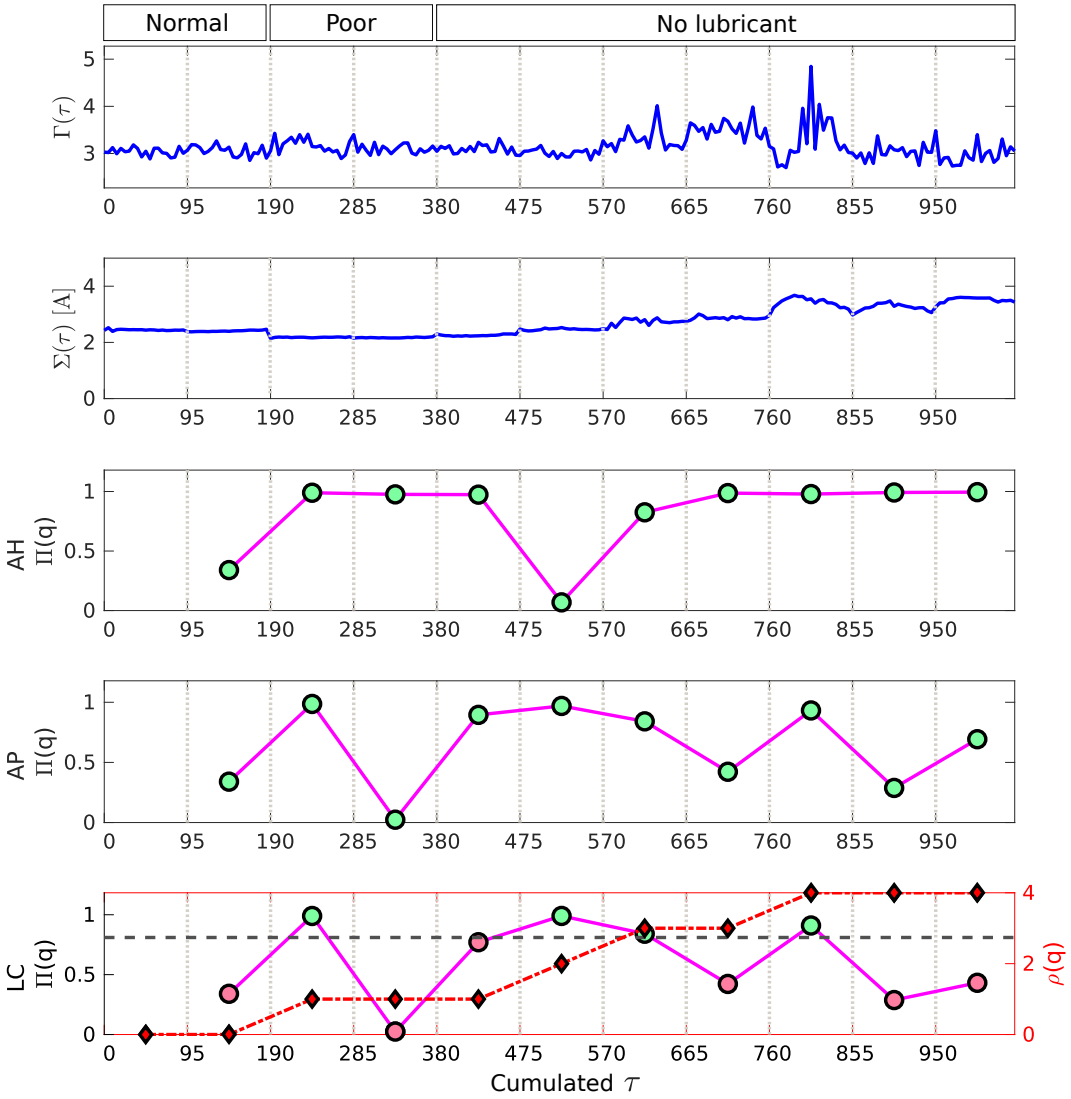

Figure 10.9: Results of the HM via three CD strategies with 0.1Hz input reference

CHAPTER 11

Conclusions and future directions

This thesis has investigated the matter of Health Monitoring (HM) via Change Detection (CD) methods based on statistical Fault Detection and Identification (FDI) techniques for the Condition Assessment (CA) of the status of degradation of the mechanical parts of an aeronautical Electro-Mechanical Actuator (EMA).

Part I: State of the art An up-to-date survey has been carried out on the state of the art of these topics in the first part of the manuscript, giving common definitions and nomenclatures in chapter 1 and considering a general approach to the matter of HM and FDI in chapter 2, describing model-based, signal-based, knowledge-based and hybrid methods. In chapter 3 great attention has been given on practical applications and analyses in the aerospace environment, giving explanations of Failure Modes and Effects Critical Analysis (FMECA) and Probabilistic Risk Assessment (PRA) and Fault Tree Analysis (FTA). Chapter 4 concludes the first part of this thesis providing an example of a FMECA on an aeronautical EMA.

Part II: Experimental setup The results of this work have been validated by means of experimental tests carried out on a test rig, described in chapter 5, in which the EMA moves a linear motor that acts as the aerodynamic counteracting load of the air on flying surfaces. The experimental tests have been carried out following a rigid procedure that is showed in chapter 6, together with the listing of the executed tests. An analysis has been carried out on the actuator to assess its

performances over time, in chapter 7. The experimental measurements revealed that the EMA maintains the same performance in achieving its primary goal (that is the reference position following task) even after degradation of the mechanical parts, in particular of the ballscrew, proved by visual inspections. For this reason the HM algorithm assumes even more importance from a CA perspective.

Part III: Health Monitoring based on Change Detection algorithms In the third part, the HM system, that is based on CD algorithms, is presented and explained together with the concepts that lay behind the final development, such as the RuLSIF algorithm, in chapter 8. The MATLAB implementation of the entire algorithm is reported in chapter 9. In the end, the work has been tested and validated in chapter 10, and considerations has been stated. Three different CD policies (Always Healthy (AH), Always Previous (AP) and Last Change (LC)) have been considered, implemented and tested, obtaining a more robust result and generalizing the proposed approach. The LC policy has been proved to provide the best response, adhering to the status of degradation of the EMA.

Future directions Now that the HM has been implemented and tested, several ways are opened for the next future:

- The HM system will soon be embedded in the ECU of the EMA and thus will be able to monitor real-time the status of degradation of the mechanical parts
- Additional tests are undergoing, to date. Hence, additional information and knowledge will be stored and the algorithm could be perfected or integrated with other FDI techniques
- Thanks to the large amount of collected data, a study on the prevision of the Remaining Useful Life (RUL) may be achieved
- If good results could be obtained by the RUL analysis, then the final achievement of the Predictive Maintenance can be accomplished, with enormous costs savings and overall reliability improvement

Bibliography

[1] R. Isermann and P. Balle, "Trends in the application of model-based fault detection and diagnosis of technical processes," Control engineering practice, vol. 5, no. 5, pp. 709–719, 1997.

[2] D. Henry, S. Simani, and R. J. Patton, "Fault detection and diagnosis for aeronautic and aerospace missions," in Fault tolerant flight control, pp. 91–128, Springer, 2010.

[3] R. J. Patton and J. Chen, "Robust model-based fault diagnosis for dynamic systems," 1999.

[4] P. M. Frank, "Analytical and qualitative model-based fault diagnosis–a survey and some new results," European Journal of control, vol. 2, no. 1, pp. 6–28, 1996.

[5] E. Y. Chow and A. S. Willsky, "Issues in the development of a general design algorithm for reliable failure detection," 1980.

[6] Z. Gao, C. Cecati, and S. X. Ding, "A survey of fault diagnosis and fault-tolerant techniques—part i: Fault diagnosis with model-based and signal-based approaches," IEEE Transactions on Industrial Electronics, vol. 62, no. 6, pp. 3757–3767, 2015.

[7] R. Isermann, Fault-diagnosis systems: an introduction from fault detection to fault tolerance. Springer Science & Business Media, 2006.

[8] R. Isermann, Combustion Engine Diagnosis. Springer Berlin Heidelberg, 2017.

[9] R. Isermann, Fault-diagnosis applications: model-based condition monitoring: actuators, drives, machinery, plants, sensors, and fault-tolerant systems. Springer Science & Business Media, 2011.

[10] R. Isermann, "Model-based fault-detection and diagnosis–status and applications," Annual Reviews in control, vol. 29, no. 1, pp. 71–85, 2005.

[11] D. van Schrick, "Remarks on terminology in the field of supervision, fault detection and diagnosis," IFAC Proceedings Volumes, vol. 30, no. 18, pp. 959–964, 1997.

[12] A. S. Willsky, "A survey of design methods for failure detection in dynamic systems," Automatica, vol. 12, no. 6, pp. 601–611, 1976.

[13] D. M. Himmelblau, Fault detection and diagnosis in chemical and petrochemical processes. Elsevier Scientific Publishing Company New York, 1978.

[14] R. Isermann, "Process fault detection based on modeling and estimation methods—a survey," automatica, vol. 20, no. 4, pp. 387–404, 1984.

[15] P. M. Frank, "Fault diagnosis in dynamic systems using analytical and knowledge-based redundancy: A survey and some new results," automatica, vol. 26, no. 3, pp. 459–474, 1990.

[16] R. Isermann and B. Freyermuth, "Process fault diagnosis based on process model knowledge," Advanced Information Processing In Automatic Control, pp. 21–34, 1990.

[17] R. Isermann, "Supervision, fault-detection and fault-diagnosis methods—an introduction," Control engineering practice, vol. 5, no. 5, pp. 639–652, 1997.

[18] J. Gertler, Fault detection and diagnosis in engineering systems. CRC press, 1998.

[19] M. Blanke, M. Kinnaert, J. Lunze, M. Staroswiecki, and J. Schröder, Diagnosis and fault-tolerant control, vol. 691. Springer, 2006.

[20] S. X. Ding, Model-based fault diagnosis techniques: design schemes, algorithms, and tools. Springer Science & Business Media, 2008.

[21] J. Chen and R. J. Patton, Robust model-based fault diagnosis for dynamic systems, vol. 3. Springer Science & Business Media, 2012.

[22] R. J. Patton, P. M. Frank, and R. N. Clark, Issues of fault diagnosis for dynamic systems. Springer Science & Business Media, 2013.

[23] P. M. Frank and X. Ding, "Survey of robust residual generation and evaluation methods in observer-based fault detection systems," Journal of process control, vol. 7, no. 6, pp. 403–424, 1997.

[24] J. Gertler, "Analytical redundancy methods in fault detection and isolation-survey and synthesis," IFAC Proceedings Volumes, vol. 24, no. 6, pp. 9–21, 1991.

[25] J. Gertler, Fault detection and diagnosis in engineering systems. Routledge, 2017.

[26] X. Ding and P. Frank, "Frequency domain approach and threshold selector for robust model-based fault detection and isolation," in Fault Detection, Supervision and Safety for Technical Processes 1991, pp. 271–276, Elsevier, 1992.

[27] A. Emami-Naeini, M. M. Akhter, and S. M. Rock, "Effect of model uncertainty on failure detection: the threshold selector," IEEE Transactions on Automatic Control, vol. 33, no. 12, pp. 1106–1115, 1988.

[28] C. Bishop, C. M. Bishop, et al., Neural networks for pattern recognition. Oxford university press, 1995.

[29] P. Frank and N. Kiupel, "Fuzzy supervision and application to lean production," International journal of systems science, vol. 24, no. 10, pp. 1935–1944, 1993.

[30] L. Ljung, System identification. Wiley Online Library, 1999.

[31] I. Gustavsson, L. Ljung, and T. Söderström, "Identification of processes in closed loop—identifiability and accuracy aspects," Automatica, vol. 13, no. 1, pp. 59–75, 1977.

[32] G. Maroni, "Il filtro particellare per la diagnostica dei guasti in ambito aerospaziale." unpublished thesis, 2015.

[33] L. Liang-Qun, J. Hong-Bing, and L. Jun-Hui, "The iterated extended kalman particle filter," in Communications and Information Technology, 2005. ISCIT 2005. IEEE International Symposium on, vol. 2, pp. 1213–1216, IEEE, 2005.

[34] M. E. Orchard and G. J. Vachtsevanos, "A particle-filtering approach for on-line fault diagnosis and failure prognosis," Transactions of the Institute of Measurement and Control, vol. 31, no. 3-4, pp. 221–246, 2009.

[35] D. ZHOU, Y. XI, and Z. ZHANG, "Non-linear adaptive fault detection filter," International journal of systems science, vol. 22, no. 12, pp. 2563–2571, 1991.

[36] X. Koutsoukos, J. Kurien, and F. Zhao, "Monitoring and diagnosis of hybrid systems using particle filtering methods," in International Symposium on Mathematical Theory of Networks and Systems, 2002.

[37] J. Marzat, H. Piet-Lahanier, F. Damongeot, and E. Walter, "Autonomous fault diagnosis: state of the art and aeronautical benchmark," in 3rd European Conference for Aero-Space Sciences, EUCASS'2009, p. 76, 2009.

[38] O. Chapelle, B. Scholkopf, and A. Zien, "Semi-supervised learning (chapelle, o. et al., eds.; 2006)[book reviews]," IEEE Transactions on Neural Networks, vol. 20, no. 3, pp. 542–542, 2009.

[39] N. M. Nasrabadi, "Pattern recognition and machine learning," Journal of electronic imaging, vol. 16, no. 4, p. 049901, 2007.

[40] J. Friedman, T. Hastie, and R. Tibshirani, The elements of statistical learning, vol. 1. Springer series in statistics New York, 2001.

[41] X. Zhu, "Semi-supervised learning literature survey," 2005.

[42] H. Ohlsson and L. Ljung, "Semi-supervised regression and system identification," in Three Decades of Progress in Control Sciences, pp. 343–360, Springer, 2010.

[43] P. A. Samara, G. N. Fouskitakis, J. S. Sakellariou, and S. D. Fassois, "A statistical method for the detection of sensor abrupt faults in aircraft control systems," IEEE Transactions on Control Systems Technology, vol. 16, no. 4, pp. 789–798, 2008.

[44] L. Hong and J. S. Dhupia, "A time domain approach to diagnose gearbox fault based on measured vibration signals," Journal of Sound and Vibration, vol. 333, no. 7, pp. 2164–2180, 2014.

[45] H. Chen and S. Lu, "Fault diagnosis digital method for power transistors in power converters of switched reluctance motors.," IEEE Trans. Industrial Electronics, vol. 60, no. 2, pp. 749–763, 2013.

[46] M. Shahbazi, E. Jamshidpour, P. Poure, S. Saadate, and M. R. Zolghadri, "Open-and short-circuit switch fault diagnosis for nonisolated dc-dc converters using field programmable gate array.," IEEE transactions on industrial electronics, vol. 60, no. 9, pp. 4136–4146, 2013.

[47] J. O. Estima and A. J. M. Cardoso, "A new algorithm for real-time multiple open-circuit fault diagnosis in voltage-fed pwm motor drives by the reference current errors," IEEE Transactions on Industrial Electronics, vol. 60, no. 8, pp. 3496–3505, 2013.

[48] N. M. A. Freire, J. O. Estima, A. J. M. Cardoso, et al., "Open-circuit fault diagnosis in pmsg drives for wind turbine applications," IEEE Transactions on Industrial electronics, vol. 60, no. 9, pp. 3957–3967, 2013.

[49] M. B. K. Bouzid and G. Champenois, "New expressions of symmetrical components of the induction motor under stator faults," IEEE Transactions on Industrial Electronics, vol. 60, no. 9, pp. 4093–4102, 2013.

[50] M. Mazzoleni, Y. Maccarana, and F. Previdi, "A comparison of data-driven fault detection methods with application to aerospace electro-mechanical actuators," IFAC-PapersOnLine, vol. 50, no. 1, pp. 12797–12802, 2017.

[51] Z. Feng and M. J. Zuo, "Fault diagnosis of planetary gearboxes via torsional vibration signal analysis," Mechanical Systems and Signal Processing, vol. 36, no. 2, pp. 401–421, 2013.

[52] N. Pan, X. Wu, Y. Chi, X. Liu, and C. Liu, "Combined failure acoustical diagnosis based on improved frequency domain blind deconvolution," in Journal of Physics: Conference Series, vol. 364, p. 012078, IOP Publishing, 2012.

[53] S. Nandi and H. A. Toliyat, "Condition monitoring and fault diagnosis of electrical machines-a review," in Industry Applications Conference, 1999. Thirty-Fourth IAS Annual Meeting. Conference Record of the 1999 IEEE, vol. 1, pp. 197–204, IEEE, 1999.

[54] M. E. H. Benbouzid, "A review of induction motors signature analysis as a medium for faults detection," IEEE transactions on industrial electronics, vol. 47, no. 5, pp. 984–993, 2000.

[55] G. M. Joksimović, J. Riger, T. M. Wolbank, N. Perić, and M. Vašak, "Stator-current spectrum signature of healthy cage rotor induction machines," IEEE Transactions on Industrial Electronics, vol. 60, no. 9, pp. 4025–4033, 2013.

[56] X. Gong and W. Qiao, "Bearing fault diagnosis for direct-drive wind turbines via current-demodulated signals," IEEE Transactions on Industrial Electronics, vol. 60, no. 8, pp. 3419–3428, 2013.

[57] Z. Feng, M. Liang, and F. Chu, "Recent advances in time–frequency analysis methods for machinery fault diagnosis: A review with application examples," Mechanical Systems and Signal Processing, vol. 38, no. 1, pp. 165–205, 2013.

[58] S. Nandi, T. C. Ilamparithi, S. B. Lee, and D. Hyun, "Detection of eccentricity faults in induction machines based on nameplate parameters," IEEE Transactions on Industrial Electronics, vol. 58, no. 5, pp. 1673–1683, 2011.

[59] Y. Gritli, L. Zarri, C. Rossi, F. Filippetti, G.-A. Capolino, and D. Casadei, "Advanced diagnosis of electrical faults in wound-rotor induction machines," IEEE Transactions on Industrial Electronics, vol. 60, no. 9, pp. 4012–4024, 2013.

[60] R. Yan and R. X. Gao, "Hilbert–huang transform-based vibration signal analysis for machine health monitoring," IEEE Transactions on Instrumentation and measurement, vol. 55, no. 6, pp. 2320–2329, 2006.

[61] V. Climente-Alarcon, J. A. Antonino-Daviu, M. Riera-Guasp, and M. Vlcek, "Induction motor diagnosis by advanced notch fir filters and the wigner–ville distribution," IEEE Transactions on Industrial Electronics, vol. 61, no. 8, pp. 4217–4227, 2014.

[62] J. F. MacGregor and T. Kourti, "Statistical process control of multivariate processes," Control Engineering Practice, vol. 3, no. 3, pp. 403–414, 1995.

[63] M. Piovoso, K. Kosanovich, and R. Pearson, "Monitoring process performance in real time," in 1992 American Control Conference, pp. 2359–2363, 1992.

[64] R. Dunia and S. J. Qin, "Joint diagnosis of process and sensor faults using principal component analysis," Control Engineering Practice, vol. 6, no. 4, pp. 457–469, 1998.

[65] J. Gertler and T. McAvoy, "Principal component analysis and parity relations-a close duality," 1997.

[66] S. T. Roweis and L. K. Saul, "Nonlinear dimensionality reduction by locally linear embedding," science, vol. 290, no. 5500, pp. 2323–2326, 2000.

[67] F. R. Bach and M. I. Jordan, "Kernel independent component analysis," Journal of machine learning research, vol. 3, no. Jul, pp. 1–48, 2002.

[68] M. Filippone, F. Camastra, F. Masulli, and S. Rovetta, "A survey of kernel and spectral methods for clustering," Pattern recognition, vol. 41, no. 1, pp. 176–190, 2008.

[69] G. Baudat and F. Anouar, "Generalized discriminant analysis using a kernel approach," Neural computation, vol. 12, no. 10, pp. 2385–2404, 2000.

[70] J. E. Jackson, A user's guide to principal components, vol. 587. John Wiley & Sons, 2005.

[71] I. Jolliffe, Principal component analysis. Wiley Online Library, 2002.

[72] C. Ding and X. He, "K-means clustering via principal component analysis," in Proceedings of the twenty-first international conference on Machine learning, p. 29, ACM, 2004.

[73] J. MacQueen et al., "Some methods for classification and analysis of multivariate observations," in Proceedings of the fifth Berkeley symposium on mathematical statistics and probability, vol. 1, pp. 281–297, Oakland, CA, USA, 1967.

[74] K. Wagstaff, C. Cardie, S. Rogers, S. Schrödl, et al., "Constrained k-means clustering with background knowledge," in ICML, vol. 1, pp. 577–584, 2001.

[75] S. Ding, "Data-driven design of monitoring and diagnosis systems for dynamic processes: A review of subspace technique based schemes and some recent results," Journal of Process Control, vol. 24, no. 2, pp. 431–449, 2014.

[76] X. Dai and Z. Gao, "From model, signal to knowledge: A data-driven perspective of fault detection and diagnosis," IEEE Transactions on Industrial Informatics, vol. 9, no. 4, pp. 2226–2238, 2013.

[77] C. Angeli and A. Chatzinikolaou, "On-line fault detection techniques for technical systems: A survey.," IJCSA, vol. 1, no. 1, pp. 12–30, 2004.

[78] M. Bo, J. Zhi-nong, and W. Zhong-qing, "Development of the task-based expert system for machine fault diagnosis," in Journal of Physics: Conference Series, vol. 364, p. 012043, IOP Publishing, 2012.

[79] D. V. Kodavade and S. D. Apte, "A universal object oriented expert system frame work for fault diagnosis," International Journal of Intelligence Science, vol. 2, no. 03, p. 63, 2012.

[80] V. Venkatasubramanian, R. Rengaswamy, S. N. Kavuri, and K. Yin, "A review of process fault detection and diagnosis: Part iii: Process history based methods," Computers & chemical engineering, vol. 27, no. 3, pp. 327–346, 2003.

[81] M. R. Maurya, R. Rengaswamy, and V. Venkatasubramanian, "A signed directed graph and qualitative trend analysis-based framework for incipient fault diagnosis," Chemical Engineering Research and Design, vol. 85, no. 10, pp. 1407–1422, 2007.

[82] G. Dong, W. Chongguang, B. Zhang, and M. Xin, "Signed directed graph and qualitative trend analysis based fault diagnosis in chemical industry," Chinese Journal of Chemical Engineering, vol. 18, no. 2, pp. 265–276, 2010.

[83] D. He, R. Li, and J. Zhu, "Plastic bearing fault diagnosis based on a two-step data mining approach," IEEE Transactions on Industrial Electronics, vol. 60, no. 8, pp. 3429–3440, 2013.

[84] J. Seshadrinath, B. Singh, and B. K. Panigrahi, "Vibration analysis based interturn fault diagnosis in induction machines," IEEE Transactions on Industrial Informatics, vol. 10, no. 1, pp. 340–350, 2014.

[85] B. M. Ebrahimi, M. J. Roshtkhari, J. Faiz, and S. V. Khatami, "Advanced eccentricity fault recognition in permanent magnet synchronous motors using stator current signature analysis," IEEE Transactions on Industrial Electronics, vol. 61, no. 4, pp. 2041–2052, 2014.

[86] A. Soualhi, G. Clerc, and H. Razik, "Detection and diagnosis of faults in induction motor using an improved artificial ant clustering technique," IEEE Transactions on Industrial Electronics, vol. 60, no. 9, pp. 4053–4062, 2013.

[87] N. Sheibat-Othman, N. Laouti, J.-P. Valour, and S. Othman, "Support vector machines combined to observers for fault diagnosis in chemical reactors," The Canadian Journal of Chemical Engineering, vol. 92, no. 4, pp. 685–695, 2014.

[88] S. Kim, I. Jung, Y. Kim, and C. Park, "Hybrid fault detection and isolation techniques for aircraft inertial measurement sensors," in AIAA Guidance, Navigation, and Control Conference and Exhibit, p. 5419, 2004.

[89] R. Isermann, "Integration of fault detection and diagnosis methods," IFAC Proceedings Volumes, vol. 27, no. 5, pp. 575–590, 1994.

[90] M. Todeschi and L. Baxerres, "Health monitoring for the flight control emas," IFAC-PapersOnLine, vol. 48, no. 21, pp. 186–193, 2015.

[91] M. Stamatelatos, W. Vesely, J. Dugan, J. Fragola, J. Minarick, and J. Railsback, "Fault tree handbook with aerospace applications," 2002.

[92] A. Bouti and D. A. Kadi, "A state-of-the-art review of fmea/fmeca," International Journal of reliability, quality and safety engineering, vol. 1, no. 04, pp. 515–543, 1994.

[93] R. Bromley and E. Bottomley, "Failure modes, effects and criticality analysis (fmeca)," in Masterclass in Systems Engineering-Part Two, IEE Colloquium on, pp. 1–1, IET, 1994.

[94] J. B. Bowles, "An assessment of rpn prioritization in a failure modes effects and criticality analysis," in Reliability and Maintainability Symposium, 2003. Annual, pp. 380–386, IEEE, 2003.

[95] Y. TANG and P. GOU, "A simple case study of fta in engineering," International Journal of Advanced Computer Science, vol. 1, no. 2, pp. 84–86, 2011.

[96] Y. Maccarana, "Modeling, identification and control of a test bench for fault detection of aeronautical electro-mechanical actuators." unpublished thesis, 2015.

[97] Y. Chen, C. Ye, B. Liu, and R. Kang, "Status of fmeca research and engineering application," in Prognostics and System Health Management (PHM), 2012 IEEE Conference on, pp. 1–9, IEEE, 2012.

[98] K. Chan, G. Southcombe, G. Trmal, and A. May, "Condition monitoring of aircraft high lift systems," Proceedings of the Institution of Mechanical Engineers, Part G: Journal of Aerospace Engineering, vol. 204, no. 2, pp. 75–82, 1990.

[99] E. Balaban, A. Saxena, S. Narasimhan, I. Roychoudhury, K. F. Goebel, and M. T. Koopmans, "Airborne electro-mechanical actuator test stand for development of prognostic health management systems," tech. rep., DTIC Document, 2010.

[100] D. S. Bodden, N. S. Clements, B. Schley, and G. Jenney, "Seeded failure testing and analysis of an electro-mechanical actuator," in Aerospace Conference, 2007 IEEE, pp. 1–8, IEEE, 2007.

[101] F. L. van der Linden, N. Dreyer, and A. Dorkel, "Ema health monitoring: An overview.," Recent Advances in Aerospace Actuation Systems and Components, pp. 21–26, 2016.

[102] C. S. Byington, M. Watson, D. Edwards, and P. Stoelting, "A model-based approach to prognostics and health management for flight control actuators," in Aerospace Conference, 2004. Proceedings. 2004 IEEE, vol. 6, pp. 3551–3562, IEEE, 2004.

[103] D. Brown, G. Georgoulas, H. Bae, G. Vachtsevanos, R. Chen, Y. Ho, G. Tannenbaum, and J. Schroeder, "Particle filter based anomaly detection for aircraft actuator systems," in Aerospace conference, 2009 IEEE, pp. 1–13, IEEE, 2009.

[104] A. Isturiz, J. Vinals, S. Fernandez, R. Basagoiti, E. d. l. Torre Arnanz, and J. Novo, "Development of an aeronautical electromechanical actuator with real time health monitoring capability," 2010.

[105] X. Jin, Y. Sun, Z. Que, Y. Wang, and T. W. Chow, "Anomaly detection and fault prognosis for bearings," IEEE Transactions on Instrumentation and Measurement, vol. 65, no. 9, pp. 2046–2054, 2016.

[106] M. Mazzoleni, S. Formentin, F. Previdi, and S. M. Savaresi, "Fault detection via modified principal direction divisive partitioning and application to aerospace electro-mechanical actuators," in Decision and Control (CDC), 2014 IEEE 53rd Annual Conference on, pp. 5770–5775, IEEE, 2014.

[107] F. Previdi, A. L. Cologni, M. G. Madaschi, N. Matteuzzi, M. Nardeschi, S. Toro, and S. M. Savaresi, "Modeling and control of an electro-mechanical ballscrew actuator for vibration active damping," in Control Applications (CCA), 2014 IEEE Conference on, pp. 177–182, IEEE, 2014.

[108] A. Isturiz, J. Vinals, J. M. Abete, and A. Iturrospe, "Health monitoring strategy for electromechanical actuator systems and components. screw backlash and fatigue estimation," Recent Advances in Aerospace Actuation Systems and Components, vol. 5, 2012.

[109] U. Forssell and L. Ljung, "Closed-loop identification revisited," Automatica, vol. 35, no. 7, pp. 1215–1241, 1999.

[110] P. M. Van Den Hof and R. J. Schrama, "Identification and control—closed-loop issues," Automatica, vol. 31, no. 12, pp. 1751–1770, 1995.

[111] T. Kanamori, S. Hido, and M. Sugiyama, "A least-squares approach to direct importance estimation," Journal of Machine Learning Research, vol. 10, no. Jul, pp. 1391–1445, 2009.

[112] S. Liu, M. Yamada, N. Collier, and M. Sugiyama, "Change-point detection in time-series data by relative density-ratio estimation," Neural Networks, vol. 43, pp. 72–83, 2013.

[113] M. Sugiyama, T. Suzuki, and T. Kanamori, Density ratio estimation in machine learning. Cambridge University Press, 2012.

[114] Y. Kawahara, T. Yairi, and K. Machida, "Change-point detection in time-series data based on subspace identification," in icdm, pp. 559–564, IEEE, 2007.

[115] K. Pearson, "On the criterion that a given system of deviations from the probable in the case of a correlated system of variables is such that it can be reasonably supposed to have arisen from random sampling," in Breakthroughs in Statistics, pp. 11–28, Springer, 1992.

[116] R. Garnett, M. A. Osborne, and S. J. Roberts, "Sequential bayesian prediction in the presence of changepoints," in Proceedings of the 26th Annual International Conference on Machine Learning, pp. 345–352, ACM, 2009.

[117] K. Yamanishi and J.-i. Takeuchi, "A unifying framework for detecting outliers and change points from non-stationary time series data," in Proceedings of the eighth ACM SIGKDD international conference on Knowledge discovery and data mining, pp. 676–681, ACM, 2002.

[118] I. Ahmed, N. Ertugrul, and W. L. Soong, "A study on the detection of fault frequencies for condition monitoring of induction machines," School of Electrical and Electronics Engineering University of Adelaide, Australia, 2005.